Coherent Optical Fibre Networking in the Nonlinear Regime

David John Ives

A thesis submitted to the University College London (UCL)
for the degree of Doctor of Philosophy (Ph.D).

Optical Networks Group
Department of Electronic and Electrical Engineering
University College London (UCL)

December 2015

I, David John Ives confirm that the work presented in this thesis is my own. Where information has been derived from other sources, I confirm that this has been indicated in the thesis.

Abstract

Optical networks form the backbone of modern communications and the Internet and with the ever increasing popularity of video streaming and other high bandwidth applications to ever more connected and mobile devices the amount of traffic is increasing rapidly. It is the overall aim of this work to investigate ways to maximise the efficient use of the backbone optical network infrastructure by considering a holistic approach optimising the whole optical network while considering the transmission impairments that degrade the optical signal.

The work begins by considering the dominant linear and nonlinear impairments to optical transmission and develops a simple model of transmission quality based on amplified spontaneous emission noise and nonlinear interference through the Gaussian noise model. The assumptions and accuracy of the model are discussed along with possible future extensions and improvements.

The quality of transmission model is used to optimise the signal to noise ratio of signals transmitted in a link and a simple three node network. It is shown that the individual signal launch powers can be adjusted to evenly distribute the signal to noise ratio margin, slightly improving the margin of the worst signal over a uniform launch power. The optimisation is extended to a mesh network where the full optimisation of modulation format, routing, wavelength and launch power are shown to increase the network throughput by upto 100 % over a fixed modulation format, fixed power, go anywhere optical signal. Finally the use of the quality of transmission model in sequential demand loaded networks is also considered.

This work will inform future planned work to include transmission impairments in the abstraction of the optical transport layer to allow for a more robust design of co-existing virtual networks.

Acknowledgements

Firstly I would like to thank my two supervisors Seb Savory and Polina Bayvel at UCL. Seb for his wide knowledge of the optical communications field and for his suggestion to join the centre for doctoral training in photonic systems development to obtain funding for this PhD. To Polina for asking the probing questions that push one towards a better understanding of the bigger picture and give greater clarity of purpose.

I would like to thank Irshaad Fatadin for beginning the collaboration between ourselves then at NPL and Seb Savory at UCL that led to his PhD and then onto this PhD. To Andrew Lord and Paul Wright at BT for providing direction from an operators perspective and supplying a sequentially loaded network simulator. I thank the EPSRC for funding through the centre for doctoral training in photonic systems development and the opportunity to learn new things and experience the broader photonics field.

A heart felt thanks goes to all my fellow students and colleagues in the Optical Networks Group and the Photonics Group in the 808 office at UCL for a friendly welcome and support. Especially to Gabriele Liga for discussions of the Gaussian noise model of nonlinear interference, to Alejandra Beghelli for pointing me in the direction of integer linear programming for optimising network routing, to Alex Alvarado for his insistence on mathematical and information rigour, to José Mendinueta for extracts from his beautiful LaTeX thesis template and finally to Domaniç Lavery for helping with modern computing and numerous illuminating discussions as a fellow physicist.

To my colleagues at Peak Rail and friends in the Matlock area that provided a break from the research, a chance to get away from the rush of London and relax with a good pint. Finally to my mother and father, brother his wife and son who have not questioned my late return to education.

Contents

List of Figures

List of Tables

List of Acronyms

3R	Re-time, Re-transmit and Re-shape
APSK	Amplitude and Phase Shift Keying
ASE	Amplified Spontaneous Emission
AWGN	Additive White Gaussian Noise
BCH	Bose Chaudhuri Hocquenghem
BER	Bit Error Ratio
BPSK	Binary Phase Shift Keying
CD	Chromatic Dispersion
CO-OFDM	Coherent Optical Orthogonal Frequency Division Multiplexing
DBP	Digital Back Propagation
DSP	Digital Signal Processing
DWDM	Dense Wavelength Division Multiplexing
EDFA	Erbium Doped Fibre Amplifier
FEC	Forward Error Correction
FWM	Four Wave Mixing
GbE	Gigabit Ethernet
GN	Gaussian
HD-BER	Hard Decision Bit Error Ratio
HD-FEC	Hard Decision Forward Error Correction

ILP	Integer Linear Programming
KSP-BLSA	k^{th} Shortest Path with Balanced Load Spectral Assignment
LOGO	Local Optimum Global Optimum
LOGON	Local Optimum Global Optimum for Nyquist channels
LP	Linear Programming
LSoHF-PSU-FFSA	Largest slots-over-hops first policy with path-set updates and first-fit spectral assignment
MILP	Mixed Integer Linear Programming
MUX	Multiplexer
NFV	Network Function Virtualisation
NLI	Nonlinear Interference
OH	Overhead
ONG	Optical Networks Group, University College London
OOK	On-Off Keying
OSNR	Optical Signal to Noise Ratio
PDL	Polarisation Dependent Loss
PMD	Polarisation Mode Dispersion
PM-BPSK	Polarisation Multiplexed Binary Phase Shift Keying
PM-mQAM	Polarisation Multiplexed m-ary Quadrature Amplitude Modulation
PM-QPSK	Polarisation Multiplexed Quadrature Phase Shift Keying
PON	Passive Optical Network
PSD	Power Spectral Density
QAM	Quadrature Amplitude Modulation
QPSK	Quadrature Phase Shift Keying
ROADM	Reconfigurable Optical Add Drop Multiplexer
RRC	Root Raised Cosine
SDN	Software Defined Network

SNR	Signal to Noise Ratio
SP-FFSA	Shortest Path with First Fit Spectral Assignment
SPM	Self Phase Modulation
WDM	Wavelength Division Multiplexing
WRON	Wavelength Routed Optical Network
WSS	Wavelength Selective Switch
XPM	Cross Phase Modulation

List of Publications

The following presentations and publications have been produced as a part of this work.

D. J. IVES & S. J. SAVORY, "Transmitter Optimized Optical Networks," *in Optical Fiber Communications Conference*, Anaheim, CA. (USA), Mar. 2013, JW2A.64.

D. J. IVES & S. J. SAVORY, "Fixed versus Flex Grid with Route Optimised Modulation Formats and Channel Data Rates of 400 Gbits and Above," *in European Conference on Optical Communications*, London (UK), Sep. 2013, P.5.11.

D. J. IVES, A. LORD, P. WRIGHT, & S. J. SAVORY, "Quantifying the Impact of Non-linear Impairments on Blocking Load in Elastic Optical Networks," in *Optical Fiber Communications Conference*, San Francisco, CA. (USA), Mar. 2014, W2A.55.

D. J. IVES, P. BAYVEL, & S. J. SAVORY, "Physical Layer Transmitter and Routing Optimization to Maximize the Traffic Throughput of a Nonlinear Optical Mesh Network," in *Optical Network Design and Modeling*, Stockholm (SE), May 2014.

D. J. IVES, P. BAYVEL, & S. J. SAVORY, "Adapting Transmitter Power and Modulation Format to Improve Optical Network Performance Utilizing the Gaussian Noise Model of Nonlinear Impairments," *Journal of Lightwave Technology*, **Vol. 32, No. 21**, Nov. 2014, pp. 3485–3494.

D. J. IVES, P. BAYVEL, & S. J. SAVORY, "Assessment of Options for Utilizing

SNR Margin to Increase Network Data Throughput," in *Optical Fiber Communications Conference*, Los Angeles, CA. (USA), Mar. 2015, M2I.3.

A. ALVARADO, D. J. IVES, S. J. SAVORY, & P. BAYVEL, "On Optimal Modulation and FEC Overhead for Future Optical Networks," in *Optical Fiber Communications Conference*, Los Angeles, CA. (USA), Mar. 2015, Th3E.1.

D. J. IVES, P. BAYVEL, & S. J. SAVORY, "Routing , Modulation , Spectrum and Launch Power Assignment to Maximize the Traffic Throughput of a Nonlinear Optical Mesh Network," *Photonic Network Communications*, **Vol. 29 , No. 3**, Mar. 2015, pp. 244–256.

A. MITRA, D. IVES, A. LORD, P. WRIGHT, & S. KAR, "Non-Linear Impairment Modeling for Flexgrid Network and its Application in Offline Network Equipment Upgrade Strategy," in *Optical Network Design and Modeling*, Pisa (IT), May 2015.

1

Introduction

OPTICAL networks, consisting of routers and switches interconnected by optical fibres, form the backbone of modern communication networks and the Internet. It was the development of low loss optical fibre combined with their high bandwidth that made optical fibre communications ideal for high speed, high capacity, long distance point-to-point communications. The development of transparent and re-configurable optical add-drop multiplexers (ROADM) allows these point-to-point links to be joined into a transparent optical network allowing the transparent wavelength routing and switching of optical signals from source to destination. This gives rise to potentially long optical paths which coupled with the high optical intensities leads to nonlinear interference and cross talk between the communication signals. The nonlinearity limits the power that can be transmitted and thus the quality of signal transmission and associated maximum data capacity. Given a network with limited resources in terms of number of fibres, connectivity, bandwidth and signal quality this work will consider how best to utilise the available resources to maximise the transport of data while placing a strong emphasis on including

the transmission impairments and their effects in a network context.

1.1 Optical Transport for the Internet

The Internet can be viewed as a layered hierarchy of interconnected networks [1–3] as illustrated in figure 1.1. At the regional operator level an optically transparent mesh network forms the core data transport layer interconnecting a small number of core nodes. These core nodes are connected via electrical edge routers to metropolitan ring networks and the metropolitan nodes are in turn connected to a local access network. The local access to the user can be provided by a passive optical network, PON, electrical ADSL or wireless network. As the transmission technology improves, it is anticipated that the range of the local access PON may be extended sufficiently to remove the need for the metropolitan ring network with the access networks connected directly to the edge routers of the regional core [4].

This work will focus on the core optical transport network where high capacity aggregated signals are transported over regional and worldwide distances.

1.2 The Capacity Crunch

Since its inception the growth of data traffic across the Internet has been relentless. Studies of data traffic [5] and future predictions of data traffic [6] in North America are shown in figure 1.2 and show a growth of approximately 50 % per annun. While historical data shows the rate of growth to be decreasing, a growth of approximately 33 % per annum was expected in 2015 [7]. In the UK the uptake of fixed line broadband connections [8, 9] is shown in figure 1.3 and has grown tremendously since 2000 but since 2008 growth slowed to approximately 6 % per annum with now almost one connection for every three people. Also over the period from 2008 to 2014 the average actual fixed line broadband speed has increased from 3.6 $\text{Mb}\cdot\text{s}^{-1}$ to 22.8 $\text{Mb}\cdot\text{s}^{-1}$ an increase of approximately 33 % per annum [10].

This growth is matched in the same period since 2009 where the BBC have reported [11] an approximately 33 % per annum growth in requests for programmes as shown in figure 1.4. Also over the period 2007 to 2015 YouTube® increased the maximum vertical

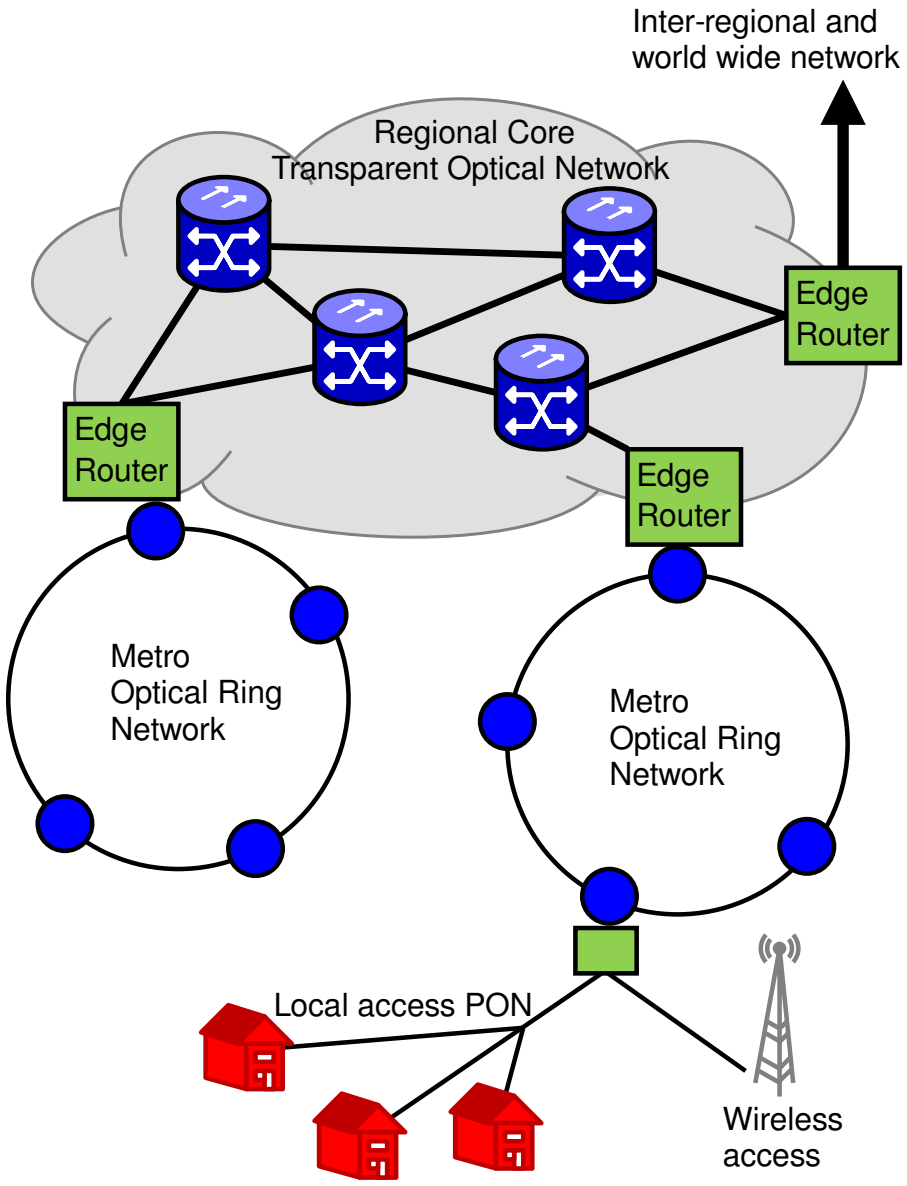

Figure 1.1: A possible view of the Internet, showing the hierarchy of networks.

resolution of its video from 240 to 4320 lines with a consequence increase in compressed data rate per video stream [1] from approximately 0.25 Mb·s^{-1} to 20 Mb·s^{-1}. This shows the growth of data traffic across the internet has been fuelled in three ways: through an increase in the number of users, an increase in the usage by individual users and through an increase in the quality and, thus, data requirements of the services provided.

It is anticpated that with the move to higher resolution video content for 4K and 8K screens that this growth in data usage will continue.

[1] Private download by author of 128 s of test video, 3.6 MB for 240 line version and 316 MB for 4320 line version `https://youtu.be/sLprVF6d7Ug`.

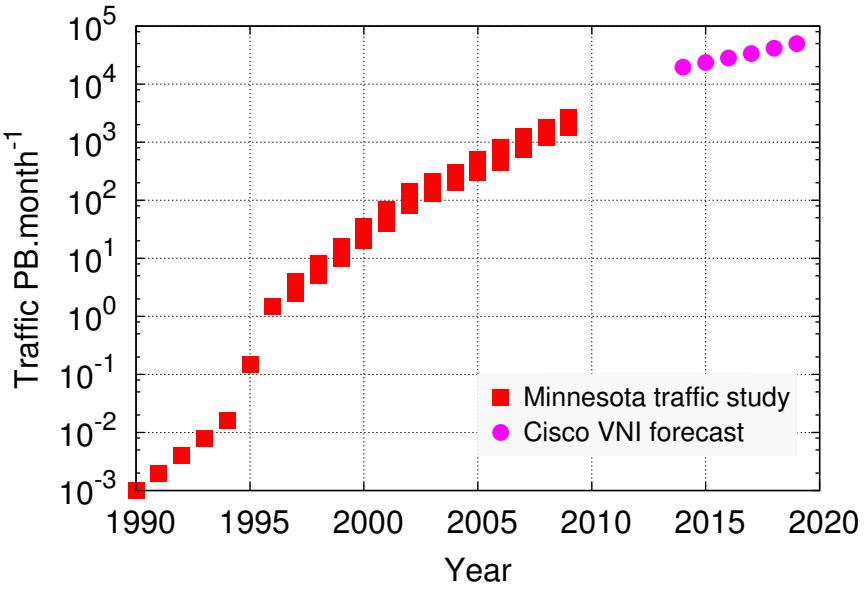

Figure 1.2: The growth of internet traffic in North America. Total traffic in Petabytes per month, historical data [5] and future forecast [6].

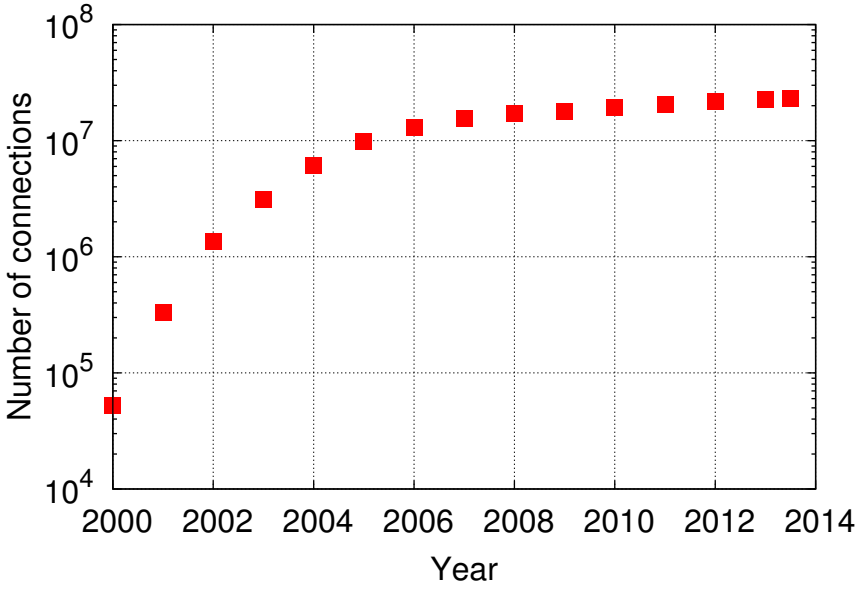

Figure 1.3: The uptake of fixed wired broadband connections in the UK [8, 9].

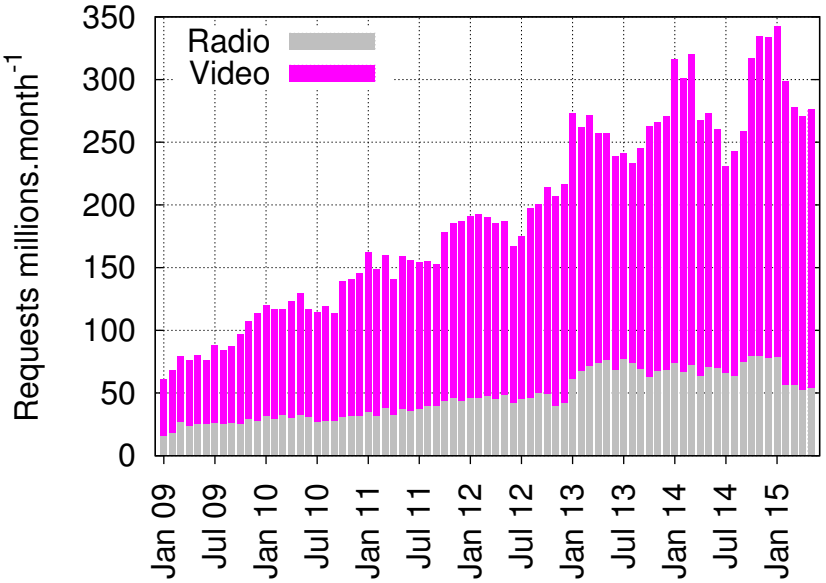

Figure 1.4: The growth of programme request to the BBC iPlayer [11].

1.3 The Problem to be Solved

This work considers a transparent wavelength routed optical network operating under the modern paradigm using high dispersion, uncompensated fibre links and polarisation multiplexed coherent optical transceivers. The overall questions are, in such a future optical network how should the transceiver operating parameters and ROADM routing be assigned to maximise the utilisation of the network resources? That is how should the installed fibre resource be used to maximise the transport of useful data?

In this work I consider both static optimised network design and sequential demand driven networks. In the first case the network would be designed and fully illuminated on day one with no further changes during its lifetime while in the second the network traffic is built up gradually by carefully adding lightpaths. It is anticipated that in the future, dynamic lightpaths will be added and removed, adapting the network to the prevailing traffic patterns. There is still considerable network research required to demonstrate to network operators that such dynamic operations are both useful and without risk to existing customers.

It is important to consider the physical transmission impairments that cause signal degradation and data loss to ensure that the network design solution is practical. A simple but effective model of nonlinear signal transmission quality is required to predict the quality

of signals that have traversed a variety of routes within the network and interacted with numerous other signals giving rise to nonlinear interference. This nonlinear impairment aware quality of transmission model is required to predict signal quality and end-to-end BER for the range of network routes and transceiver parameters that may exist in the network.

In such an impairment constrained nonlinear network what are the limited resources that we wish to utilise more effectively? Within each link the resources are bandwidth and in some way signal power. The bandwidth is clearly a resource that is utilised to transport data and has a total sum constraint, but signal power? This is in some way a resource as signals with high signal power necessarily restrict the SNR and thus data capacity of other signals through nonlinear interference, thus if some signals do not use power then other signals may be able to use more power to increase their SNR and increase their capacity. So signal power is a limited resource but the constraint is not a simple sum.

In an impairment constrained nonlinear optical network how should the transceiver and ROADM parameters be set? That is the transceiver signal parameters of modulation format, symbol rate, carrier frequency, FEC overhead, launch power and the ROADM parameters setting wavelength dependent switching and thus signal routing. This work begins by looking at the specific problem of maximising the useful data throughput of a given network topology with a fixed fibre resource and traffic pattern. With the associated secondary optimisation to minimise the number of transmitters, and maximise the available SNR margin to minimise the BER of each transmission.

It is hoped these initial optimisations will provide insight into generic rules that restrict the overall parameter space of the transceiver and ROADM where the optimum solutions are found. This will be used to inform future control plane algorithms, cognitive or virtual control planes, about how the scarce network resources should be best utilised.

1.4 Outline of Existing Solutions

In order to support this growth in traffic demand, optical communications have evolved with the continuing goal to transmit more data for the same or lower cost [12–14]. The throughput of point-to-point optical transmission links has been continuously increased, starting with simple OOK the throughput was limited by transmission losses and the

bandwidth of the terminal equipment. The transmission losses were overcome through the development of the EDFA [15] leaving the throughput limited by chromatic dispersion and PMD. Further gains in link throughput were achieved by adding multiple channels onto a single fibre through wavelength division multiplexing [12]. The development of coherent optical receivers with digital signal processing allowed the mitigation of the linear transmission impairments [16] and the development of high order polarisation multiplexed modulation formats where each modulated symbol can represent multiple information bits [17]. Modulation formats as high as PM-2048QAM with 22 bits·symbol^{-1} have been demonstrated [18]. In terms of overall data transport a total throughput of 102.3 Tb·s^{-1} over a single fibre 240 km link [19] and 61.9 Tb·s^{-1} over a 5920 km single fibre link [20] have been demonstrated.

The mitigation of linear impairments leaves the transmission limited by noise from ASE and noise like nonlinear interference. In dispersion managed networks utilising low symbol rate OOK signals the dominant source of nonlinear interference is from FWM between the equally spaced DWDM channels. For OOK the residual optical carrier has a high PSD leading to a strong nonlinear interaction between the channel carriers. Also the dispersion management reduces walk-off allowing a longer interaction length for FWM to build up. The reduced dispersion also increases the SPM and XPM but these lead to a nonlinear phase noise . This does not directly affect the signal amplitude but causes timing jitter. The FWM between DWDM channels can be reduced by offsetting the carrier frequencies from the channel centre in such a way as to ensure the FWM products do not impact on other channels [21]. This is only suitable where the DWDM channel spacing is much greater than the signal bandwidth. For coherent systems operating with high dispersion and with high bandwidths, digital signal processing in the form of digital back propagation [22] attempts to mitigate the nonlinear interference by backward simulation of the transmission link. This is limited by available receiver bandwidth and incomplete knowledge of stochastic processes within the link, ASE noise and the exact build up of PMD [23].

The most recent development in high throughput point-to-point links have looked at using multiple cores or multiple modes to increase throughput through spatial division multiplexing with upto 36 cores or 15 modes being demonstrated [24, 25].

The development of wavelength selective ROADMs [26] has allowed the interconnection of point-to-point fibre links such that optical signals can be transparently routed from one

fibre link to another, dropped to receivers or added from transmitters to allow local data to enter and leave the network. ROADMs allow the fibre links to be interconnected as a mesh network and allow the transparent end-to-end routing of signals based on their wavelength. This changes the situation from point-to-point communications, we still wish to support growth in traffic but must transport traffic between different sources and destinations as required. This leads to a varying load across the network with some links more congested than others and also a variety of transmission impairments on signals depending on their route through the network.

Wavelength routed optical networks traditionally used a fixed grid of frequencies spaced at 100 GHz and more recently 50 GHz for the signal carrier frequencies [27]. This gives all signals the same bandwidth leading to wasted bandwidth where low data rate channels are used and intermediate guard bands where two or more channels are co-routed. Flexible or elastic grid networking allows the establishment and routing of an adjustable bandwidth signal path. Finer granularity, typically 12.5 GHz, wavelength slots can be selected to provide a stepwise and more importantly allows multiple slots to be co-routed providing a continuous variable bandwidth signal path [28]. This allows a more efficient use of the available transmission bandwidth and has been shown to increase link throughput and gives a greater impact on overall network throughput [29].

The variety of route lengths and paths through a wavelength routed optical mesh network leads to a variety of transmission impairments giving signals with different quality of transmission. Traditionally the approach was to use transmitters capable of error free transmission over all routes within the network [30]. However the overall network efficiency can be increased by matching the modulation format to the route. Network design utilising mixed line rates, using OOK at 10 Gb·s^{-1}, DQPSK at 40 Gb·s^{-1} and PM-QPSK at 100 Gb·s^{-1} has been used to increase throughput and reduce capital expenditure on transmitters [31].

Given knowledge of the transmission impairments it is possible to use models to predict the transmission quality and use this information to inform the routing process [32, 33]. Much of this work has been carried out for direct detection OOK transmission but recently a number of models suitable for dispersion unmanaged transmission with polarisation multiplexed coherent signals have been developed [34–36].

The development of software defined transceivers [37–39] allows the automatic and

remote reconfiguration of transceiver parameters including modulation format to allow better and real time optimisation of the network throughput. For a given quality of transmission the modulation format can be adapted, but this leads to large steps in the required SNR. To fully utilise the available SNR between these steps the FEC overhead can be adapted to maximise the error free information rate [40].

For nonlinear transmission the transmitter launch power is an important factor controlling the quality of transmission. Too little power results in a poor signal to noise given the fixed amplifier ASE noise. While too great a launch power results in increased nonlinear interference and also increases the interference on neighbouring channels. The launch power can be optimised globally based on a worst case with fully loaded links to either maximise the signal SNR [41] or maximise the linear OSNR margin [42]. Some launch power adjustment around a global optimum [43] has been shown to slightly improve network throughput while Birand et al. [44] examined dynamic power control to maintain transmission performance while minimising interference. Recently the GN model has been used to optimise individual channel launch powers [45, 46]

1.5 The Approach of this Thesis

In this work it is assumed that maximising the data transported is the driving force and that the network resources will be heavily utilised. As such the investigation will consider how to operate the network in a resource scarce regime to maximise the throughput with little regard to complexity or cost. It will be assumed the network is using the most modern technology and will be operated in the high dispersion unmanaged regime with only polarisation-multiplexed coherent transmission formats.

It is intended to take a holistic approach and optimise the whole network to achieve these aims. Ideally the whole network would be optimised through a multi-parameter optimisation where routing, wavelength assignment and transmitter parameters such as symbol rate, modulation format , FEC OH and launch power are all considered together. In this work the optimisation space has been reduced by considering only fixed grid DWDM systems which avoids the complexity of routing with wavelength contiguity constraints. The optimisation was also separated into a multi-stage optimisation allowing the routing, wavelength, modulation and FEC OH to be assigned separately to the optimisation of

the launch power. This leaves the possibility of further improvements in the optimum if a technique that optimises all the transmission parameters together can be found with suitably low complexity.

An important optimisation metric of this work is the network throughput. Network throughput is here defined through equation (3.15). It is the total client data transported by the network that satisfies the traffic profile. It is the sum of all ingress client data, which is equal to the sum of the egress client data, that satisfies the traffic profile. In this work the traffic profile is uniform with equal traffic between all node pairs. Thus all the client data flows between all node pairs must be equal to satisfy the traffic profile and so the network throughput is equal to the minimum client data flow between any source destination pair taken over all possible source destination pairs multiplied by the number of source destination pairs.

Another important metric is the signal quality of transmission described by the symbol SNR. In this work I consider the symbol SNR as the SNR measured at the input to the decision circuit within the receiver. Since in this work I only consider hard decisions this is the point where the processed sampled analogue signal is mapped to received bits. The symbol SNR includes many sources of noise but in this work I include just the dominant components of optical amplifier noise and nonlinear interference. It is assumed that other noise sources in the transmitter and receiver both electrical and digital can be neglected.

Within a network context the signal traverses links and nodes it will be assumed that the nodes do not degrade the quality of transmission. The affect of amplifier noise in the nodes can be mitigated by pre-compensating for the ROADM loss giving a higher signal power within them. The effects of filtering and isolation within the ROADM nodes, non-ideal wavelength flatness of amplifiers and PDL are neglected as a source of transmission impairment. Such effects are dependent on specific technologies and are not a fundamental limitation. It is assumed that in the future such impairments can be significantly reduced and are thus not included in this work.

The key differences between the approach of this work and previous works are;

1) to consider a network with only polarisation-multiplexed coherent transmission formats operating in the the high dispersion unmanaged paradigm and use the GN model of nonlinear impairments

2) to place a strong emphasis on the launch power and how this affects the nonlinear impairments and how its adjustment can improve network performance

3) to maximise network throughput, rather than for example minimise cost, by adjusting all the transmitter parameters in particular the launch power.

The throughput of a mesh network is increased by improving the throughput of each point-to-point link but the overall benefits to the network depend on the traffic profile and the ability to route individual transmitters without wavelength collisions. It is intended that this investigation will lead to an understanding of the scarce limited resources in a network and how best they should be utilised to maximise the transport of data.

1.6 Outline of the Remainder of this Thesis

The remainder of this thesis is organised as follows. In chapter 2 a more detailed review of the literature and previous work is provided. This is followed by a description of the essential background ideas required to understand the main work in chapter 3.

Chapter 4 describes in detail the quality of transmission model used, based on ASE noise and nonlnear interference from the GN model . The originality of this work relates to the adaptation of the GN model to a network context. The GN model was also simplified to a matrix multiplication that calculates the nonlinear interference on all the signals depending on the power in all the other signals. The chapter also discusses the assumptions used in the simplification and also assesses the errors caused by their use.

The quality of transmission model is used in chapter 5 to optimise a point-to-point link and a simple three node, two link, inline network. The launch power of individual channels is adapted to achieve a number of network wide optimisation goals; maximising the even SNR, maximising the throughput... The operating bandwidth used in this chapter is small allowing the wavelength assignment to be investigated through brute force trial of all possible allocations. The work results in a number of heuristic rules that give near optimal performance.

The ideas of launch power adaptation are extended to realistic mesh networks in chapter 6. ILP is used to solve the routing, wavelength and modulation format assignment problem to maximise the data throughput given a fixed uniform traffic profile. The individual launch powers are optimised to maximise the SNR margin evenly on each signal and this margin is subsequently used in the ILP to increase the data throughput further. The chapter also explores the use of different FEC OH to bridge the SNR gap between the discrete modulation formats.

Chapter 7 considers a sequential demand driven network . This work was carried out in parallel with the work of chapters 5 and 6. For large networks the use of ILP to solve the routing and wavelength assignment is not tractable due to its complexity. In all likelihood in real installed networks the traffic will increase and transceivers will be added lighting more paths until the network can accept no further traffic. In particular the work of this chapter included nonlinearity into a demand driven network simulator and explored how this affects the blocking probability of demands in the network.

Finally the work is summarised in chapter 8 and some directions for further work are considered.

2

Review of the Published Literature

THIS chapter contains a review of the literature relating to network optimisation. Much of the previous work considers direct detection OOK transmission with associated assumptions and approximations. The work of this thesis will differ in many cases by assuming that the transmission systems of the future will operate with polarisation multiplexed coherent formats and that the transmission medium will have high unmanaged dispersion and operate in a nonlinear region.

2.1 Impairment Aware Networking

In transparent DWDM optical networks the transmission of data is affected by physical layer impairments. Thus to guarantee error free transportation of data the signal path must deliver a suitable quality of transmission. Impairment aware networking aims to consider the impairments in the design and routing of optical transport signals. Numerous papers have been published and summarised in a number of reviews [32, 33, 47]. Within these the most popular transmission rate is 10 Gb·s^{-1} OOK utilising direct detection, on a fixed

100 GHz DWDM grid [33].

The inclusion of transmission impairments has been carried out in a number of ways; through a post routing and wavelength assignment verification that there is a suitable quality of transmission, through a quality of transmission constraint applied within the routing and wavelength assignment and through a joint quality of transmission aware, routing and wavelength assignment that tries to maximise the quality of transmission. In some instances a simplified model of the quality of transmission is used to avoid complexity issues. In such cases the quality of transmission of the final solution may be verified or the quality of transmission constraint is given a sufficiently large margin to guarantee the final quality of transmission.

There are many choices for a quality of transmission metric, the most popular in the published literature [33] are; BER, OSNR, Q-factor, cross talk, power and equivalent length. While BER is popular as it reflects the ultimate requirement when uncoded or hard decision FEC is used, for example in traditional OOK transmission, the accumulation of this metric over multiple links is complex. The second and third most popular choices OSNR and Q-factor can, in traditional OOK transmission, be accumulated from the addition of a sequence of penalties for the various impairment. In this work the related symbol SNR is used as the quality of transmission metric as it is both easy to accumulate while also modulation format and symbol rate agnostic. The symbol SNR is outlined in section 1.5 defined in section 4.1 and includes both linear and nonlinear noise sources.

2.2 Mixed Line Rate Networking

One way to improve network utilisation is to use transmitters with different data rates for different connections. This may be useful where different demands exist for different connections and the cost of provisioning equipment can be reduced by using cheaper slower transmitters where demand does not require higher cost, high speed transmitters. It is also useful in a network context since in general shorter routes have fewer impairments allowing high speed transmitters to transport more data while longer routes are more affected by impairments such that error free transmission is only possible for slower transmitters. Thus mixed line rate networking allows the adaptation of the transmitter rate based on either the traffic demand and/or the physical layer impairments to optimise global network goals.

The term mixed line rate refers to the use of transmitters with different client data rates and also includes mixed technology types. For example Nag et al. [31, 48, 49] consider mixed line rate networking with transmitters capable of 10, 40 and 100 Gb·s^{-1} utilising OOK, DQPSK and PM-QPSK formats. An impairment model based on linear impairments and noise is used to assess the suitability of each modulation format on a given light path. The routing and line rate assignment is carried out with both a flow based ILP and a heuristic with the objective to minimise the network cost. Quantifiable benefits are difficult to extract; in [31] it is concluded that *"... one can save quite a bit of capital expenditure..."* through the utilisation of a multi-line rate approach. In their earlier paper [49] looking at the modified 14 node, 22 link NSF network with a total traffic of 10 Tb·s^{-1} they demonstrate a cost saving of 48 % by moving from 10 Gb.·s^{-1} fixed line rates to mixed line rates and a reduction in the number of transceivers from 1050 to 277. This advantage comes from the improved spectral efficiency. They also point out that the network can not support 20 Tb·s^{-1} utilising 10 Gb·s^{-1} line rates alone while it can using a mixed line rate approach. The work is extended in [50] to introduce nonlinear impairments and shows that the network cost is influenced by the transmitter launch power. Finally the emphasis is changed to minimise the energy cost in [51, 52], where it is shown that transparent optical networks reduce energy usage over translucent or opaque optical networks. Nag et al. [52] also introduce an ILP formulation robust against traffic variation.

The use of mixed optical line rates to design a network to transport ethernet over ethernet paths and tunnels is shown by Batayneh et al. [53, 54]. While Aparicio-Pardo et al. [55] describe an ILP to design a mixed line rate network with due regard for the quality of transmission that also simultaneously designs the virtual topology to minimise the network cost for a given traffic demand. Christodoulopoulos et al. [56, 57] use a reach based transmission constraint to optimise a mixed line rate network. The effective length of each link depends on the network state and allows the inclusion of the adverse nonlinear effects between different line rates.

The above work is related to static network design, similar techniques have been applied to dynamic demand driven networks [58, 59] again with 10, 40 and 100 Gb·s^{-1} rates provided by OOK, DQPSK and PM-QPSK each within a fixed 100 GHz channel. The routing algorithm was based on a expansion of the network graph one for each wavelength channel where the edges and nodes are weighted by the physical impairments. Heuristic

weights for chromatic dispersion, PMD, SPM, XPM and ROADM filtering were included. The algorithm finds the minimum weighted route on each wavelength graph before carrying out a BER estimation. The route and wavelength with the minimum BER is chosen. Before the request is set up the effect on all existing light paths is checked. There is a small improvement of around 3 % in the accepted network load at the relatively high blocking probability of 10 % in comparison with the basic shortest path first fit wavelength allocation.

In general the ideas of mixed line rate networking are used in this thesis through the adaptation of the modulation format, utilising higher order modulation formats where the quality of transmission allows. The use of different technologies, direct detection or coherent detection, is not considered in this work.

2.3 Flexible Optical Networks

Elastic optical networking was introduced and demonstrated in [60, 61] where the bandwidth of the optical path can be elastically expanded to match the bandwidth required for a given transmission data rate. This avoids wasted bandwidth by only utilising the bandwidth required. The concept and benefits of elastic optical networks were further outlined in [28, 62, 63] showing that the advantage of the technique is a saving of wasted bandwidth for low data rate channels and a reduction of guard bands by combining channels to form continuous high bandwidth channels for high data rate applications. The releasing of locked bandwidth has been shown to give a greater multiplicative increase in a network context. Wright et al. [29] show that using 400 Gb·s^{-1} PM-16QAM in an 87.5 GHz bandwidth is 128 % more efficient than using 4 off 100 Gb·s^{-1} PM-QPSK on a 50 GHz grid for a point-to-point link but when the same is used in a dynamic demand driven network simulation the network throughput was increased by 166 % for the same blocking probability.

Much of the advantage of flexible grid networks is due to the improved overall spectral efficiency by reducing wasted bandwidth. These gains apply equally to point-to-point and network contexts. These flexible grid ideas become more interesting when combined with bit rate adaptation allowing the reduction of spectral usage when the signal transmission quality allows for a higher modulation format. The idea of bit rate adaptation in elastic optical networks was described by Kozicki et al. [64]. They show that by adapting the

bit rate to the transmission distance the overall spectral efficiency can be increased. An experimental demonstration utilising DQPSK and 16APSK both at 42.7 Gb·s^{-1} gave an improvement in spectral efficiency of 45 % when 10 out of 16 channels traversed a short distance and were suitable for the 16APSK modulation.

These ideas were developed in [30, 65–67] based around three modulation formats PM-16QAM at 14 Gbaud using 37.5 GHz of optical bandwidth, PM-QPSK at 28 Gbaud using 50 GHz of optical bandwidth and PM-QPSK at 28 Gbaud using 62.5 GHz of optical bandwidth. Each format provides a data rate of 100 Gb·s^{-1} and had a reach of 5, 10 and $>$10 hops were each hop was just 50 km and the maximum hop count was determined from a full system simulation but neglecting nonlinear impairments. With static network routing using this approach [30] shows a 45 % improvement in spectral efficiency for a 12 node ring topology with uniform traffic while [65] show an 18 % improvement in spectral efficiency for a 6x6 square grid mesh network. For dynamic, demand driven loading [66] shows a 42 % increase in load for a 7x7 square mesh network and a 63 % increase in load for the COST266 European topology, both for a blocking probability of 1 %.

Zhang et al. [68] select the highest order modulation format and then use CO-OFDM bandwidth adaptation to match the required data rate. They develop a number of routing algorithms and compare these with SP-FFSA and KSP-BLSA. Considering the 14 node, 22 link NSF topology they show their LSoHF-PSU-FFSA algorithm gives improvements of several orders in blocking probability at low loads over SP-FFSA, but this is a simplistic algorithm, and a 10 % increase in accepted load at 1 % blocking over the KSP-BLSA routing algorithm.

The optimisation of the bandwidth and modulation format is tackled in [69, 70] where ILP formulations suitable to solve the routing, modulation level and spectral assignment problem are presented along with a number of heuristics. The techniques are tested on the 14 node, 23 link German telecommunication network. It is shown that the advantage of elastic bandwidths is largest for light traffic loads where the bandwidth used is reduced by more than 60 % over the fixed grid. The use of adaptive modulation level reduces the bandwidth used by approximately 25 % for all network loads.

In this thesis a simpler fixed grid is used leaving the advantages and complexities of a flexible grid to be investigated in further work.

2.4 Four Wave Mixing Mitigation

One of the areas considered in this thesis is the mitigation of nonlinear interference through routing, wavelength and launch power assignment. In traditional dispersion managed OOK systems, FWM between DWDM signals is a significant nonlinear impairment. It has been shown that for a sparsely populated spectrum by careful allocation of the channel centre frequency away from a regular grid the FWM components can be generated away from the transmission signals eliminating the interference at the expense of an increase in bandwidth usage [21, 71]. Thing et al. [72] showed that by fractionally adjusting the optical carrier frequency within the 100 GHz grid the average BER of eight 10G OOK channels could be decreased by a factor of 20. Adhya et al. [73, 74] considered FWM in the design of a logical network on the physical layer and equalised the SNR across channels by routing longer paths to the outer parts of the spectrum to reduce the number of interfering FWM components. They used a simple count of FWM components to assess the FWM impact. In this work given the use of the new high dispersion paradigm such that FWM is considerably reduced and the use of coherent transmission formats, the nonlinear interference is dominated by SPM and XPM. Also in this work adjustment to the optical carrier frequencies, to mitigate FWM, was not possible since most of the optical bandwidth was fully occupied.

2.5 Launch Power Control

The optimisation of launch power has been examined both from a global and individual channel point of view. Serena and Bononi [75] showed for a link that in the asymptotic limit of a large operating bandwidth the signal power spectral density, PSD, that minimises the nonlinear interference for a given total power is a uniform PSD across the operating bandwidth. Palkopoulou et al. [76] investigated optimised static network design using simulated annealing with variable symbol rate transponders. They showed that maintaining a constant launch PSD used less spectrum and fewer transponders than maintaining a constant launch power per transponder. The former launches more power for higher Baud transmission.

Poggiolini et al. [77] show that the optimum launch power for a complete path is obtained when the SNR degradation in each link is locally minimised. This is the LOGO

concept where the launch power into each span can be locally optimised to obtain the path global optimum. To simplify this further the assumption of high network loads and thus fully loaded fibres with Nyquist spaced channels leads to the LOGON model [35, 77] for network design where the SNR degradation of each link is calculated assuming fully loaded fibres at the optimum launch power.

Pastorelli et al. [42, 78, 79] compared network optimisation for two situations; global maximisation of the linear part of the OSNR margin to give the system maximum headroom for OSNR degradation and global maximisation of the BER margin giving the minimum BER. It is shown that a more robust network design is possible following the maximisation of BER margin.

Beyranvand and Salehi [80] use a closed form approximation of the GN model to optimise the global launch power to maximise the transmission reach. They use this physical layer model in a dynamic demand driven network to find the most dominant route and show the most dominant route selection leads to lower blocking, and higher OSNR in the 14 node, 22 link NSF mesh network and the 24 node, 43 link USA backbone.

Birand et al. [44, 81] examined dynamic power control based on a measured step wise differentiation of the SNR with launch power. The technique uses optical performance monitors to adapt the launch power to maintain a network performance guarantee. Recently Nakashima et al. [82] have developed a margin balancing algorithm that reduces the power of high margin signals and increases the power of low margin channels while also applying nonlinear compensation. The approach balances the margin and increases the number of channels providing sufficient quality of transmission.

A small amount of work has been carried out on launch power adaptation in networks. Power adaptation in OFDM signals is common in RF communications and has been shown by Yang et al. in CO-OFDM [83]. They demonstrate an optimal power distribution between sub-carriers such that a 4QAM modulated 10.7 Gb·s^{-1} signal can be uprated to 13.3 Gb·s^{-1} by moving half the sub-carriers to 8QAM modulation. The demonstration was carried out in the linear transmission regime.

In [43] an impairment aware routing is upgraded to include some basic power adaptation. A quality of transmission model based on linear cross talk and XPM weights is used and a single step wise power adjustment ± 1 dB is made to achieve a target weight. The small power adjustment is made around a previously optimised reference point [59] and resulted

in a small improvement in blocking in a dynamic, demand driven simulation of the 14 node, 21 link NSF mesh network. The technique is developed in [84] where the weight calculated from the auxiliary graph is directly linked to the launch power through a look up table.

Gao et al. [85] include power control in the routing and wavelength assignment of a dynamic demand driven network with mixed line rates. The route with the minimum power requirement is selected. On the 24 node 43 link USA backbone network blocking is less than or equal to the optimum fixed launch power. A 0.2 dB margin was found to be optimal at light path set up in order to provide some buffer against future blocking. The blocking advantage over a fixed optimal launch power appears to only occur at high blocking levels.

More recently Yan et al. [46] presented a formulation to jointly optimise any combination of bandwidth, power, and SNR margin, through optimal joint selection of modulation formats, carrier frequencies, and PSDs in flexible-grid optical networks. They demonstrate the formulation for a three node network showing a reduce spectral usage in comparison to a fixed grid baseline [34].

2.6 Code Rate Adaptation

The code rate of the transmission can be adapted to give error free data transmission where the SNR is insufficient for a preferred fixed FEC OH. Gao et al. [86] described a family of HD-FEC codes that can be used to provide adapted rate transmission. Savory [87] assumed an ideal HD-FEC based on a binary symmetric channel to show that adaptation of the FEC OH can be used in statically loaded networks. Arabaci et al. [88] described a family of soft decision codes while Mello et al. [40] considered a theoretical variable soft decision FEC based on a performance gap between a single realised soft decision FEC code and the ideal format constrained capacity.

Thanh et al. [89] used a variable code rate in conjunction with a flexible grid and showed that the number of channels on each link is significantly reduced for a given load and that around three times more traffic could be supported in comparison to using mixed line rates alone. Li et al. [90] considered three generations of FEC and choose a FEC depending on the channel OSNR. They found that in a network context adapting the FEC OH allowed an overall reduction in the FEC OH. Alvarado et al. [91] showed that a variable

HD-FEC overhead can significantly improve the throughput of a network compared to a fixed HD-FEC OH. He went on to show that most of the throughput gains can be obtained using a limited number, of just two optimised HD-FEC OH.

2.7 Theoretical Advantage of Adaptation

In 2010 Korotky et al. [92] published a paper estimating the potential increase in traffic that a network can support by moving to bit rate adaptive modulation. The paper reports headline figures of up to a 4 fold increase in network traffic by changing from a fixed network wide modulation to a light path specific bit rate adapted modulation. The calculation is based on the statistical distribution of light path lengths within the network and the distribution of traffic across the network. A couple of points regarding this headline 4 fold improvement in network throughput. The calculation is based on taking an existing routing assignment for a fixed network wide modulation, fixing the number of light paths and looking at the increase in traffic supported if the modulation is adapted for each light path. This will change the distribution of traffic across the network and is not equivalent to giving each existing user a 4 fold increase in capacity. Also the larger increases in network throughput are based on an inaccurate physical layer model where the bit rate distance product is assumed constant. The latter part of the paper uses a SNR based approach where the SNR is inversely proportional to the transmission distance and the bit rate depends on the logarithm to the base 2 of the SNR. This approach is consistent, under certain assumptions, with the quality of transmission model described in chapter 4. So while the lower figure of a 1.7 fold increase in network throughput, for the mesh network with lumped amplifiers covering ¾ of the contiguous USA, is less attractive it is more realistic. Although given the first point regarding the change of traffic distribution this is still likely to be optimistic.

More recently Makovejs et al. [93] looked at the potential increase in average transponder capacity where low loss fibre or shorter span lengths are used. It is shown that by using the most modern low loss Vascade EX2000® fibre in the German telecommunication network that PM-16QAM at 200 Gb·s^{-1} can be transmitted error free without regeneration across the whole network. By comparison when using standard single mode fibre only 32 % of connections can support PM-16QAM at 200 Gb·s^{-1}. They show that the average transponder capacity can be increased from 169 Gb·s^{-1} to 250 Gb·s^{-1} when changing from

standard SMF to Vascade EX2000 fibre and suggest this would lead to a corresponding increase in network capacity. However similar to Korotky et al. [92] an increase in average transponder capacity does not necessarily translate into network capacity as we must ensure the traffic profile is not changed and this requires a new routing and wavelength assignment solution for the uprated transponders.

3

Background

THIS chapter includes descriptions of a minimal set of ideas, concepts and technologies that are required to understand the work of this thesis.

3.1 Wavelength Routed Optical Networks

WRONs are formed of nodes containing optical transmitter, receivers and ROADMs, connected by optical links [3, 94–97]. The optical signals are routed from the transmitter to the receiver by virtue of their wavelength. The ROADMs contain wavelength selective switches that can route individual wavelengths from input port to output port. They can also route a wavelength from an input port to a receiver, a drop or from a transmitter to an output port, an add. The links contain optical fibre pairs each that operate unidirectionally and consist of fibre spans interspersed by optical amplifiers to compensate for the transmission loss. The optical network provides a transparent link between the transmitter and receiver without any intermediate signal processing beyond basic amplification. This means network elements are signal agnostic allowing the upgrade of transmitter and receiver without

affecting the intermediate elements.

WRONs have been extended with the use of non transparent intermediate elements such as wavelength conversion, format conversion and 3R regenerators. In this work the WRON will be taken as the basic transparent version with ROADM nodes connected by optical fibre links, if the additional functionality of wavelength, format conversion or 3R regeneration is required it is assumed this will be implemented by optical-electrical-optical conversion at ROADM nodes and utilising the installed network transceivers.

The WRON architecture routes signals based on their wavelength. Traditionally, this has meant routing signals on the ITU-T grid but more recently elastic optical networking has allowed routing of finer wavelength slots that can be grouped to build up the required transparent bandwidth [62, 63]. Traditional DWDM switches will operate on a 100 or 50 GHz grid switching either 100 or 50 GHz of optical bandwidth. The switches are such that if two adjacent 50 GHz grid wavelengths are switched together there can still be a small blocked band between the two switched channels. In elastic optical networking groups of smaller bandwidth slots can be switched forming a continuous optical channel that potentially has larger continuous bandwidth than with fixed grid technology. In this work a traditional 50 GHz fixed grid wavelength routed optical network was considered.

The aim of this work is to explore nonlinear networks near their capacity limit as it is the growth of internet traffic that drives the research in optical networking. Thus only the latest spectrally efficient modulation formats based on coherent transmission technologies are considered. The phase and amplitude polarisation multiplexed, 4 dimensional, modulation formats of PM-BPSK, PM-QPSK, PM-16QAM, ... PM-mQAM will be used. With the development of software-defined transceivers [37–39] the transmitter can be re-configured allowing the transmission parameters and modulation format to be adapted to the current network conditions. This allows the physical network resources of bandwidth and power to be used more efficiently.

Throughout this thesis the fibre, signal and networking parameters shown in table 3.1 will be assumed unless otherwise explicitly stated.

Table 3.1: Simulation parameters used throughout this thesis, except where explicitly shown.

Parameter	Symbol	Value	
Fibre Parameters			
Span Length	L	80	km
Attenuation Coefficient	α	0.0507	km^{-1}
		(0.22	$dB{\cdot}km^{-1}$)
Chromatic Dispersion Coefficient	β_2	-21.3	$ps^2{\cdot}km^{-1}$
		(16.7	$ps{\cdot}nm^{-1}{\cdot}km^{-1}$)
Non-linear Coefficient	γ	1.3	$W^{-1}{\cdot}km^{-1}$
Amplifier Parameters			
Noise Figure	NF	5	dB
Signal Parameters			
Carrier Frequency	ν	193.5	THz
Symbol Rate	R	32	Gbaud
Spectral Roll off		0.0	
DWDM fixed grid		50	GHz
DWDM Channels		80	

3.2 Nonlinear Optical Propagation

The propagation of electromagnetic waves in silica glass is weakly nonlinear and this leads to transmission impairments that cause interactions between co-propagating signals.

Within a dielectric medium the electric field, E, causes the bound charges to move creating an electric polarisation field, P. The electric displacement field, D is defined as the sum of these two fields [98]

$$D = \varepsilon_0 E + P = \varepsilon_0 \varepsilon_r E \tag{3.1}$$

where ε_0 is the permittivity of free space and ε_r is the relative permittivity of the medium. The solution of Maxwell's equations within a medium is similar to the solution in free space and gives a plane wave with velocity of propagation $(\varepsilon_r \varepsilon_0 \mu_r \mu_0)^{-1/2}$ where μ_0 is the permeability of free space and μ_r is the relative magnetic permeability and is typically

equal to the 1 for the material of interest here. The polarisation of the medium leads to a speed of propagation slower than in free space and a refractive index $n = \sqrt{\varepsilon_r \mu_r}$.

The polarisation field P depends on the electric field E through the electric susceptibility and is given by [99]

$$P_i = \varepsilon_0 \sum_{j=1}^{3} \chi_{ij}^{(1)} E_j + \varepsilon_0 \sum_{j=1}^{3}\sum_{k=1}^{3} \chi_{ijk}^{(2)} E_j E_k + \varepsilon_0 \sum_{j=1}^{3}\sum_{k=1}^{3}\sum_{l=1}^{3} \chi_{ijkl}^{(3)} E_j E_k E_l + \ldots \tag{3.2}$$

where $i = 1,2,3$ denote the three spatial dimensions and $\chi^{(1)}$, $\chi^{(2)}$, and $\chi^{(3)}$ represent the first, second and third order susceptibility tensors. The first order susceptibility $\chi^{(1)}$ gives rise to the usual linear refractive index. For amorphous material such a glasses $\chi_{ij}^{(1)} = \chi_{11}^{(1)}$ for $i = j$, 0 otherwise and $\varepsilon_r = 1 + \chi_{11}^{(1)}$. The higher order susceptibility tensors $\chi^{(2)}$, $\chi^{(3)}$ ... give rise to nonlinear effects as the polarisation field is no longer a linear function of the electric field. For materials with inversion symmetry $\chi^{(2)}$ is zero such that $\chi^{(3)}$ is the most significant cause of nonlinearity. The $\chi^{(3)}$ tensor has 81 elements but for amorphous materials only 21 of these are non zero and they can all be related to $\chi_{1111}^{(3)}$ by symmetry.

Solving Maxwell's equations for the propagation of electromagnetic waves in an amorphous material leads to a nonlinear index of refraction, the Kerr effect where the refractive index depends on the optical intensity,

$$n = n_0 + n_2 I \tag{3.3}$$

where n_0 is the linear refractive index, n_2 is the nonlinear refractive index and I the optical intensity. The optical fibre silica glass medium is very weakly nonlinear with a nonlinear refractive index $n_2 \approx 3 \times 10^{-20}$ m^2·W^{-1} [100] such that at every day optical intensities of 1000 W·m^{-2} the refractive index of a camera lens would change but merely 3×10^{-17}, insignificant in comparison to the bulk refractive index around 1.45. Even at the relatively high optical intensities within the fibre core, 100 mW in a 10 μm diameter giving of order 1 GW·m^{-2} the refractive index is hardly changed, just by of order 3×10^{-11}. It is the guiding structure of the optical fibre that maintains the high optical intensity for extended transmission lengths, 10s km allowing this nonlinearity to build and become significant.

The effect of the nonlinear refractive index on the transmission signal is to create an intensity dependent optical phase shift since the change in refractive index alters the propagation velocity. This leads to the effect of self phase modulation. This nonlinear phase shift is more simply described by

$$\phi_{NL} = \gamma p L \tag{3.4}$$

where p is the optical power, L the propagation distance and γ is the nonlinear coefficient. The nonlinear coefficient is a combination of the third order susceptibility and other optical and dimensional properties of the optical fibre and allows the optical intensity to be replaced by the more easily measured optical power.

In the linear propagation regime where $\chi^{(3)}$ can be neglected the polarisation field is a linear function of the electric field caused by the signal. This linearity means that the polarisation field due to the sum of the electric field of two signals is the same as the sum of the polarisation fields caused by the two electric fields separately. This linear property means the electric fields of two signals act independently and separably and thus do not interact. In the nonlinear regime the polarisation field depends on the optical intensity within the optical fibre and since the intensity depends on the square of the total field within the fibre there will be cross terms between the signal fields causing interference between copropagating signals. This gives rise to cross phase modulation where the intensity variations in one channel causes optical phase variations on another. It also gives rise to the phenomena of four wave mixing.

The most important nonlinear phenomena in this work is four wave mixing where three waves mix to create a fourth. Physically this can be seen as the effect of two waves beating to create a time vary intensity that subsequently phase modulates the third wave generating the fourth. In reality if three waves were injected into an optical fibre with sufficient power nine new waves would be generated from the various combinations. The nonlinear phenomena of SPM and XPM will be viewed as the result of FWM between the spectral components of the signal channel alone and between the spectral components of the signal and interfering channel respectively.

Traditionally four wave mixing was considered between the carrier tones of each channel but with the modern coherent signal formats the carrier is suppressed giving a broadband signal channel. Under this new paradigm the four wave mixing being considered is between all signal spectral components and as such all four waves may exist within a single DWDM channel or between many DWDM channels. The four wave mixing generates nonlinear interference that is viewed as a source of noise degrading the transmitted signal quality.

3.3 A Brief Review of Transmission Impairments

The optical signal is degraded by the non-ideal transmission path such that the received signal is a distorted version of the transmitted signal leading to errors in the received data. The signal is degraded through the accumulation of stochastic noise and through transmission impairments causing signal distortions [99, 101]. The transmission impairments can be either linear or nonlinear in nature, where linear impairments scale linearly with the optical signal field while nonlinear impairments tend to increase more rapidly than linear with increasing optical signal and also causes interference between co-propagating signals.

There are numerous sources of stochastic noise in the transmission path in the electrical, optical and digital domains. In the transmitter there is the potential for digital noise from the non-ideal nature of any digital to analogue conversion, electrical and thermal noise in the drive electronics, and laser relative intensity noise and phase noise from the optical source. As the optical signal will be assumed to be transmitted over some distance the signal loss of the optical fibre will be regained by amplification. The optical amplification process will introduce noise in the form of amplified spontaneous emission, ASE. Finally at the receiver there will be shot noise in the detector due to the quantum nature of the light, further electrical and thermal noise in the electronics before digitizing noise in the analogue to digital converters and digital noise in the receiver DSP. Careful transmitter and receiver design can minimise many of these noise sources such that for long distance (multiple span) transmission the only significant stochastic noise source is the ASE noise from the intermediate optical amplifiers.

Linear impairments cause signal distortion that are proportional to the signal field strength such that the distorted shape of the signal is independent of signal strength. Such impairments include chromatic dispersion where the signal velocity is dependent on its frequency and polarisation mode dispersion where the signal velocity depends on its polarisation state. Both effects lead to a broadening of features within the signal waveform causing transmitted symbols to overlap with previous and future symbols. Spectral filtering caused by narrow band optical filters or by the limited electrical bandwidth also distort the signal. Finally there can be linear cross talk between signals where two signals on the same DWDM carrier frequency are poorly isolated in a ROADM node. In coherent receivers where the receiver detects the signal field the linear transmission impairments

of chromatic dispersion and polarisation mode dispersion can be equalised and removed within the receiver DSP [102, 103]. The effects of spectral filtering and limited electrical bandwidths can be reduced by design while cross talk within ROADMs can be reduced by using higher isolation components.

Nonlinear impairments give signal distortions that are not proportional to the optical signal field strength but tend to increase more rapidly with increasing optical signal strength. These include nonlinear impairments caused by the Kerr effect, through the third order electric susceptibility and also nonlinear interactions between the optical field and the media, through molecular vibrations within the material, the Brillouin and Raman effects [99]. The Kerr effect causes the refractive index of the transmission media to be dependent on the instantaneous optical intensity and gives rise to the phenomena of self phase modulation(SPM), cross phase modulation(XPM) and four wave mixing(FWM). The SPM interference can be mitigated using digital back propagation(DBP) [22] and with full knowledge of all the transmitted channels could be extended to mitigate XPM and FWM [23, 104]. In a real network signals may co-propagate for just a short distance being combined and separated at intermediate ROADMs. Thus signals may interact without the direct knowledge of the transmitter or receiver such that only SPM can be fully mitigated. Thus nonlinear interference caused by XPM and FWM are significant signal degradations that can not be fully mitigated and SPM will also need to be included if the complexity of DBP is considered excessive.

There are also nonlinear interactions between the optical field and the media through molecular vibrations within the material. These interactions manifest themselves as Brillouin scattering and Raman scattering where the optical field interacts with acoustic and optical phonons respectively. Brillouin scattering is a significant scattering mechanism for narrow linewidth signals however for the high capacity high Baud signals in modern communications, Brillouin scattering is reduced by virtue of the broad signal spectrum. Raman scattering is used as an amplification mechanism where a pump is deliberately scattered into the signal. The Raman shift (the difference between the pump wavelength and scattered wavelength) is of the order 100 nm thus if all the signals are within the c-band any signal generated Raman scattering will give rise to noise outside of the c-band as the c-band is $<$40 nm wide.

3.4 Quality of Transmission Models

To ensure that error free data transmission is possible across a network it is important to consider the physical layer transmission impairments and the quality of transmission of signals across the network. To maximise the use of physical resources it is necessary to consider the impairments along with the routing and spectral assignment giving impairment aware network optimisation. The impairment models used in this optimisation must be simple yet sufficiently accurate to capture and predict the impairments.

Physical layer impairment aware routing has seen a lot of interest and is well reviewed [32, 33]. Much of the prior work has been aimed at direct detection OOK systems with dispersion managed links, in this context a popular quality of transmission metric is the Q-factor defined for OOK by

$$Q \triangleq \frac{\mu_1 - \mu_0}{\sigma_1 + \sigma_0} \tag{3.5}$$

where μ_1, μ_0 are the mean level for a 1 or 0 bit, and σ_1, σ_0 are the standard deviation of the level for a 1 or 0 bit, all taken at the decision point. The Q-factor can be converted to BER using

$$\text{BER} = \tfrac{1}{2}\text{erfc}\left[\tfrac{Q}{\sqrt{2}}\right] \tag{3.6}$$

where

$$\text{erfc}[x] \triangleq \frac{2}{\sqrt{\pi}} \int_x^\infty e^{-t^2} \mathrm{d}t. \tag{3.7}$$

For BPSK and Gray coded QPSK modulation formats the Q-factor is still relevant such that Q^2 is equal to the symbol SNR and the BER formula (3.6) still applies.

For transmission in a network the Q-factor is estimated based on the accumulated noise and including penalties for other impairments [58, 105, 106]. The noise is estimated from ASE [105] but can also include XPM and FWM as noise sources. XPM noise is given for direct detection OOK as a function of the signal power, the interfering power and a frequency dependent transfer function [107–111]. This form has similarities with the Gaussian noise model that includes XPM as a source of optical noise but differs since direct detection leads to a signal noise beating and the dispersion management leads to a different frequency dependent transfer function between phase and amplitude noises. FWM has also been included in [110, 111]. The linear impairments of chromatic dispersion and PMD are included as penalties estimated by extensive simulation and interpolation [112–114]. Other authors also treat the impairments separately setting constraints on OSNR, CD, PMD and

nonlinear phase noise that must all be met for error free transmission.

One simpler approach is to calculate the reach (the maximum transmission distance) of the transmitter to be used in the network [48, 115]. The reach is calculated by simulation under some assumed network conditions; fibre type, channel spacing, channel load. These are usually a worst case to allow robust transmission. When routing through the network an equivalent length [116] is calculated based on the fibre length and some equivalent length for other component impairments and the reach must be greater than this equivalent length for guaranteed error free transmission. Jinno and Takagi [30, 65, 66] use a reach based approach in their optimisation of elastic optical networks but simplify this further to a maximum number of ROADM hops in their network.

For polarisation multiplexed coherent transmission in high dispersion unmanaged paradigm the Gaussian noise, GN, model [41, 117–120] has proved a useful tool to estimate the signal quality through the SNR using an additive Gaussian white noise approach. The use of the GN model as a quality of transmission modelling method will be fully described in chapter 4.

3.5 Erbium Doped Fibre Amplifier Noise

EDFAs are used to amplify the optical signal in a lumped fashion, that is over a distance much shorter than the span length. Such amplifiers add noise to the onward propagating signal in the form of ASE. For a single mode fibre amplifier supporting 2 polarisation modes the single sided noise PSD generated at the laser output is given by N_0 (W·s^{-1}) [121]

$$N_0 = 2\eta_{sp} h\nu \,(G-1) \tag{3.8}$$

where h is Planck's constant (6.626×10^{-34} J·s), ν is the channel carrier optical frequency (Hz), G is the amplifier gain and η_{sp} is the inversion factor given by

$$\eta_{sp} = \frac{n_2}{n_2 - n_1 \frac{g_2}{g_1}} \tag{3.9}$$

where $\eta_{sp} > 1$ and n_1 and n_2 are the density of erbium atoms in the ground and excited states respectively and g_1 and g_2 are the ground state degeneracy and excited state emission degeneracy respectively, these are often replaced by $\sigma_{1,2} \propto \frac{1}{g_{1,2}}$ the transition cross sections [122]. For commercially available amplifiers the noise performance is specified using a noise figure, denoted F in linear units or NF in (dB). The noise figure gives the ratio of

the SNR at the output to the SNR at the input and represents an SNR degradation. Note the definition of noise figure is very specific [123] and does apply to a general input SNR. The SNR at the input is taken as the electrical SNR measured on an ideal photodiode for a single polarisation optical signal that is purely shot noise limited. The SNR at the output is taken as the electrical SNR measured on an ideal photodiode where the optical signal is shot and ASE noise limited. The noise figure is given by, F, as

$$F = 2\eta_{sp}\frac{G-1}{G}. \tag{3.10}$$

So substituting into (3.8) gives,

$$N_0 = Fh\nu G. \tag{3.11}$$

For real amplifiers the noise figure is measured for a small input signal where the amplifier provides the full small signal gain. The noise figure, F, is limited by the inversion and also by component losses that give an overall gain less than that due to the amplifying medium alone.

In this work there is the requirement for a variable gain optical amplifier such that any span loss or component loss can be ideally compensated. If we consider adjusting the amplifier gain by adjusting the pump power then this will reduce the density of excited states and increase the overall noise figure. Thus it will be assumed that the amplifier is always run at its optimum gain and any excess gain is reduced by a following attenuator. Both the gain and the noise will be reduced by the attenuator such that equation (3.11) still applies where G now refers to the overall gain of the amplifier and attenuator combination.

3.6 Nonlinearity Mitigation by Digital Back Propagation

Coherent receivers provide linear detection of the electric field of the optical signal and this allows complex DSP algorithms to mitigate transmission impairments. Algorithms to mitigate the linear impairments of chromatic dispersion and polarisation mode dispersion are a well established part of coherent receiver technology. The mitigation of nonlinear impairments is possible using DBP [22], where the received electric field is reverse propagated by simulation to estimate the transmitted electric field. The technique requires considerable mathematically effort and cannot ideal compensate all the transmission impairments. The main sources of error are received noise which is back propagated as

if it was signal, nonlinear interference between signal and ASE [86] which cannot be estimated as the ASE is an unknown stochastic process, incomplete knowledge of the transmission medium in particular PMD, as shown in [23, 86], and incomplete knowledge of co-propagating signals outside the receiver bandwidth. As such DBP is considered useful to remove SPM from the nonlinear interference noise. Even for SPM the accuracy of DBP is significantly dominated by PMD where the detail of the polarisation evolution of the signal through the transmission medium is unknown and changes with time such that DBP should only be considered for transmission distances with low PMD accumulation.

The paper by Liga et al. [23] shows that it is possible to reduce SPM noise to 10 % of its uncompensated impact, that is the overall symbol SNR improves by approximately 3 dB, for a total PMD of 2 ps (3200 km at 0.035 ps·km$^{-1/2}$) and a total signal bandwidth of 160 GHz. This suggests a PMD bandwidth product of $PMD \times BW \leq 0.3$ is required for good SPM compensation. Thus for good SPM compensation of a single 32 GBaud channel a total PMD of less than 10 ps is required which will be achieved for 0.1 ps·km$^{-1/2}$ over 8000 km or 0.05 ps·km$^{-1/2}$ over 32000 km. These PMD values are achievable with good quality modern single mode fibre.

3.7 ROADM Design

For this work the ROADM nodes within the network had a design as shown in figure 3.1. This basic design [26, 124] is contention-less and allows the non blocking routing of wavelengths between the links, but importantly, allows without blocking the same wavelength to be injected into or dropped from two or more different links. Thus, if none of the signals were passed through the node the full 80 DWDM channels could be added to each link without contention. This ROADM design is conceptually suitable for this work but in practice, since it is not colourless or direction-less, reconfiguration is difficult as it may involve physical relocation and reconnection of transceivers to the correct DWDM multiplexer or demultiplexer port. A more sophisticated ROADM design would also be colourless, allowing any transceiver port to be used with any wavelength and direction-less allowing any transceiver port to be routed to any link. Such a design would allow a bank of transceivers to be used as a reconfigurable resource without manual intervention.

In establishing the ROADM loss the component losses in table 3.2 were assumed. The

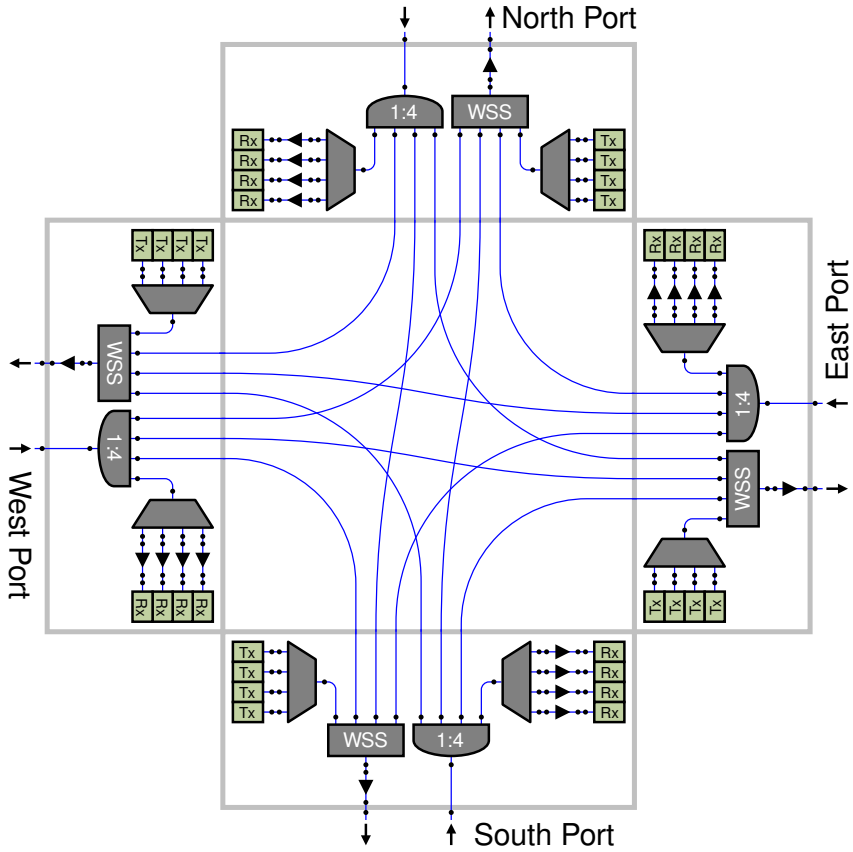

Figure 3.1: A possible ROADM design showing the components and interconnections. The dots correspond to mated connector pairs.

Table 3.2: Loss assumptions of the optical components used in the ROADM and the network spans.

Symbol	Loss (dB)	Component Name	Example Model
WSS	6.5	Wavelength selective switch	Finisar DWPf
1:4	6.0	1 to 4 balanced splitter	
MUX	6.0	DWDM multiplexer	MRV RD-DMDXA80M
·	0.3	Mated connector pair	FC/PC

loss preceding the EDFA, of ≈14 dB, is practically the same for link input to receiver, transmitter to link output and from link input to link output.

While the path loss within the ROADM is practically around 14 dB the signal degradation due to ASE noise need not be as bad as for a fibre span with a similar loss. In a fibre span the launch power is restricted by the nonlinear interference such that the fibre loss must precede the amplifier. In the case of the ROADM there is limited nonlinearity as the loss is

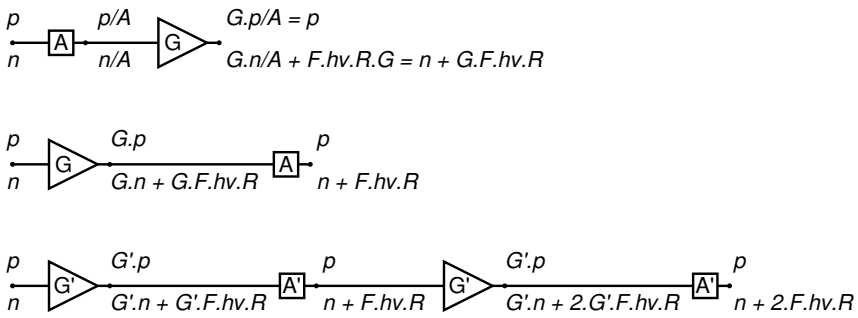

Figure 3.2: The build up of signal power and noise through multiple amplifiers.

mainly due to mismatch within optical components and between fibre and component. Thus the amplifier can precede the ROADM leading to a reduced noise impact since the signal is greater. Figure 3.2 illustrates the different amplifier placement options and the signal power and noise generated. Where the attenuating element is placed before the compensating amplifier the ASE noise is increased by $GF h\nu R$ however if the compensating amplifier is placed before the attenuating element the overall ASE noise is only increased by $F h\nu R$. It can be seen that where the compensating amplifier precedes the attenuating element the output power requirements of the amplifier are larger. That is for signal powers around 1 mW per DWDM channel an amplifier with around 2 W of output power is required to compensate the ROADM. The final option is to split the compensation of the attenuating elements into two reducing the gain of each amplifier and reducing the required output power to ≈ 400 mW at the expense of an increase in ASE noise to $2F h\nu R$. For comparison the noise generated by an EDFA compensating for a 80 km span is $58F h\nu R$. Thus by careful design the ROADM can have negligible impact on the overall quality of signal transmission.

ROADM designs have been advanced such that they are colourless, direction-less and contention-less, CDC. Colourless allows any transceiver module to operate at any desired wavelength and be connected through regardless of its physical connection, direction less allows any transceiver to be connected through to any ROADM port regardless of its physical connection and contention less allows any transceivers operating at the same wavelength to be connected to their respective (different) ports. CDC-ROADMS designs [26, 125] are more complex than the basic design and have a resource pool of transceivers that can be used to add or drop from any port on any wavelength without contention making reconfiguration fully software driven.

Table 3.3: Details of the network topologies tested.

Name	Nodes (N)	Links (L)	Diameter (km)	Avg. Node Degree
DTAG/T-Systems [128]	14	23	1000	3.3
NSF Net [129]	14	21	6000	3.0
Google B4 [130]	12	19	32000	3.2

The basic ROADM design illustrated in figure 3.1 is a broadcast and select ROADM where each input port is broadcast to all of the output ports and the drop port. A wavelength selective switch selects the correct input port for forwarding to the output. In this design the isolation of the wavelength selective switch is critical to block signals from other ports on the same wavelength [126]. An alternative design is to use wavelength selective switches at both the input and output port increasing the isolation but the concatenation of numerous wavelength selective elements leads to a narrowing of the pass band [127] reducing signal quality. In this work the reductions of signal quality due to pass band narrowing and isolation are assumed negligible by careful design of the ROADM and choice of components.

3.8 Realistic Example Mesh Network Topologies

In order to understand the possible capacity gains, through optimisation of the transmitter parameters, alongside the routing and spectral allocation algorithms, a number of realistic example mesh networks were used. The use of optimal routing solvers based on linear programming restricts the size of such networks as the complexity increases rapidly with the number of nodes and the linear programming problem is know to be NP hard. As such the networks topologies chosen were the 14 node, 23 link Germany backbone DTAG/T-systems network [128]; the 14 node, 21 link NSF net [129]; and the 12 node, 19 link Google B4 network [130]. The topologies are shown in figures 3.3, 3.4 and 3.5 and there statistics summarised in table 3.3. It is not know if these networks have ever been operated as transparent wavelength routed optical networks but the topologies are representative of networks with three different scales; country, continental and global.

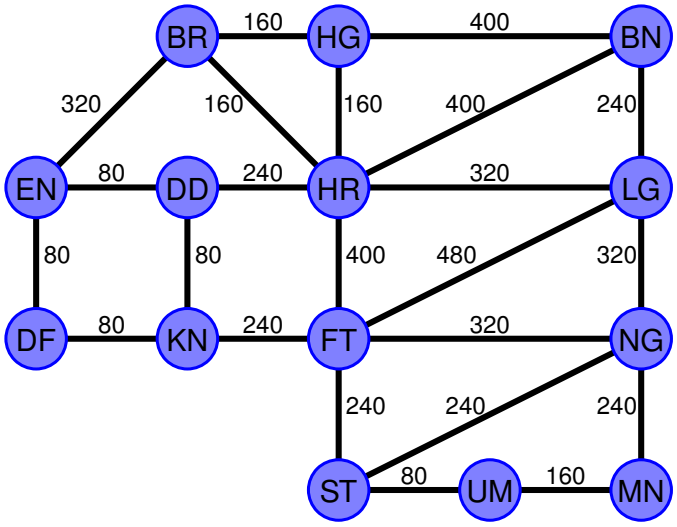

Figure 3.3: Topology of the 14 node, 23 link DTAG/T-systems mesh network showing the fibre link lengths used in km.

The node locations were taken from the references shown and converted to latitude and longitude using online tools. The link lengths, Z (km), were calculated from the great circle distance between the nodes, Z_{GC} (km), using [131]

$$Z = \begin{cases} 1.50Z_{GC}, & Z_{GC} \leq 1000 \text{ km} \\ 1500, & 1000 \text{ km} \leq Z_{GC} \leq 1200 \text{ km} \\ 1.25Z_{GC}, & Z_{GC} \geq 1200 \text{ km} \end{cases} \tag{3.12}$$

where the great circle distance between the nodes was calculated from the latitude and longitude of the nodes using the Haversine formula [132, 133].

$$Z_{GC} = 2R_e \arcsin\left(\sqrt{\sin^2\left(\frac{\phi_1 - \phi_2}{2}\right) + \cos(\phi_1)\cos(\phi_2)\sin^2\left(\frac{\lambda_1 - \lambda_2}{2}\right)}\right) \tag{3.13}$$

where R_e is the radius of the earth taken as 6367 km and ϕ and λ are the latitude and longitude of the nodes. The link lengths were rounded to the nearest 80 km so that all the spans are identical for simplicity. Each link within the network was assumed to consists of a fibre pair with the simulation parameters given in table 3.1.

3.9 Traffic Matrices

In order to understand and optimise the network data throughput a traffic demand matrix is required specifying the demand between each node pair. There is no point provisioning

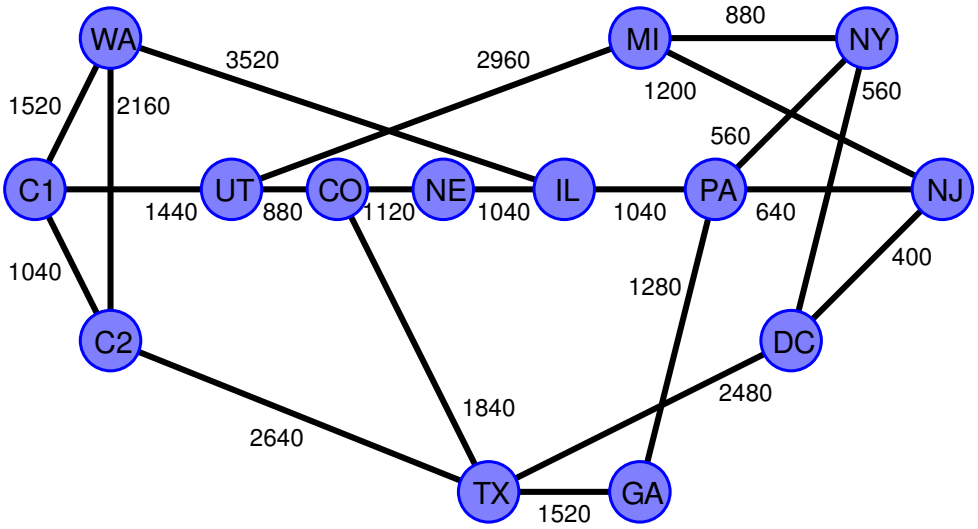

Figure 3.4: Topology of the 14 node, 21 link NSF mesh network showing the fibre link lengths used in km.

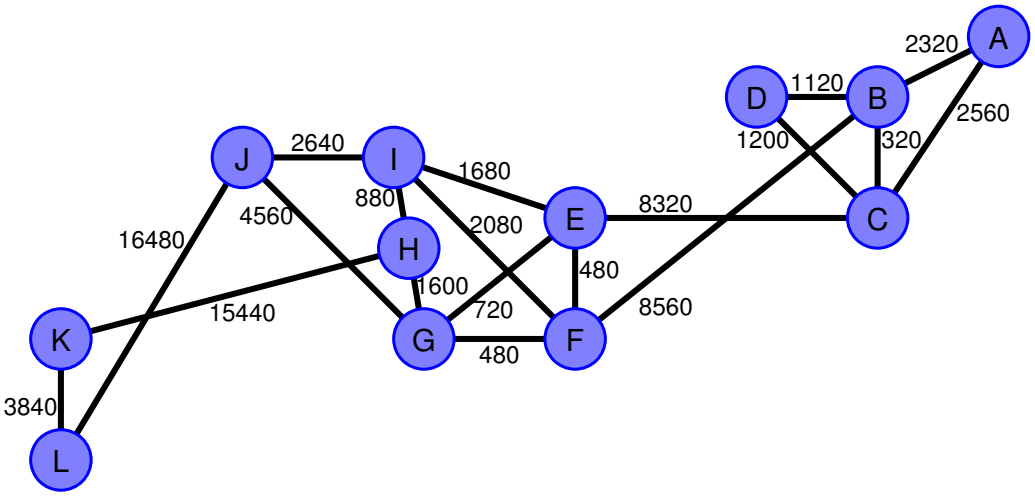

Figure 3.5: Topology of the 12 node, 19 link Google B4 mesh network showing the fibre link lengths used in km.

capacity between nodes if there is no traffic demand between them. The actual traffic matrix is difficult to obtain, even network operators have only basic information like the total ingress and egress at each node or the traffic volume in each link. Thus to obtain the full traffic matrix a model is often used. "Gravity" models have been used in many situations for estimating traffic flow from telephony [134, 135], trade [136] and transport [137]. Such models are based on the product of some source and destination weight and divided by some weight depending on the distance between the source and destinations. Maximum entropy models have been used to estimate traffic matrices where the total link loads were known [138] and where the total ingress and egress from each node was known [92, 139]. The model produces an exponential distance dependence when transport pricing is linearly dependent on the transmission distance. When there is detailed network knowledge of the locations of servers and peering points a service based estimate of traffic can be made [140].

In this work without any prior knowledge the traffic matrix is assumed to be uniform with equal traffic demand between all node pairs. A normalised traffic profile, **T**, is given by

$$T_{s,d} = \begin{cases} \frac{1}{N(N-1)} & s \neq d \\ 0 & s = d \end{cases} \tag{3.14}$$

where N is the total number of nodes in the network. A traffic demand matrix, **D**, is then given by

$$\mathbf{D} = c\,\mathbf{T}, \tag{3.15}$$

where c is a multiplier defining the total network throughput.

One of the metrics of the advantages of the ideas described in this work is the network throughput. Network throughput is here defined through equation (3.15). It is the total client data transported by the network that satisfies the traffic profile. It is the sum of all ingress client data, which is equal to the sum of the egress client data, that satisfies the traffic profile. In the case of uniform traffic as described by equation (3.14) then all the client data flows must be equal to satisfy the traffic profile so the network throughput is equal to the minimum client data flow between any source destination pair taken over all possible source destination pairs multiplied by the number of source destination pairs, $N(N-1)$.

4

Quality of Transmission Model

In this chapter a quality of transmission model suitable for coherent optical networks operating in the dispersion unmanaged weakly nonlinear propagation regime is described that allows the rapid assessment of signal quality in a transmission link. In this work the metric used to describe signal quality is the received symbol SNR. This model should allow the rapid testing and optimisation of the transmitter power and DWDM channel allocation to obtain a symbol SNR suitable for the chosen modulation formats. This chapter is a mixture of background and new work. The adaptation of the GN model to a network context and its simplification to a matrix form along with the detailed assessment of the model errors are the originality of this work.

4.1 Symbol SNR

Consider a digital transmission system, as illustrated in figure 4.1, where a stream of data bits at discrete times are first converted to symbols from a discrete alphabet. These symbols are encoded onto the optical signal through modulation giving a continuous time analogue

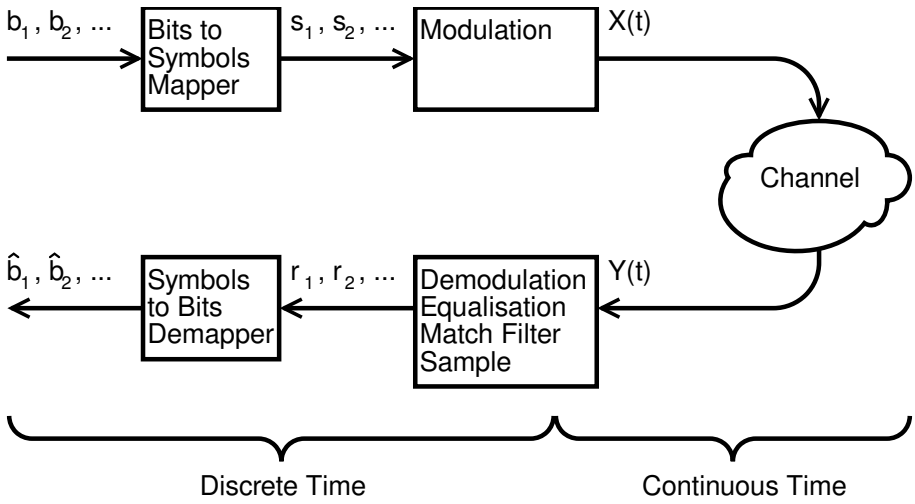

Figure 4.1: Illustration of the elements of a digital transmission link.

waveform that is transmitted across the channel. At the receiver the distorted version of the continuous waveform is demodulated and equalised through DSP. A matched filtered is applied before sampling to get recovered symbols (with noise) at discrete times. The data bits at are then recovered from the symbols.

So the receiver output is a sequence of discrete time measurements, r_i, given by

$$r_i = s_i + e_i \tag{4.1}$$

where s_i is the i^{th} transmitted symbol and e_i is the noise on the i^{th} received symbol. The time average signal power is given by

$$S = \lim_{N\to\infty} \frac{1}{N} \sum_{i=1}^{N} s_i \cdot s_i^* \tag{4.2}$$

where s_i^* represents the complex conjugate of s_i. The time average noise power is given by

$$n = \lim_{N\to\infty} \frac{1}{N} \sum_{i=1}^{N} e_i \cdot e_i^* \tag{4.3}$$

and thus the symbol SNR is define as

$$SNR \triangleq \frac{S}{n}. \tag{4.4}$$

In a well designed balanced coherent optical receiver the optical field is directly transformed by a linear scaling into the digital domain. For white optical noise the receiver matched filter limits the effective noise bandwidth to the symbol rate, R (s^{-1}), such that the symbol noise is given by

$$n \propto N_0 R \tag{4.5}$$

and the symbol signal power is given by

$$S \propto p \tag{4.6}$$

leading to a symbol SNR given by

$$SNR = \frac{p}{N_0 R} = \frac{\varepsilon_s}{N_0} \tag{4.7}$$

where p is the average optical signal power (W), N_0 is the optical noise PSD (W·Hz^{-1}) and ε_s is the optical energy per symbol (J). Both p, ε_s and N_0 are here defined as the totals for both polarisation modes and N_0 is defined as a single sided PSD, such that the power transmitted by a physical optical bandpass filter of width, $\Delta\nu$, is given by $N_0\Delta\nu$ (W).[1]

For a coherent receiver where the noise is limited by ASE noise alone the symbol SNR at the decision circuit depends linearly on the OSNR and the relationship between the symbol SNR and the OSNR is given by

$$SNR = OSNR\frac{B_{ref}}{R} \tag{4.8}$$

where here both SNR and $OSNR$ are in linear units and B_{ref} is the OSNR reference bandwidth usually specified as 0.1 nm such that near 1550 nm $B_{ref} \approx$ 12.5 GHz.

4.2 Dependence of BER on SNR

In this work symbol wise hard decision detection is considered such that an approximation for the BER based only on nearest neighbour errors is given by [142, eq. (2)] derived from [143, eq. (7)]

$$\text{BER} \simeq G_p \frac{N}{\log_2[M]} \frac{1}{2} \text{erfc}\left[\frac{d}{\sqrt{2}\sigma}\right] \tag{4.9}$$

where N is the average number of nearest neighbours, G_p is the Gray penalty (the average number of bit errors per symbol error), M is the size of the symbol alphabet, $2d$ is the Euclidean distance between nearest neighbours and σ^2 is the noise variance on the I or Q signal component.

[1] It should be noted that in many communications texts, for example [141], the noise power spectral density is defined as a double sided spectrum with noise power at both positive and negative frequencies. The noise power spectral density is then defined as $\frac{N_0}{2}$ so that the single sided noise power spectral density is equal to N_0 as defined here.

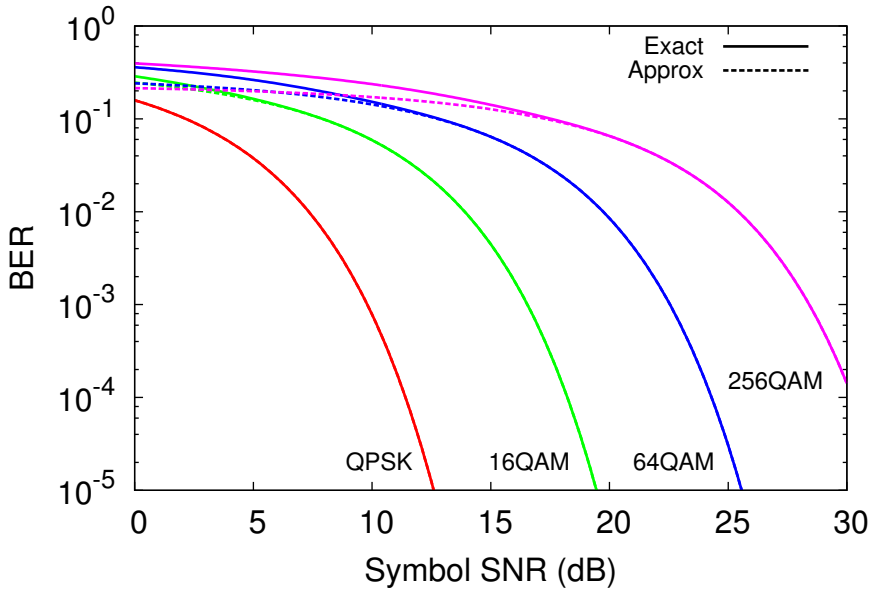

Figure 4.2: BER vs symbol SNR for various formats showing the approximate and exact curves.

The ratio of the nearest neighbouring decision boundary distance, d, to the noise, σ, is related to the symbol SNR ,SNR, by

$$\frac{d^2}{2\sigma^2} = SNR\frac{d^2}{S} \tag{4.10}$$

where S is the mean square symbol, averaged over all symbols and is proportional to the signal power while $2\sigma^2$ is proportional to the noise power with the same constant of proportionality.

The approximation of equation (4.9) can be summarised for all modulation formats as

$$\text{BER} \simeq A \text{ erfc}\left[\sqrt{B\ SNR}\right], \tag{4.11}$$

with the values of A and B for the various PM-mQAM modulation formats given in table 4.1. Figure 4.2 shows the exact [144, eq. (14) & (16)] and approximate values for BER as a function of symbol SNR for square mQAM formats. The approximation is sufficiently accurate for BER less than 0.1.

4.3 Required SNR

Two strengths of FEC will be considered both based on hard decisions. The use of hard decision FEC decouples the FEC from the decision process allowing the use of

Table 4.1: Parameters for the approximate BER expression in equation (4.11).

Format	Bit Loading bit·symbol^{-1}	A	B
PM-BPSK	2	$\frac{1}{2}$ = 0.500	1
PM-QPSK	4	$\frac{1}{2}$ = 0.500	$\frac{1}{2}$
PM-8QAM	6	$\frac{5}{8}$ = 0.625	$\frac{1}{3+\sqrt{3}}$
PM-16QAM	8	$\frac{3}{8}$ = 0.376	$\frac{1}{10}$
PM-32QAM	10	$\frac{1417}{3840}$ = 0.369	$\frac{1}{20}$
PM-64QAM	12	$\frac{7}{24}$ = 0.292	$\frac{1}{42}$
PM-128QAM	14	$\frac{11861}{43008}$ = 0.276	$\frac{1}{82}$
PM-256QAM	16	$\frac{15}{64}$ = 0.234	$\frac{1}{170}$
PM-512QAM	18	$\frac{96685}{442368}$ = 0.219	$\frac{1}{330}$
PM-1024QAM	20	$\frac{31}{160}$ = 0.194	$\frac{1}{682}$

equation (4.11) to estimate the pre-FEC BER and the valid assumption that provided the pre-FEC BER is below some threshold the FEC can deliver error free performance.

The performance of FEC is often specified by a net coding gain. The net coding gain, *NCG*, is given by [145]

$$NCG = QdB_{10^{-15}} - QdB_{preFEC} + 10\log_{10}[r_c] \tag{4.12}$$

where $QdB_{10^{-15}}$ = 18 dB is the signal Q for a BER of 10^{-15}, QdB_{preFEC} is the required FEC decoder input Q in dB to achieve an output BER of 10^{-15} and r_c is the coding rate. The signal Q in dB is given by

$$QdB = 20\log_{10}\left[\sqrt{2}\,\text{inverfc}(2\,\text{BER})\right] \tag{4.13}$$

where inverfc$(\cdot)$ is the inverse complimentary error function defined by the inverse of equation (3.7).

Two implemented continuously interleaved BCH codes with capability to correct four errors were considered [146–148]. These give net coding gains of 9.35 dB and 10.5 dB for 6.7 % and 20 % FEC overhead. When a 5 % overhead is added for OTU framing these are suitable for 28 GBaud and 32 GBaud transmission giving an error free client symbol rate of 25 GBaud.

Table 4.2: Symbol SNR requirements for various formats and preFEC BER, (dB)

Format	Bit Loading	Required SNR (dB) for a pre-FEC BER	
	bit·symbol^{-1}	0.004	0.015
PM-BPSK	2	5.46	3.72
PM-QPSK	4	8.47	6.73
PM-8QAM	6	12.45	10.81
PM-16QAM	8	15.13	13.24
PM-32QAM	10	18.12	16.22
PM-64QAM	12	21.06	19.01
PM-128QAM	14	23.89	21.81
PM-256QAM	16	26.84	24.65
PM-512QAM	18	29.63	27.38
PM-1024QAM	20	32.62	30.27

The net coding gains allow a pre-FEC BER of 0.004 and 0.015 respectively for the 6.7 % and 20 % FEC OH. Table 4.2 give the required symbol SNR in dB for each modulation format for the two required pre-FEC BERs.

4.4 The Quality of Transmission Model

In this work we consider optical transmission in the modern high dispersion paradigm utilising the latest coherent technology. That is the transmission fibres have high chromatic dispersion that is uncompensated in the line except at the receiver and/or the transmitter. The transmitted signals are assumed to be polarisation multiplexed such that the transmitted signal appears to be, on average, depolarised with equal average power in the two orthogonal polarisation modes.

It is assumed that the transmitter and receiver are well designed such that the only significant source of stochastic noise is ASE noise from the optical amplifiers in the links. It is further assume that all the linear transmission impairments are compensated in the receiver DSP, that the receiver bandwidth does not impact signal distortion, and the ROADM are designed with components with sufficient isolation and bandwidth to avoid signal degradation and crosstalk. The nonlinear transmission impairments caused by

photon-phonon interactions within the transmission medium are neglected as the signals are broadband reducing Brillouin scattering and contained within the c-band avoiding stimulated Raman gain. Thus it is assumed that the symbol SNR is limited by ASE noise and nonlinear interference through the third order electric susceptibility, the Kerr effect.

ASE noise is a source of additive Gaussian noise and will also be assumed to be white in nature. For an uncompensated link the nonlinear interference between DWDM channels caused by the Kerr effect has been shown to manifests itself as a source of additive Gaussian noise [149–154]. The Gaussianity of the nonlinear interference is a foundation of the Gaussian noise model and occurs as a result of the accumulated dispersion in uncompensated transmission systems. The dispersion acts in two important ways. First it causes the original transmitted signals to disperse, causing inter-symbol interference that gives the time domain waveform of the signal a pseudo Gaussian distribution, making the transmitted signals appear like Gaussian distributed noise. Secondly the nonlinearity causes an instantaneous nonlinear phase noise which is converted to a circular symmetric Gaussian noise by the dispersion in the onward transmission. At the receiver, the transmission path dispersion is compensated returning the signal to its undistorted constellation, but the nonlinear phase noise is generated along the link such that besides noise generated near the transmitter this noise will be overcompensated at the receiver leaving residual dispersion that distributes the noise as a circular Gaussian field on the IQ plane. Thus, it is anticipated that for short links with limited chromatic dispersion the Gaussian model will fail with both incorrect noise power and also a non circular symmetric Gaussian distributed noise.

Under the Gaussian noise model it is assumed the nonlinear interference is Gaussian noise and combines incoherently with the additive white Gaussian noise due to ASE. The symbol SNR, SNR_i, of the i^{th} DWDM channel is given by

$$SNR_i = \frac{p_i}{n_{ASE,i} + n_{NLI,i}} \tag{4.14}$$

where p_i is the received signal power, $n_{ASE,i}$ is the ASE noise power and $n_{NLI,i}$ is the nonlinear interference noise power, all within the receiver matched filter bandwidth, of the i^{th} DWDM channel. It is assumed that the ASE noise is a source of AWGN and that the symbol rate is constant such that $n_{ASE,i} = n_{ASE}$ is independent of the channel number. The transmission loss is fully compensated by EDFAs so that the received signal power is

equal to the transmitter launch power and the ASE noise power is given by

$$n_{ASE} = 10^{\frac{NF}{10}} h\nu R \sum_{k} \left(10^{\frac{A_k}{10}}\right) \tag{4.15}$$

where the summation, k, is taken over all EDFAs in the optical path, NF is the amplifier noise figure (dB), h is Planck's constant (6.626×10^{-34} J·s), ν is the channel optical carrier frequency (193.5 THz), R is the symbol rate (Baud) and A_k are the individual transmission losses (dB) between the $(k-1)^{\text{th}}$ and k^{th} EDFA. The transmission losses A_k can include the fibre span losses and ROADM losses.

The nonlinear interference noise can be identified as SPM for nonlinear interference caused solely within the i^{th} channel, XPM for interference on the i^{th} channel caused by signals in the j^{th} channel and FWM for interference caused by signals in multiple channels. It is assumed the nonlinear interference noise due to FWM can be ignored as insignificant [118] and that the signal channels are well spaced to avoid the nonlinear interference noise generated on one channel spreading into the matched filter of neighbouring channels. The nonlinear interference noise due to SPM and XPM can be written as [34, 45]

$$n_{NLI,i} = p_i \sum_{j} X_{i,j} p_j^2 \tag{4.16}$$

where p are the channel launch powers and the summation j is over all co-propagating channels, $X_{i,j}$ is a nonlinear efficiency factor accumulated over the light path. $X_{i,j\neq i}$ is a XPM factor and $X_{i,i}$ is a SPM factor. Similar nonlinear interference noise models have been subsequently published in the literature [35, 36].

4.5 The Gaussian Noise Model

The GN, model is often attributed to the group at Politecnico di Torino [41] but has origins that are older, see e.g. [117–120] and has been independently suggested by other authors, e.g. [155]. The GN model is a perturbation model and assumes that the nonlinear Kerr effect produces a Gaussian distributed noise like interference. This interference is a summation of all the four wave mixing products generated from combinations of spectral components from across the transmitted spectrum. The key result is a noise spectral density that depends on a double integral across the signal spectrum and has been derived in several ways by a number of authors, see e.g. [119, 152, 155–159]. In this work with ideal compensation of the span loss after each span using lumped amplifiers, ignoring higher

order dispersion and assuming identical spans, the GN model reference equation [41, eq. (1)] can be written as

$$G_{NLI}(f) = \frac{16}{27}\gamma^2 \int_{-\infty}^{\infty}\int_{-\infty}^{\infty} G(f_1)G(f_2)G(f_1+f_2-f)\rho(f_1,f_2,f)\chi(f_1,f_2,f)\,\mathrm{d}f_1\,\mathrm{d}f_2. \tag{4.17}$$

where $G_{NLI}(f)$ is the nonlinear interference noise power spectral density (W.Hz^{-1}) generated at frequency, f (Hz), $G(f)$ is the signal power spectral density (W·Hz^{-1}) at frequency, f (Hz), γ is the nonlinear coefficient (W^{-1}·km^{-1}), ρ and χ are the "four wave mixing factor" and "phased-array factor" respectively. ρ is given by

$$\rho(f_1,f_2,f) = \frac{1+e^{-2L_s\alpha}-2e^{-L_s\alpha}\cos\left[4\pi^2\beta_2\left(f_1-f\right)\left(f_2-f\right)L_s\right]}{\alpha^2+\left[4\pi^2\beta_2\left(f_1-f\right)\left(f_2-f\right)\right]^2} \tag{4.18}$$

where L_s is the span length (km), α is the fibre attenuation coefficient (km^{-1})[2] and β_2 is the chromatic dispersion coefficient (s^2·km^{-1}). The "phased-array factor" accounts for the summation of NLI generated by multiple spans and is given by χ as

$$\chi(f_1,f_2,f) = \frac{\sin^2\left[2\pi^2\left(f_1-f\right)\left(f_2-f\right)\beta_2 L_s N_s\right]}{\sin^2\left[2\pi^2\left(f_1-f\right)\left(f_2-f\right)\beta_2 L_s\right]} \tag{4.19}$$

where N_s is the number of concatenated spans.

One of the key advantages of the GN model is that the nonlinear interference noise spectrum is independent of the modulation format. This allows a decoupling of the quality of transmission from the choice of modulation format which greatly simplifies any modulation format optimisation process. There is some debate about the validity of the GN model in particular it has been shown that the nonlinear interference can depend on the modulation format [160, 161] although for engineering purposes the difference is small. A further discussion of this is included in section 4.9.

4.6 The Nonlinear Interference Efficiency Factor

The nonlinear interference efficiency factor, $X_{i,j}$, describes the strength of the interference on the i^{th} channel caused by the j^{th} channel and depends on the frequency spacing between channels i and j, the spectral shape of the channels, their symbol rates and the linear and nonlinear transmission properties of the optical fibre. For similar channels on a fixed

[2]It should be noted that the attenuation here refers to the more usual power attenuation and is thus twice that used in [41]

regularly spaced frequency grid $X_{i,j}$ is a function of $|i-j|$. It is independent of the exact modulation format subject to the general assumption of it being a polarization multiplexed coherent transmission. The efficiency factor $X_{i,j}$ was calculated by numerical integration of the GN model reference equation (4.17).

Consider just two DWDM channels with the same spectral shapes, such that the signal spectrum can be written as $G(f) = p_0 g(f) + p_1 g(f-\Delta f)$ where p_0 is the launch power in the data channel, p_1 is the launch power in the interfering channel, $g(f)$ is the spectral shape of the channel normalised such that $\int_{-\infty}^{\infty} g(f)df = 1$ and Δf is the channel separation. $g(f)$ is centred around $f = 0$ and assumed to fall entirely within a single DWDM channel. For the two DWDM channel case the multiplication of the three PSD terms in the double integral of equation (4.17) gives eight cross terms. Expanding equation (4.17) gives,

$$\begin{aligned}
G_{NLI}(f) \quad = \quad & p_0^3 \frac{16}{27}\gamma^2 \int_{-\infty}^{\infty}\int_{-\infty}^{\infty} g(f_1)g(f_2)g(f_1+f_2-f)\rho(f_1,f_2,f)\chi(f_1,f_2,f)\mathrm{d}f_1\mathrm{d}f_2 \\
& + p_0\, p_1^2 \frac{16}{27}\gamma^2 \int_{-\infty}^{\infty}\int_{-\infty}^{\infty} g(f_1-\Delta f)g(f_2)g(f_1+f_2-f-\Delta f)\rho(f_1,f_2,f)\chi(f_1,f_2,f)\mathrm{d}f_1\mathrm{d}f_2 \\
& + p_0\, p_1^2 \frac{16}{27}\gamma^2 \int_{-\infty}^{\infty}\int_{-\infty}^{\infty} g(f_1)g(f_2-\Delta f)g(f_1+f_2-f-\Delta f)\rho(f_1,f_2,f)\chi(f_1,f_2,f)\mathrm{d}f_1\mathrm{d}f_2 \\
& + p_0\, p_1^2 \frac{16}{27}\gamma^2 \int_{-\infty}^{\infty}\int_{-\infty}^{\infty} g(f_1-\Delta f)g(f_2-\Delta f)g(f_1+f_2-f)\rho(f_1,f_2,f)\chi(f_1,f_2,f)\mathrm{d}f_1\mathrm{d}f_2 \\
& + p_0^2\, p_1 \frac{16}{27}\gamma^2 \int_{-\infty}^{\infty}\int_{-\infty}^{\infty} g(f_1-\Delta f)g(f_2)g(f_1+f_2-f)\rho(f_1,f_2,f)\chi(f_1,f_2,f)\mathrm{d}f_1\mathrm{d}f_2 \\
& + p_0^2\, p_1 \frac{16}{27}\gamma^2 \int_{-\infty}^{\infty}\int_{-\infty}^{\infty} g(f_1)g(f_2-\Delta f)g(f_1+f_2-f)\rho(f_1,f_2,f)\chi(f_1,f_2,f)\mathrm{d}f_1\mathrm{d}f_2 \\
& + p_0^2\, p_1 \frac{16}{27}\gamma^2 \int_{-\infty}^{\infty}\int_{-\infty}^{\infty} g(f_1)g(f_2)g(f_1+f_2-f-\Delta f)\rho(f_1,f_2,f)\chi(f_1,f_2,f)\mathrm{d}f_1\mathrm{d}f_2 \\
& + p_1^3 \frac{16}{27}\gamma^2 \int_{-\infty}^{\infty}\int_{-\infty}^{\infty} g(f_1-\Delta f)g(f_2-\Delta f)g(f_1+f_2-f-\Delta f)\rho(f_1,f_2,f)\chi(f_1,f_2,f)\mathrm{d}f_1\mathrm{d}f_2
\end{aligned} \tag{4.20}$$

Given that $g(f)$ is only significant around $f = 0$ then the eight noise terms are generated around different frequencies. The first term generates interference around $f = 0$ and is SPM on the data channel. The second and third terms generate interference around $f = 0$ and are XPM caused by the interfering channel on the data channel. The fourth term generate interference around $f = 2\Delta f$ and is a traditional FWM term. The fifth and sixth terms generate interference around $f = \Delta f$ and are XPM caused by the data channel on the interfering channel. The seventh term gernerates interference around $f = -\Delta f$ and is another FWM term. The final eighth term generates interference around $f = \Delta f$ and is SPM on the interfering channel. Therefore only three of these terms produce interference noise within the data channel bandwidth, a single SPM term and two degenerate XPM

terms. Thus the NLI PSD due to XPM, G_{XPM}, is given by

$$G_{XPM}(f) = 2\frac{16}{27}\gamma^2 p_0 p_1^2 \int_{-\infty}^{\infty}\int_{-\infty}^{\infty} g(f_1-\Delta f)g(f_2)g(f_1-\Delta f+f_2-f) \rho(f_1,f_2,f)\chi(f_1,f_2,f)\,\mathrm{d}f_1\,\mathrm{d}f_2 \quad (4.21)$$

and that due to SPM is half this with $p_1 = p_0$ and Δf set to zero.

This noise spectral power density will be filtered in the coherent receiver by a matching filter to maximise the SNR. Provided the overall noise is dominated by AWGN, caused by ASE, the matching filter is given by $H(f) = Rg(f)$. Combining equations (4.18) , (4.21) and apply the match filter, for a single span the nonlinear interference noise due to XPM, $n_{XPM,ss}$ can be written as

$$n_{XPM,ss} = p_0\, p_1^2 X_{0,1,ss} = p_0\, p_1^2 \frac{32}{27}\gamma^2 R\cdot \int_{-\infty}^{\infty}\int_{-\infty}^{\infty}\int_{-\infty}^{\infty} \frac{1+e^{-2L_s\alpha}-2e^{-L_s\alpha}\cos\left[4\pi^2\beta_2(f_1+\Delta f-f)(f_2-f)L_s\right]}{\alpha^2+\left[4\pi^2\beta_2(f_1+\Delta f-f)(f_2-f)\right]^2} \cdot g(f_1)\,g(f_2)\,g(f_1+f_2-f)\,g(f)\,\mathrm{d}f_1\,\mathrm{d}f_2\,\mathrm{d}f. \quad (4.22)$$

Similarly for SPM, $n_{SPM,ss}$ is given by

$$n_{SPM,ss} = p_0^3 X_{0,0,ss} = p_0^3 \frac{16}{27}\gamma^2 R\cdot \int_{-\infty}^{\infty}\int_{-\infty}^{\infty}\int_{-\infty}^{\infty} \frac{1+e^{-2L_s\alpha}-2e^{-L_s\alpha}\cos[4\pi^2\beta_2(f_1-f)(f_2-f)L_s]}{\alpha^2+[4\pi^2\beta_2(f_1-f)(f_2-f)]^2} \cdot g(f_1)\,g(f_2)\,g(f_1+f_2-f)\,g(f)\,\mathrm{d}f_1\,\mathrm{d}f_2\,\mathrm{d}f. \quad (4.23)$$

The values of the nonlinear interference efficiency factor, $X(\Delta f)$, were calculated by numerical integration of equations (4.22) or (4.23). Note in the earlier paper [162] a change of variables was applied to integrate over a frequency space where the four wave mixing factor ρ was fixed as this proved more reliable for the numerical integration routine in Mathematica®. More recently the numerical integral has been calculated using a Monte Carlo integration routine in Matlab® and having the power spectral density function, $g(f)$, fixed in frequency space, as shown here, has proved more useful. The Monte Carlo method randomly samples the integrand such that the mean of the samples gives the integral and the variance of the samples allows an estimation of the uncertainty of the integral. The number of samples was increased until the uncertainty of the integral was less than 10^{-4} of the integral, an error of less than 0.001 dB. Both the Mathematica® and the MATLAB® Monte Carlo approaches gave numerically equal results.

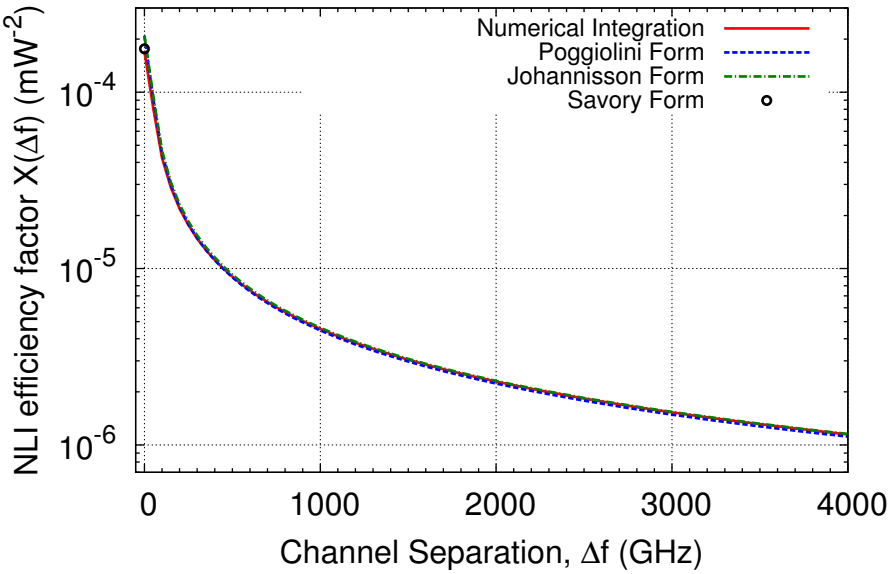

Figure 4.3: The NLI efficiency factor for SPM and XPM as a function of channel spacing Δf. Note $\Delta f = 0$ refers to SPM. Single span of length 80 km with fibre parameters as in table 3.1

The red curve in figure 4.3 shows the numerically integrated values of the NLI efficiency factor as a function of the channel separation. It clearly shows how the nonlinear interference reduces as the channel separation increases and is approximately $\propto {}^{1}/_{\Delta f}$ for large Δf. The transmission fibre properties used are given in table 3.1.

Also shown for comparison in figure 4.3 are values of the nonlinear interference efficiency factor calculated using closed form solutions published in the literature [35, 36, 163]. Figure 4.4 shows the difference between the closed form solutions and the numerical integrated values used in this thesis. The differences occur for a number of reasons. The closed form solutions of Poggiolini and Johannisson both assume the NLI noise is uniform across the signal and equal to that at the signal centre, this is a worst case assumption for SPM. The span length dependence of $\left(1-e^{-\alpha L_s}\right)^2$ is incorrect for large channel separations, as it tends towards $\left(1-e^{-2\alpha L_s}\right)$, leading to an underestimate of the NLI efficiency factor by approximately 0.16 dB.

For completeness, the closed form solutions of Poggiolini et al. [35], Johannisson et al. [36] and Savory [163] are given below where these have been transposed to keep notational consistency with this thesis. Poggiolini et al. have an XPM efficiency described

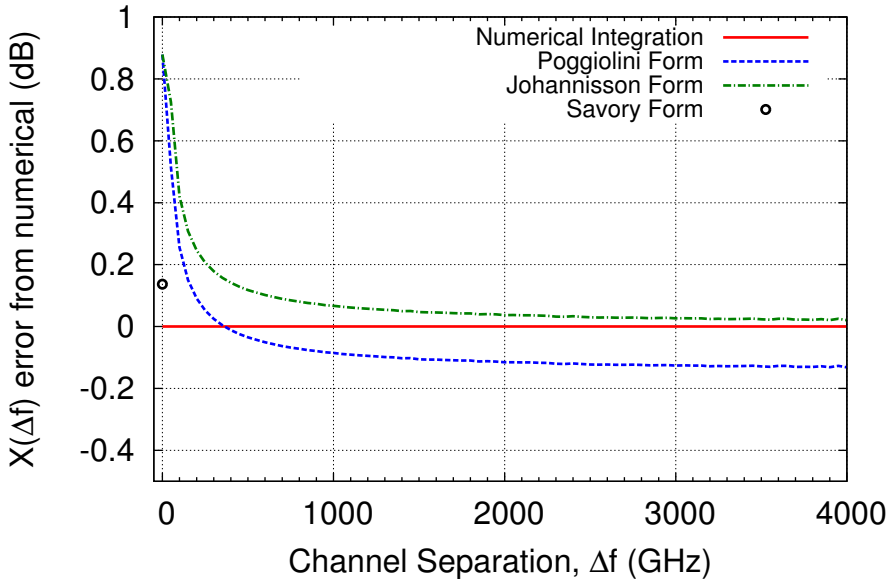

Figure 4.4: The ratio between different closed form solutions for the NLI efficiency factor for SPM and XPM and the numerical integrated value. Note $\Delta f = 0$ refers to SPM. Span length 80 km with fibre parameters as in table 3.1

by [35, eq. (41) & (42)]

$$X_{ss}(\Delta f) = \frac{32}{27}\frac{\gamma^2\left(1-e^{-\alpha L_s}\right)^2}{4\pi\alpha\beta_2 R^2}\left(\operatorname{asinh}\left[\frac{\pi^2\beta_2}{\alpha}(\Delta f+\tfrac{R}{2})R\right]-\operatorname{asinh}\left[\frac{\pi^2\beta_2}{\alpha}(\Delta f-\tfrac{R}{2})R\right]\right) \tag{4.24}$$

and SPM efficiency described by [35, eq. (41) & (43)]

$$X_{ss}(0) = \frac{32}{27}\frac{\gamma^2\left(1-e^{-\alpha L_s}\right)^2}{4\pi\alpha\beta_2 R^2}\operatorname{asinh}\left[\frac{\pi^2\beta_2}{2\alpha}R^2\right]. \tag{4.25}$$

Johannisson uses an XPM efficiency described by [36, eq. (16)]

$$X_{ss}(\Delta f) = \frac{32}{27}\frac{\gamma^2}{4\pi\alpha\beta_2 R^2}\log_e\left(\frac{\Delta f+\frac{R}{2}}{\Delta f-\frac{R}{2}}\right) \tag{4.26}$$

and SPM efficiency described by [36, eq. (16)]

$$X_{ss}(0) = \frac{32}{27}\frac{\gamma^2}{4\pi\alpha\beta_2 R^2}\log_e\left|\frac{\pi^2\beta_2}{\alpha}R^2\right|. \tag{4.27}$$

Finally, Savory defines a SPM efficiency by [163, eq. (12)] as

$$X_{ss}(0) = \frac{32}{27}\frac{\gamma^2\left(1-e^{-\alpha L_s}\right)^2}{4\pi\alpha\beta_2 R^2}\frac{2}{\pi}\mathrm{Ti}_2\left(\frac{2\pi^2|\beta_2|}{3\alpha}R^2\right) \tag{4.28}$$

where $\mathrm{Ti}_2(x)$ is the inverse tangent integral defined by

$$\mathrm{Ti}_2(\mathrm{x}) = \int_0^{\mathrm{x}}\frac{\operatorname{atan}(\mathrm{u})}{\mathrm{u}}\mathrm{du} \tag{4.29}$$

and can be approximated by the following piecewise function as [163, eq. (17)]

$$Z = \begin{cases} x - \left(\frac{x}{2.1962}\right)^3 + \left(\frac{x}{2.4313}\right)^5, & x \leq 1.533 \\ \frac{\pi}{2}\log_e(x) + \frac{1}{x} - \frac{1}{9x^3}, & x > 1.533 \end{cases}. \tag{4.30}$$

The incoherent GN model assumes that the noise from multiple spans add incoherently, such that the NLI from N_S spans would be $n_{NLI} = n_{NLI,ss}\, N_S$. From a network perspective this would be a useful assumption as it is only required to know the number of spans over which signals interfere and not if they are consecutive. It is possible two signals could co-propagate, diverge and then latter re-converge and co-propagate again. The coherent extension to the GN model [164] provides a better approximation of the NLI, n_{NLI}, from N_s spans as,

$$n_{NLI} = n_{NLI,ss} N_s^{1+\varepsilon} \tag{4.31}$$

where ε is a small number. The NLI noise was calculated by numerical integration of equation (4.17) for a single span and for 100 spans and the ε factor calculated using,

$$\varepsilon = \frac{\log(n_{NLI,100}) - \log(n_{NLI,1})}{\log(100)} - 1. \tag{4.32}$$

Figure 4.5 shows the ε factor as a function of channel separation for the SPM and XPM interference. It can be seen that the ε factor drops rapidly with channel separation and can be considered 0 except for the case of SPM. Thus it is considered suitable to use the following approximation for multiple spans,

$$X_{i,j} = \begin{cases} X_{i,i,ss} N_s^{1+\varepsilon}, & i = j \\ X_{i,j,ss} N_s, & i \neq j \end{cases}. \tag{4.33}$$

Figure 4.6 shows the nonlinear interference noise as a function of the number of spans calculated by numerical integration and also the noise based on the incoherent assumption. It shows that for the XPM interference the incoherent model leads to small errors of less than 0.13 dB for the closest channel separation at the largest distance but there are large errors for the SPM interference. Also show on figure 4.6 is the SPM interference noise for the coherent GN model with ε=0.2186 which reduces the error to less than 0.6 dB in the range 1 to 500 spans (80 to 40000 km).

4.7 Check of the Model Assumptions

During the derivation of the quality of transmission model described in section 4.4 a number of assumptions were made that should be confirmed.

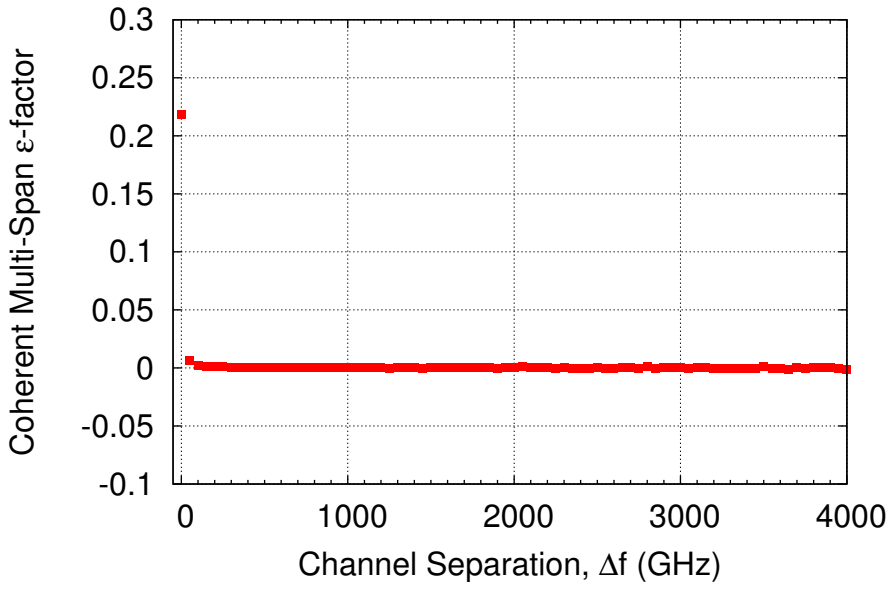

Figure 4.5: The ε coherence factor as a function of the channel separation.

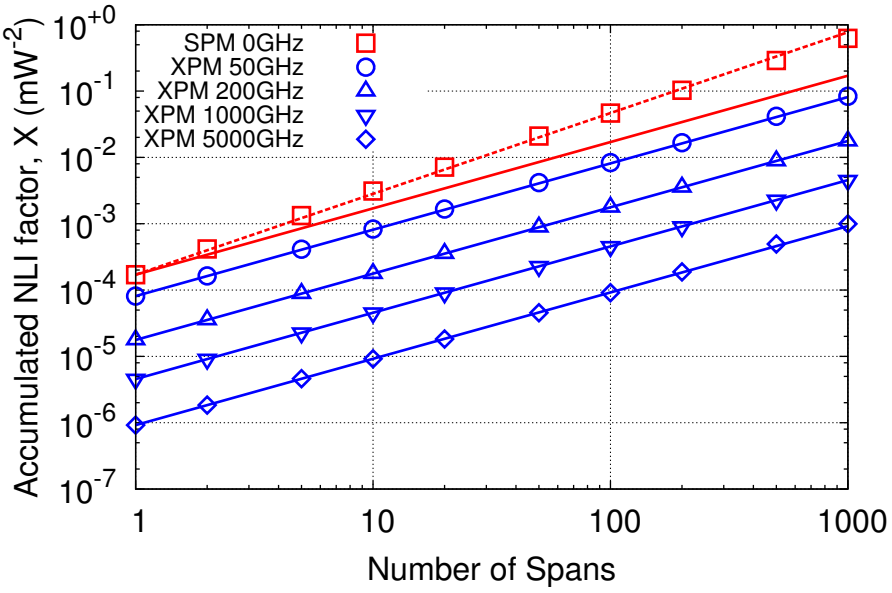

Figure 4.6: The nonlinear interference efficiency factor as a function of the number of spans. Symbols show exact numerical integration with solid lines the incoherent model and dashed lines the coherent model (for SPM only).

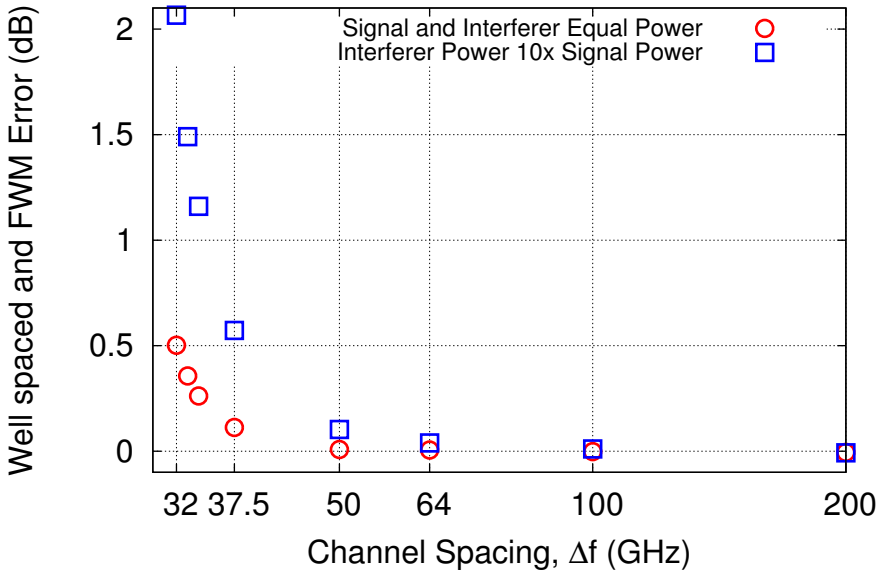

Figure 4.7: Error between the total NLI and that caused by SPM and XPM alone shown as a function of channel spacing for equal launch powers and the worst case where interferes have 10 times more power.

It was assumed that the channels were well spaced and that FWM was insignificant. This assumptions is needed to reduce the NLI noise calculation to a single summation across the DWDM channels. Poggiolini et al. [35] states that the channels must be spaced by more than 1.5 times the channel bandwidth. This is only true for the calculation of noise generated at the channel centre and this needs to be expanded to 2 times the channel bandwidth to avoid all noise generated within the match filter bandwidth. In reality the "four wave mixing factor", $\rho(f_1, f_2, f)$, of equation (4.18) reduces the bandwidth over which significant noise is generated such that much smaller guard bands may be acceptable. To assess the error caused by these two assumptions, well spaced channels and negligible FWM, the nonlinear interference noise on a central channel of an 80 channel DWDM system was calculated by both numerical integration of the full c-band spectrum and through equation (4.16). Figure 4.7 shows the error in (dB) between the full nonlinear interference and that caused by SPM and XPM alone as a function of the channel spacing where all the channels have equal power and the worst case where the interfering channels have 10 times more power than the central signal channel. It shows that errors of just over 2 dB exist if the channels are spaced by their bandwidth and the interferes have 10 times more power but the error drops to ≈0.1 dB when the channels are spaced by 50 GHz or more.

There is also the assumption in section 4.6 that the noise is white and that the matched filter is thus shaped like the signal spectrum. Following the tutorial of Turin [165] the ideal matched filter in the presence of white noise $H(f) = kS(f)^*$ where k is a complex constant and $S(f)$ is the signal field spectrum. The filtered signal power is given by

$$\left| \int_{-\infty}^{\infty} S(f)H(f)\mathrm{d}f \right|^2 \tag{4.34}$$

and the filtered noise power by

$$\int_{-\infty}^{\infty} N(f)\,|H(f)|^2\,\mathrm{d}f \tag{4.35}$$

where $N(f)$ is the noise power spectral density and the square can be brought inside the integral since the spectral components of the noise are independent and uncorrelated. Choosing k such that $\int_{-\infty}^{\infty} |H(f)|^2\,\mathrm{d}f = R$ where R is the symbol rate normalises the filter such that the average filtered signal power is equal to the average signal power. In the case of signals using Nyquist sinc shaped pulses $H(f) = 1$ for $|f| < \frac{R}{2}, 0$ elsewhere.

In the case where the noise is coloured the matched filter can be found by first whitening the noise by applying a whitening filter $H_w(f)$ such that $|H_w(f)|^2 = \frac{1}{N(f)}$ and then matching the whitened signal such that matching filter is given by $H(f) = kH_w(f)^* S(f)^*$. For the case of signals using Nyquist sinc shaped pulses all the signal frequency components are independent and uncorrelated so the filtered signal power can be written

$$\int_{-\infty}^{\infty} G(f)\,|H_w(f)|^2\,|H(f)|^2\,\mathrm{d}f = pk\int_{-\infty}^{\infty} g(f)\frac{g(f)}{N(f)^2}\mathrm{d}f \tag{4.36}$$

where the substitution $G(f) = p \cdot g(f)$ has been used from section 4.6. For the case of signals with spectra wider than the symbol rate the correlation between $S(f)$ and $S(f+R)$ will need to be taken into account. Choosing k such that the average filtered signal power is equal to the average signal power gives a normalising factor k of

$$\frac{1}{k} = \int_{-\infty}^{\infty} \frac{g(f)^2}{N(f)^2}\mathrm{d}f \tag{4.37}$$

and thus the filtered noise power is given by

$$n = k\int_{-\infty}^{\infty} N(f)\frac{g(f)}{N(f)^2}\mathrm{d}f = \frac{\int_{-\infty}^{\infty} \frac{g(f)}{N(f)}\mathrm{d}f}{\int_{-\infty}^{\infty} \frac{g(f)^2}{N(f)^2}\mathrm{d}f}. \tag{4.38}$$

Remembering in the case of signals using Nyquist sinc shaped pulses $g(f) = \frac{1}{R}$ for $|f| < \frac{R}{2}, 0$ elsewhere and substituting into equation (4.38) gives the ideal matched filtered

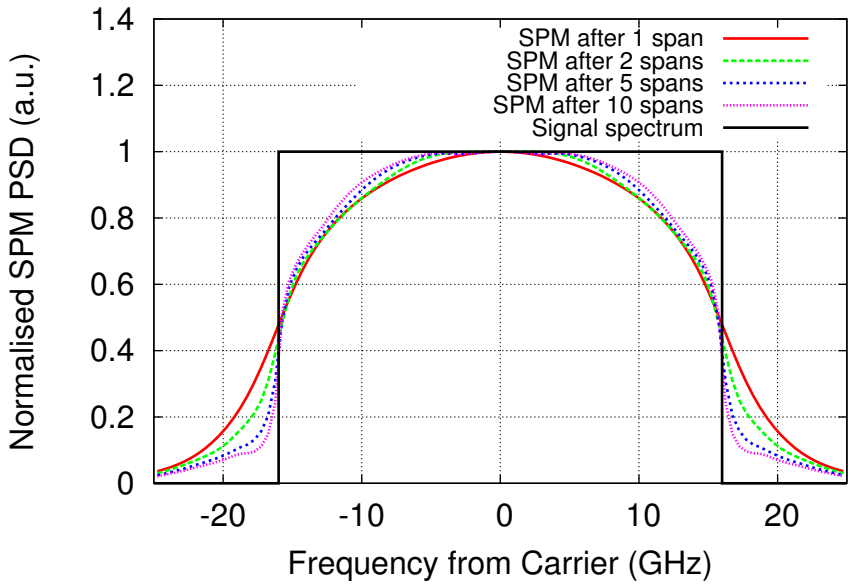

Figure 4.8: Nonlinear interference spectrum for SPM, normalised to f=0 for transmission through 1,2,5 and 10 spans.

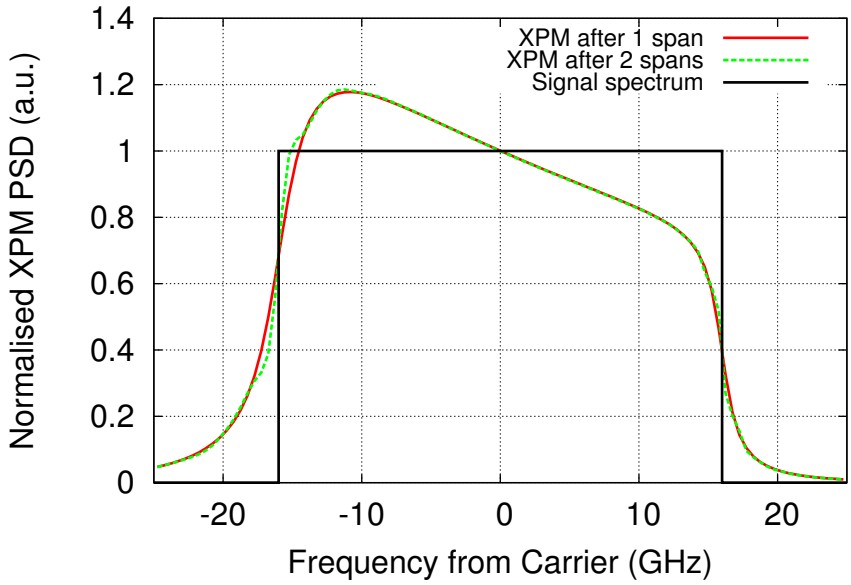

Figure 4.9: Nonlinear interference spectrum for XPM from an interfering channel separated by 50 GHz, normalised to f=0 for transmission through 1 and 2 spans.

noise power, n, as

$$n = R\frac{\int_{-\frac{R}{2}}^{\frac{R}{2}} \frac{1}{N(f)}\mathrm{d}f}{\int_{-\frac{R}{2}}^{\frac{R}{2}} \frac{1}{N(f)^2}\mathrm{d}f}. \tag{4.39}$$

In order to assess the error due to the incorrect matched filter the actual nonlinear

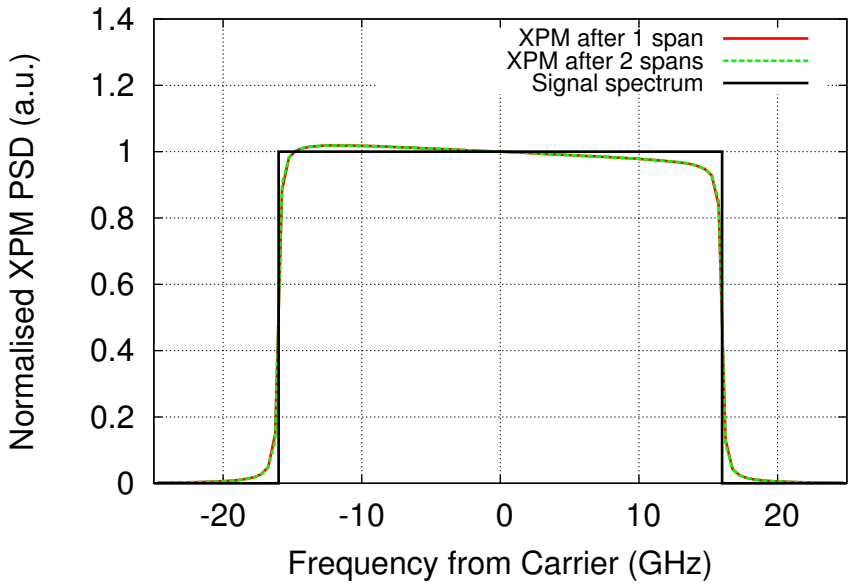

Figure 4.10: Nonlinear interference spectrum for XPM from an interfering channel separated by 500 GHz, normalised to f=0 for transmission through 1 and 2 spans.

interference noise shape was calculated by numerical integration of equation (4.17) and the noise calculated for the incorrectly assumed and actual match filter response. Figure 4.8, 4.9 and 4.10 show the NLI noise spectrum for SPM, XPM for a channel separation of 50 GHz and XPM for a channel separation of 500GHz respectively. It can be seen that the NLI noise spectrum becomes flatter across the signal spectrum as the number of spans increases and as the separation between the signal and interfering channel increases. The reduction in NLI noise when using the ideal matched filter as compared to a filter following the transmitted signal spectrum was calculated and is shown in Table 4.3. The results show that an improvement in NLI noise of less than 0.4 dB can be obtained, however when white ASE noise equal to twice the peak NLI is included this improvement is reduced to $<$0.03 dB strongly suggesting that in the operating network the error from the incorrect matched filter assumption is small.

The NLI noise generated by the Kerr effect appears as a phase noise at the point of generation and it is the effect of uncompensated dispersion that circularises this noise on the IQ plane. How many spans need to be traversed before the NLI noise can be approximated by a circular symmetric Gaussian noise field? A split step time domain simulation of 7 DWDM channels of 32 Gbaud PM-QPSK on a 50 GHz grid transmitted through 1 to 20 spans was carried out, after each span the signal was restored to its

Table 4.3: Noise improvement through ideal matched filter compared to filter following the transmitted signal spectrum.

Nonlinear Interference	Channel Separation (GHz)	No. of Spans Interfering	Noise Improvement using ideal Matched Filter	
			NLI only	NLI + ASE
SPM	0	1	0.33	0.02
SPM	0	2	0.34	0.02
SPM	0	5	0.32	0.02
SPM	0	10	0.28	0.02
XPM	50	1	0.35	0.03
XPM	50	2	0.31	0.03
XPM	500	1	0.01	0.00
XPM	500	2	0.01	0.00

original power by ideal noiseless amplifiers. The output signal of the central channel was corrected for chromatic dispersion and the average nonlinear phase shift to obtain the IQ constellation. Figure 4.11 shows the output recovered constellations overlaid for the different transmission distances, the smallest elliptic constellation occurs after a single span while the largest more circular constellation occur after 20 spans. Using knowledge of the transmitted data the constellation was collapsed and rotated to 1,0 on the IQ plane. The noise in the I and Q dimensions was calculated and corresponds to the noise in the radial and angular directions. Figure 4.12 shows the ellipticity, e, of the NLI noise defined as

$$e \triangleq \frac{\mathrm{var}(Q) - \mathrm{var}(I)}{\mathrm{var}(Q)} \tag{4.40}$$

where var(.) is the variance function. It can be seen that after 5 spans the noise power shows ellipticity less than 20 % such that the noise field will show ellipticity less than 10 %. Also calculated for comparison was the NLI noise ellipticity for a signal that had been subject to considerable, 10000 km, of pre-dispersion. This gave NLI noise power ellipticity less than 5 %.

In order to assess the degrading effect of this ellipticity in the noise, the SNR penalty

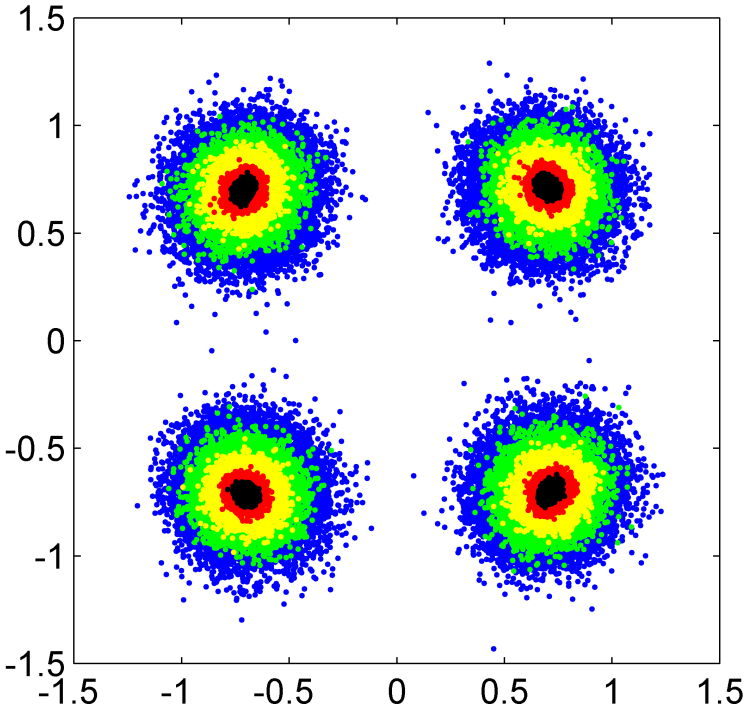

Figure 4.11: Overlaid output QPSK constellations after transmission through 1 (black), 2 (red), 5 (yellow), 10 (green) and 20 (blue) spans.

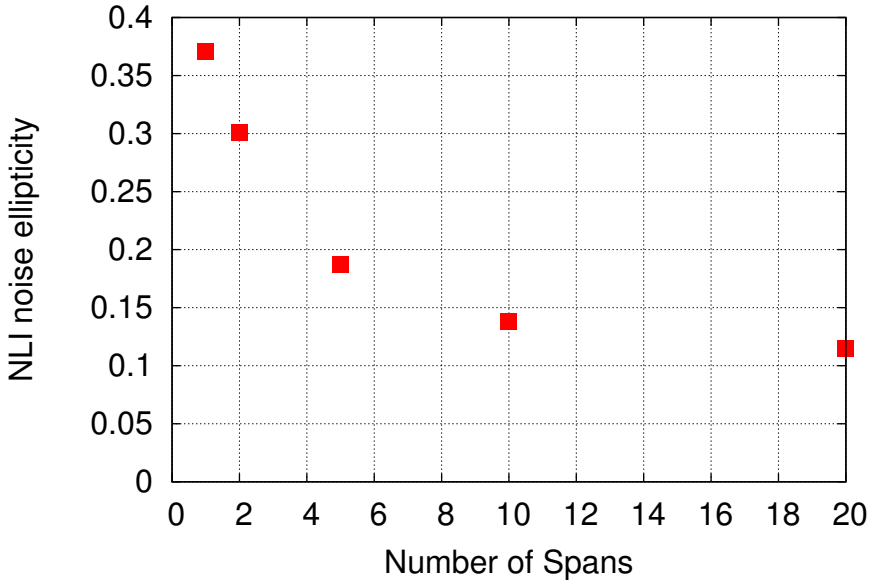

Figure 4.12: Ellipticity of the constellation noise as a function of the number of fibre spans transmitted.

was estimated from the probability density of the noise. The probability density of the noise was assumed to be the convolution of a Gaussian circular symmetric component and a Gaussian angular component. The probability of receiving a complex signal z given a transmitted complex symbol z_c is given by $P(z|z_c)$ as,

$$\begin{aligned} P(z|z_c) &= \int_{-\infty}^{\infty} P(\theta)\, P(z|(z_c,\theta))\, \mathrm{d}\theta \\ &= \int_{-\infty}^{\infty} \frac{1}{\sqrt{2\pi\sigma_\theta}} e^{-\frac{\theta^2}{2\sigma_\theta^2}} \frac{1}{2\pi\sigma} e^{-\frac{\left|z-z_c e^{\mathrm{i}\theta}\right|^2}{\sigma^2}}\, \mathrm{d}\theta \end{aligned} \tag{4.41}$$

where σ_θ^2 is the variance of the angular component and σ^2 is the variance of the circular symmetric component. For PM-QPSK with ideal Gray coding the HD-BER is given by,

$$\mathrm{BER} = \int_{-\infty}^{0} P(z|(\tfrac{1}{\sqrt{2}} + \mathrm{i}\tfrac{1}{\sqrt{2}}))\mathrm{d}z. \tag{4.42}$$

The BER was calculated by numerical integration of equation (4.42) and the . σ_θ and σ were chosen to give the required ellipticity while maintaining an overall SNR. Figure 4.13 shows the SNR penalty due to the ellipticity of the noise calculated from the BER as a function of the ellipticity and input SNR. For ellipticity < 0.15 the penalty is less than 0.1 dB. When the effect of the ASE noise that will be circular symmetric is included, at the optimum launch power, the ellipticity will be reduced by 3. This will give a penalty of < 0.05 dB for 5 or more spans of transmission such that this noise ellipticity is not significant for most of the routes considered in chapter 6.

4.8 The Model in a Network Context

Consider a mesh network of nodes formed of ROADMs and links, l, formed of fibre pairs. Consider a number of transmission signals routed across the network between source, s, and destination, d, nodes. For simplicity only signals transmitted from low to high nodes are considered and it is assumed that a parallel transmission from high to low node will be carried on the second fibre of the pair along an identical route with identical transmission format and properties. This means if a route traverses a link then regardless of its direction both fibres will contain an equal load.

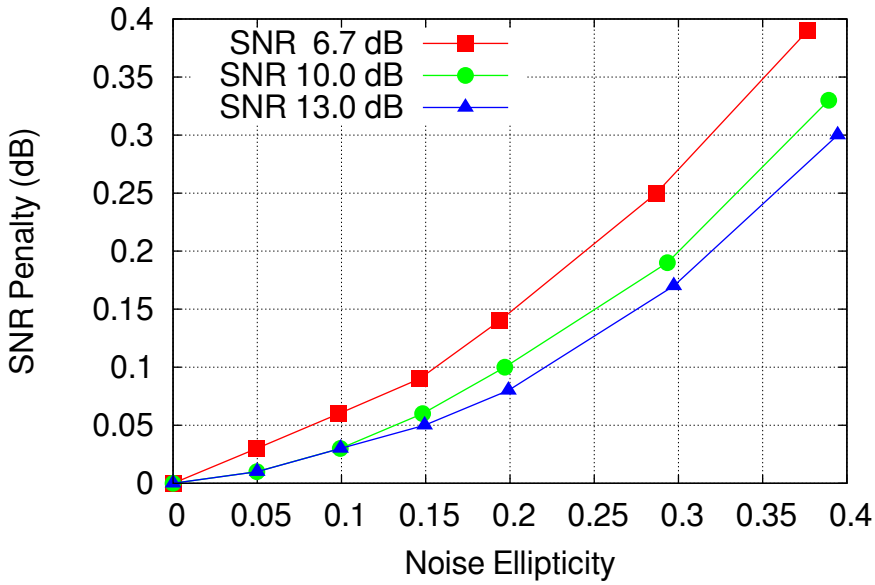

Figure 4.13: SNR penalty to maintain HD-BER performance as a function of noise ellipticity in the IQ constellation. For PM-QPSK modulation a SNR of 6.7 dB leads to a HD-BER of 0.015.

The ASE noise accumulated on the transmission signal, i, $n_{ASE,i}$ is given by

$$n_{ASE,i} = 10^{\frac{NF}{10}} h\nu R \sum_l \left[\delta_{i,l}^L N_{s,l} 10^{\frac{A_{span}}{10}} \right] \tag{4.43}$$

where $N_{s,l}$ is the number of spans in link l and $\delta_{i,l}^L$ is 1 if the signal from the i^{th} transmitter-receiver pair traverses link l, zero otherwise. Similarly the nonlinear interference is given by a summation of the nonlinear interference accumulated on the i^{th} transmitted signal as it traverses each link on its route, thus the accumulated nonlinear efficiency, $X_{i,j}$, is given by

$$X_{i,j} = \begin{cases} X_{ss}(0) \left(\sum_l \delta_{i,l}^L N_{s,l} \right)^{1+\varepsilon}, & i = j \\ X_{ss}\left(|\nu_i - \nu_j| \right) \sum_l \delta_{i,l}^L \delta_{j,l}^L N_{s,l}, & i \neq j \end{cases} \tag{4.44}$$

where $X_{ss}(\Delta\nu)$ is the single span efficiency for the nonlinear interference between signals spaced by a frequency, $\Delta\nu$. Thus the final model of SNR in a network context is such that the SNR on the i^{th} transmission signal, SNR_i, is given by

$$SNR_i = \frac{p_i}{n_{ASE,i} + p_i \sum_j X_{i,j} P_j^2}. \tag{4.45}$$

4.9 Extensions and Corrections to the Model

As shown in section 4.7 the simple summation model of section 4.4 can have significant errors when the channels are closely spaced. Figure 4.14 shows the integration space for widely spaced and closely spaced channels for nonlinear interference generated at zero frequency for five equal DWDM signals . It shows that as the channels become closer, FWM islands appear in the integration space that are significant due to their closeness to the frequency axis ($f_1 = 0$ or $f_2 = 0$) where the "four wave mixing factor" is largest. The most significant additional terms, coloured red in figure 4.14 could be included in the model via an additional summation of the form

$$P_i \sum_j X_{i,j}^{(E)} P_j P_{j-1} \tag{4.46}$$

where $X_{i,j}^{(E)}$ is the NLI efficiency correction term between channels i and j. In this work the channels are well spaced such that there is no need for this term. Further terms would be required to capture all of the FWM terms further away from the frequency axis. It is noted that the analytical closed form solution used by Johannisson [36] is calculated by integration over a rectangle which includes these red coloured FWM islands, provided the signals have equal PSD.

The GN model has been derived on the assumption that both the signal and noise are Gaussian distributed. Where the signal has been highly dispersed it appears Gaussian distributed while the interference generated can also appear Gaussian distributed if the interference is also highly dispersed. Thus the GN model is most applicable to uncompensated links where the signal has undergone some prior dispersion. The need for prior dispersion means the GN model is not fully applicable to the first few spans in a link.

There is some debate about the validity of the GN model. It has been shown that the nonlinear interference can depend on the modulation format and is not always a circular complex Gaussian noise [160, 166, 167]. It should be noted that these results have been obtained including the first span of the link where the signal has not been dispersed. It is also pointed out that the signal is never a truly Gaussian stochastic process since after some linear equalization a non-Gaussian signal constellation can be recovered. A number of extensions to the original GN model have been proposed to improve the applicability of the model to all situations [160, 168, 169]. These extensions considerably increase the models complexity.

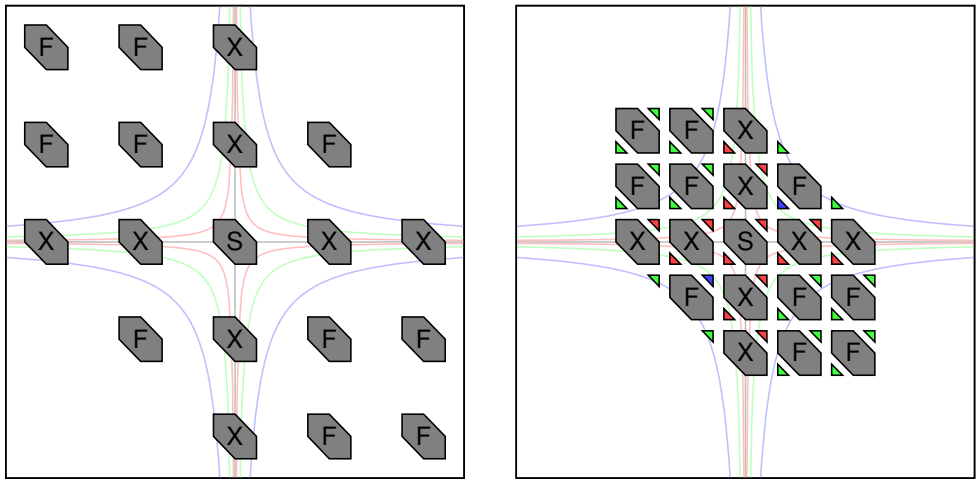

Figure 4.14: The integration region for NLI generated at f=0 for (left) widely spaced DWDM channels and (right) for closely spaced DWDM channels. Nonlinearity is marked as S=SPM, X=XPM, F=FWM. The coloured islands generate the errors in the model for closely spaced channels and are marked red, blue and green in order of significance. Also shown are contours of the "four wave mixing factor" at 10 dB intervals. The signals are at 32 Gbaud with rectangular Nyquist spectra.

The paper of Dar et al. [168] concentrates on correction terms for XPM while Carena et al. [169] provides corrections for all NLI terms. For well spaced channels the enhanced Gaussian noise, EGN, model gives the nonlinear interference noise due to XPM as

$$n_{XPM,i,j} = p_i p_j^2 \left(\kappa_{11,i,j} - \Phi_j \kappa_{12,i,j}\right) \tag{4.47}$$

where Φ_j depends on the modulation format of the j^{th} interfering channel and is given by

$$\Phi_j = \frac{\mathrm{E}\left[|s|^4\right]}{\mathrm{E}\left[|s|^2\right]^2} - 2 \tag{4.48}$$

where s are the symbols and $\mathrm{E}[\cdot]$ represents the expectation over the symbol set. Φ_j is equal to 0 for Gaussian distributed symbols, -1 for QPSK and $\frac{-17}{25}$ for 16QAM modulation. The factor $\kappa_{11,i,j}$ is identical to the original GN model. Define $\mu(f_1, f_2, f)$ as

$$\mu(f_1, f_2, f) = e^{4\pi^2 \beta_{2,p}(f_1-f)(f_2-f)} \frac{1 - e^{-\alpha L + 4\pi^2 \beta_2 (f_1-f)(f_2-f)L}}{\alpha - 4\pi^2 \beta_2 (f_1-f)(f_2-f)} \frac{1 - e^{4\pi^2 \beta_2 (f_1-f)(f_2-f)LN_s}}{1 - e^{4\pi^2 \beta_2 (f_1-f)(f_2-f)L}} \tag{4.49}$$

where $\beta_{2,p}$ is the signal pre-dispersion before its launch into the fibre. Thence for signals with Nyquist sinc pulses such that $g(f) = \frac{1}{R}\mathrm{rect}\left[\frac{f}{R}\right]$ where $\mathrm{rect}[x]$ defines the rectangle

function and is equal to 1 for $|x| < \frac{1}{2}$, 0 elsewhere, κ_{11} and κ_{12} are given by

$$\kappa_{11,i,j} = \frac{32}{27}\frac{\gamma^2}{R^3}\int_{-\frac{R}{2}}^{\frac{R}{2}}\int_{-\frac{R}{2}}^{\frac{R}{2}}\int_{-\frac{R}{2}}^{\frac{R}{2}} \mathrm{rect}\left[f_1+f_2-f\right]\mu(f_1,f_2+\Delta f,f)\mu(f_1,f_2+\Delta f,f)^*\mathrm{d}f_1\mathrm{d}f_2\mathrm{d}f \tag{4.50}$$

where Δf is the carrier frequency separation of the i and j channels and

$$\kappa_{12,i,j} = \frac{80}{81}\frac{\gamma^2}{R^4}\int_{-\frac{R}{2}}^{\frac{R}{2}}\int_{-\frac{R}{2}}^{\frac{R}{2}}\int_{-\frac{R}{2}}^{\frac{R}{2}}\int_{-\frac{R}{2}}^{\frac{R}{2}} \mathrm{rect}\left[f_1+f_2-f\right]\mathrm{rect}\left[f_1+f_3-f\right] \cdot\mu(f_1,f_2+\Delta f,f)\mu(f_1,f_3+\Delta f,f)^*\mathrm{d}f_1\mathrm{d}f_2\mathrm{d}f_3\mathrm{d}f. \tag{4.51}$$

The EGN model was used to calculate the nonlinear interference noise due to XPM on a central channel by 6 interfering channels on a 50 GHz grid. Figure 4.15 shows the result with the EGN model giving lower interference than the GN model. Figure 4.15 also shows the most surprising result in that a heavily pre-dispersed[3] signal while initially giving nonlinear interference in agreement with the GN model shows a deviation from the model as the number of spans and thence total dispersion increases. The deviation from the GN model approaches 2.3 dB for QPSK, 1.4 dB for 16QAM and 1.2 dB for high order QAM modulation formats. When this is combined with ASE noise at the optimum launch power these discrepancies will be reduced by a $\frac{1}{3}$ in the log domain.

The GN models is derived from a first order perturbation and does not follow the physical conservation of energy principle. Recently a spectral solution to the NLSE based on turbulent flow [170] has been proposed that is more accurate and less complex for strong nonlinearity where higher order perturbations must be considered. The recent work of Secondini [161,171] also points out a correlation of the NLI between symbols that could allow for some blind NLI compensation.

[3]Where the signal has been dispersed with the same sign as the fibre such that during propagation the signal will become even more dispersed.

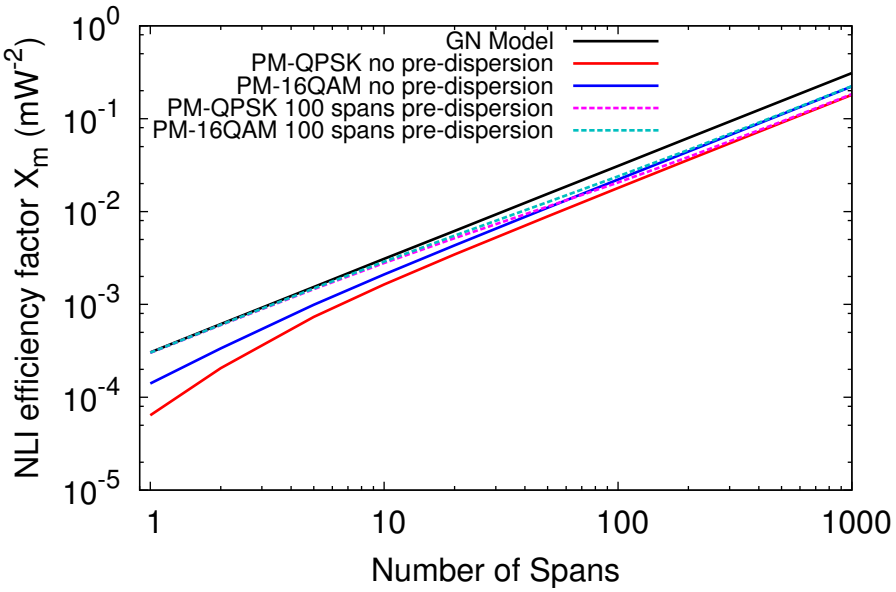

Figure 4.15: Nonlinear interference factor X_m on central channel due to XPM from six neighbouring channels as a function of number of transmitted spans. X_m based on the GN and EGN models shown for QPSK and 16QAM modulation with and without 100 spans of pre-dispersion.

5

Link and Simple Network Optimisations

THE GN model has been used to define optimum system operating points under a variety of assumptions. P. Serena and A. Bononi [75] showed that in the asymptotic limit of a large operating bandwidth the signal power spectral density, PSD, that minimises the nonlinear interference for a given total power is a uniform PSD across the operating bandwidth.

P. Poggiolini et al. [41] show that in the case of a uniform signal PSD the launch power that minimises the BER, and maximises the SNR, is such that the nonlinear interference noise is half the ASE noise. They go on to show [77] that the optimum launch power for a complete path is obtained when the SNR degradation in each link is locally minimised. This is the local optimum global optimum, LOGO, concept where the launch power into each span can be locally optimised to obtain the path global optimum. To simplify this further the assumption of high network loads and thus fully loaded fibres with Nyquist spaced channels leads to the LOGON model [35, 77] for network design where the SNR degradation of each link is calculated assuming fully loaded fibres at the optimum launch

power.

R. Pastorelli et al. [42, 78] looked at a global maximisation of the linear part of the OSNR margin to give the system maximum headroom for OSNR degradation from ageing components, amplifiers etc. They found the linear part of the OSNR margin is maximum when the SNR due to NLI is three times the linear OSNR FEC transmission limit.

In this chapter the nonlinear transmission model described in chapter 4 is used to optimise the transmitter launch power in a link and in a simple three node network. These ideas were first shown at the Optical Fiber Conference in Anaheim 2013 [34] and published as an extended paper in 2014 [162]. The potential improvement in SNR and information throughput are assessed for a number of different optimisation strategies. The transmission parameters used throughout this chapter are shown in table 3.1.

5.1 Link Optimisation

The nonlinear transmission model, described by equation (4.16) of chapter 4 was used to optimise the performance of a single point-to-point link. Consider a traditional link where all of the transmitters launch the same uniform signal power, p, then for a transmission link operating in the nonlinear propagation regime there is an optimum launch power which maximises, the minimum symbol SNR of the worst channel. From equation (4.14) the minimum symbol SNR, SNR_m, is given by

$$SNR_m = \frac{p}{n_{ASE} + p^3 X_m} \tag{5.1}$$

where n_{ASE} is the accumulated ASE noise over the link and is assumed constant for all channels and X_m is the maximum accumulated nonlinear interference efficiency factor on the worst channel given by

$$X_m = \max_i \sum_j X_{i,j} \tag{5.2}$$

where $X_{i,j}$ is the accumulated nonlinear interference efficiency for nonlinear interference noise generated on channel i by channel j. For an equally spaced grid of similar spectrally shaped channels this maximum will occur for the central channel. Solving equation (5.1) to obtain the launch power, p_0, to maximise, the minimum symbol SNR gives

$$p_0 = \sqrt[3]{\frac{n_{ASE}}{2X_m}} \tag{5.3}$$

and the minimum symbol SNR is given by

$$SNR_m = \frac{2p_0}{3n_{ASE}}. \tag{5.4}$$

So at the optimum uniform launch power the maximised minimum symbol SNR occurs when the nonlinear interference noise is half the ASE noise [41][1].

A link consisting of 12 spans of 80 km with the transmission fibre parameters as shown in table 3.1 was considered. Figure 5.1 illustrates the launch power and symbol SNR for each channel transmitted in the 960 km link under two different SNR optimisation strategies. In the first optimisation, all the channels are launched with the same power as calculated using equation (5.3), the maximised symbol SNR of the channel with the worst quality of transmission was 17.8 dB and 18.6 dB respectively for transmission with CD compensation only and for CD and SPM compensation. The channels towards the edge of the band show higher SNR since the nonlinear interference is reduced as there are fewer neighbouring channels. In the second optimisation the individual channel powers have been optimised to maximise the uniform symbol SNR of all the channels. This leads to all the channels having a symbol SNR of 17.9 dB and 18.7 dB respectively for CD only or for CD and SPM compensation. By redistributing the channel powers the symbol SNR of the worst channel has been slightly increased by around 0.1 dB. It can also be seen that the advantage of ideal SPM compensation is only 0.8 dB and this advantage will decrease if the number of channels is increased or the channel spacing decreased as either will increase the strength of XPM interference.

A third optimisation where the Gaussian noise limited Shannon capacity was maximised is shown in figure 5.2. The metric, b, given by

$$b = \sum_i \log_2 \left[SNR_i + 1 \right], \tag{5.5}$$

was maximised by optimising the individual channel powers, actually $\frac{1}{b}$ was minimised using the MATLAB® unconstrained minimisation function. This leads to a Gaussian noise limited Shannon capacity of the link is $2bR$ where R is the symbol rate and the factor 2 accounts for the polarisation multiplexing. Figure 5.2 shows the symbol SNR and launch powers of the optimised channels where the Gaussian noise limited Shannon capacity was

[1] It should be noted that with large operating bandwidths n_{ASE} and X_m increase linearly with the number of spans such that the optimum launch power p_0 is independent of the transmission length to first order.

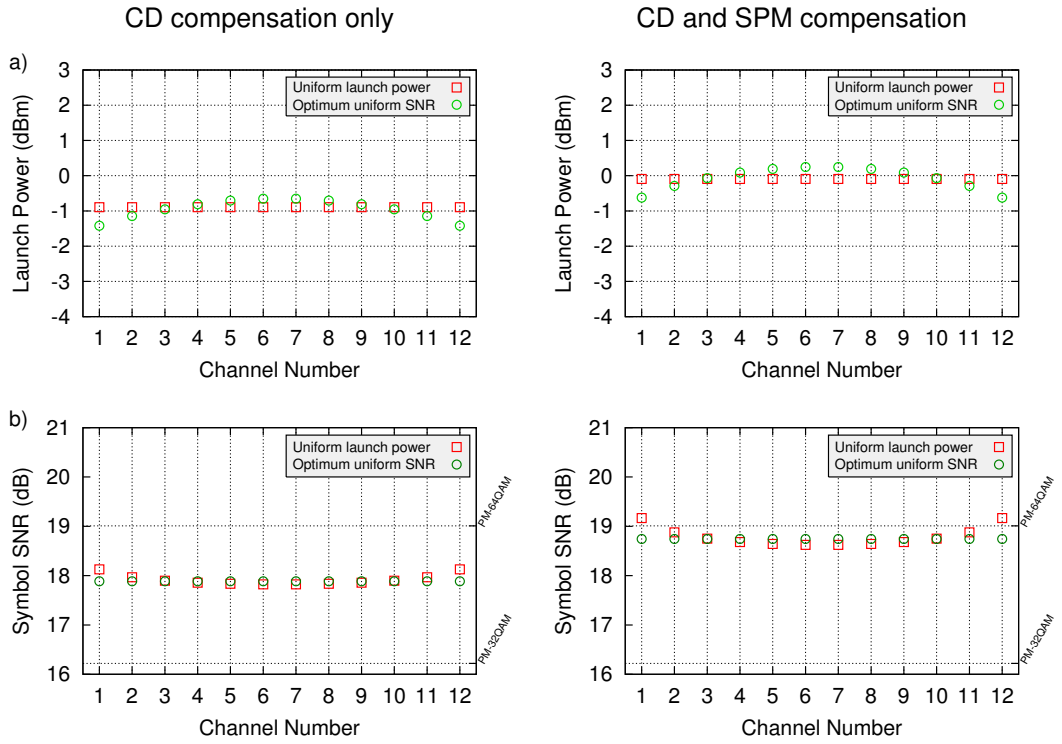

Figure 5.1: The launch power a) and symbol SNR b) for each channel under two SNR optimisation strategies. The results are shown for CD compensation only (left) and for CD and SPM compensation (right). The symbol SNR thresholds for 0.015 preFEC BER are also marked for various modulation formats.

found to be 4.59 Tb·s^{-1} and 4.82 Tb·s^{-1} respectively for CD only or for CD and SPM compensation.

The final optimisation, also shown in figure 5.2, was to maximise the throughput of the link utilising PM-mQAM formats. The power of each channel was optimised to achieve the required symbol SNR of the modulation formats as shown in table 4.2. For the transmission rate of 32 Gbaud this would give an error free data rate of 50, 100, 150, 200, 250 and 300 Gb·s^{-1} for the PM-BPSK, PM-QPSK, PM-8QAM, PM-16QAM, PM-32QAM and PM-64QAM modulation formats, respectively. For the link under consideration the maximised flat symbol SNR lies between that required for PM-32QAM and PM-64QAM so the optimal link throughput will be achieved for a mixture of these formats. The individual launch powers were iteratively optimised to achieve the required symbol SNR while the channel allocation and formats were optimised by exhaustive search to achieve the maximum throughput. The maximised throughput of the link was 3.00 Tb·s^{-1} and 3.50 Tb·s^{-1} respectively for CD only or for CD and SPM compensation with a final

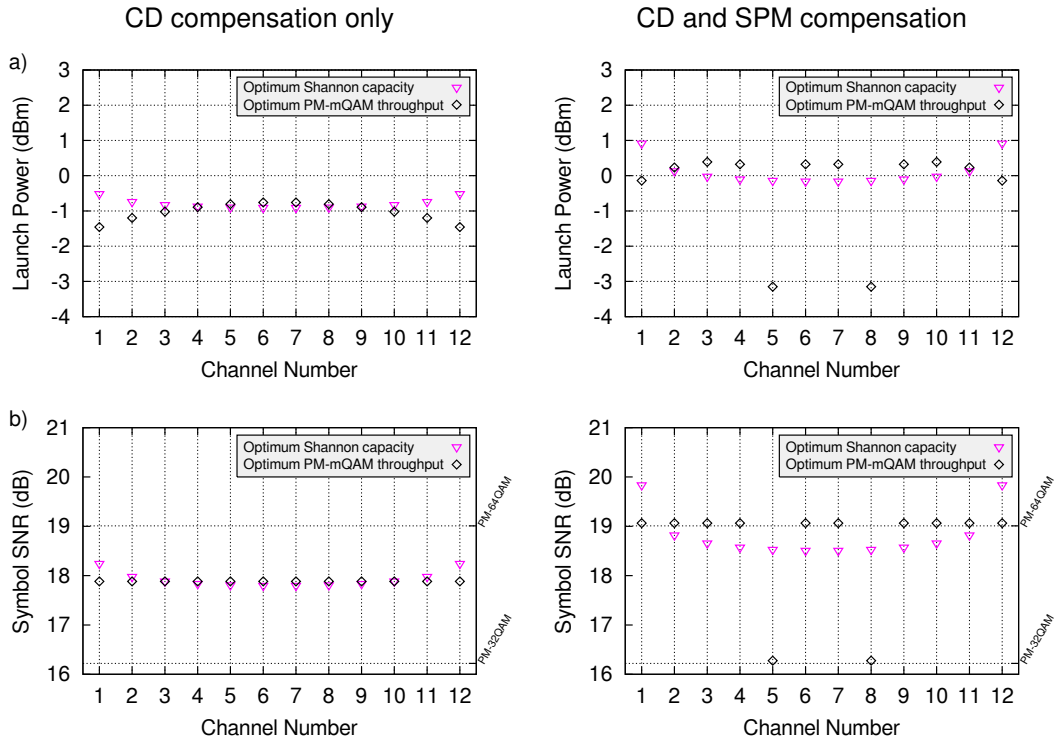

Figure 5.2: The launch power a) and symbol SNR b) for each channel under two capacity optimisation strategies. The results are shown for CD compensation only (left) and for CD and SPM compensation (right). The symbol SNR thresholds for 0.015 preFEC BER are also marked for various modulation formats.

achievable SNR margin of 1.7 dB and 0.1 dB respectively. The launch powers and achieved symbol SNR are shown in figure 5.2. It is observed that the optimisation has placed lower power channels between high SNR channels reducing the nonlinear interference noise on them, also lower SNR channels have been placed towards the centre of the transmission band where nonlinear interference noise tends to be higher. It is interesting that in figure 5.2 (a left) the channel launch powers increase towards the band edge for the Shannon capacity optimisation but decrease for the PM-mQAM throughput optimisation. In this result, the PM-mQAM throughput optimisation returns a single modulation format. So the optimisation will effectively maximise the uniform SNR across all channels and will thus decrease the launch power towards the edge, where there is less noise. For the Shannon capacity optimisation, the channels at the band edge influence fewer channels such that increasing their launch power will increase their capacity but will degrade fewer channels leading to an overall increase in capacity.

Table 5.1 summarises the optimisation strategies along with the minimum symbol SNR,

Table 5.1: Summary of four different link optimization strategies

Optimisation Strategy	Metric	CD only	CD and SPM
Uniform power	min SNR (dB)	17.8	18.6
	Throughput (Tb·s^{-1})	3.00	3.10
Uniform SNR	min SNR (dB)	17.9	18.7
Shannon capacity	Capacity (Tb·s^{-1})	4.59	4.82
PM-mQAM throughput	Throughput (Tb·s^{-1})	3.00	3.50
	with SNR margin (dB)	1.7	0.1

the Shannon capacity and the PM-mQAM throughput based on the modulation formats and required symbol SNR described above.

These optimisations of a link have shown that by optimising the transmitter launch power the SNR of the worst channel can be improved at the expense of reducing the SNR of the better channels. These gains are possible since the outer channels have fewer neighbours and, thus, experience less nonlinear interference. By optimising the SNR to that required for error-free transmission and reducing the SNR margin where it is not required it is possible to increase the SNR of other channels to allow for a higher order modulation format transmitting more data. It can also be seen that the effect of SPM mitigation has a small effect around 0.8 dB on the SNR but in this instance allows for an increases in the PM-mQAM realised throughput . It should be noted that in this instance the granularity of the required SNR for higher order modulation has left a 1.7 dB margin for CD only compensation case which can not be converted to increased throughput . It can be seen however that under ideal coding the Shannon capacity is only marginally increased by mitigating SPM.

5.2 Optimisation of a Three Node Network

Next consider the very simple three node network shown in figure 5.3. It consists of two links each of 6 spans of 80 km connected by an idealised, loss less, ROADM.

Using the nonlinear transmission model described in chapter 4, three SNR optimisations

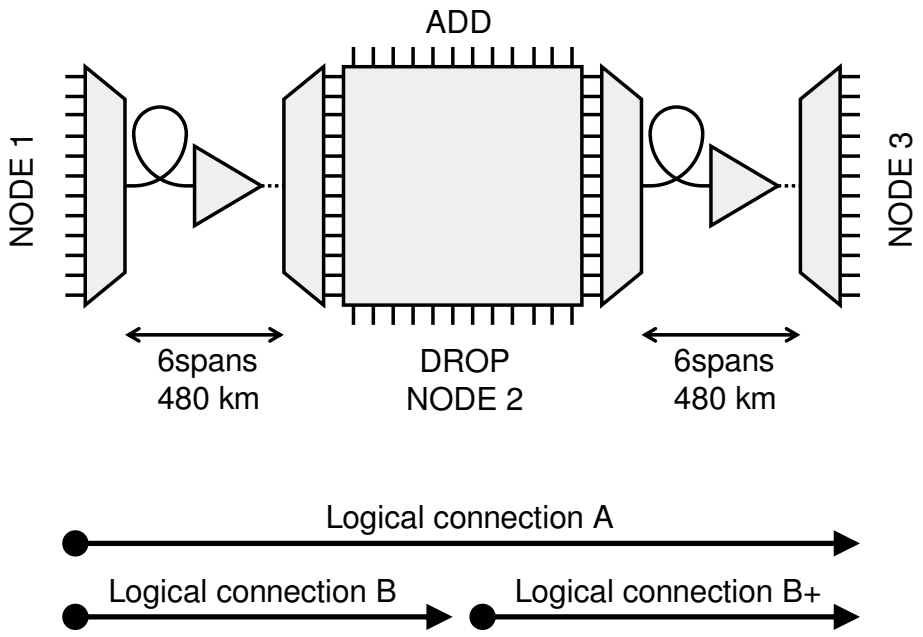

Figure 5.3: A simple three node network showing the logical connections

of a 12 DWDM channel three node network were performed, the results are shown in figure 5.4. Initially grouping the connections such that the first 6 DWDM channels provide connections "A" from node 1 to node 3 and the final 6 DWDM channels provide connections "B" from node 1 to node 2 and are re-used for "B^+" from node 2 to node 3. The optimum uniform launch power was calculated using equation (5.3) of section 5.1 and gave a maximised worst case symbol SNR of 17.8 dB and 18.6 dB respectively for CD only or for CD and SPM compensation on the longest central channel with the second group of connections "B" and "B^+" achieving an approximately 3 dB higher SNR. Maintaining the grouped channel allocations and optimising the individual channel powers allowed the maximised uniform symbol SNR to be raised to 18.1 dB and 19.2 dB respectively for CD only or for CD and SPM compensation at the expense of a significant reduction in the SNR of the shorter connections. In each link there are 12 DWDM channels 6 for connection "A" and 6 for "B" or "B^+". Thus there are 12! permutations of these channels but since all the "A" or "B" channels are equivalent there are just $\frac{12!}{6!\times 6!} = 924$ unique combinations. So finally optimising the channel allocations by an exhaustive search of all 924 possible combinations while optimising the individual launch powers a maximised uniform symbol SNR of 18.5 dB and 19.9 dB respectively for CD only or for CD and SPM compensation was achieved. It can been seen that in this situation the inclusion of SPM compensation allows the optimisation gains in SNR to be increased from 0.7 dB to 1.3 dB.

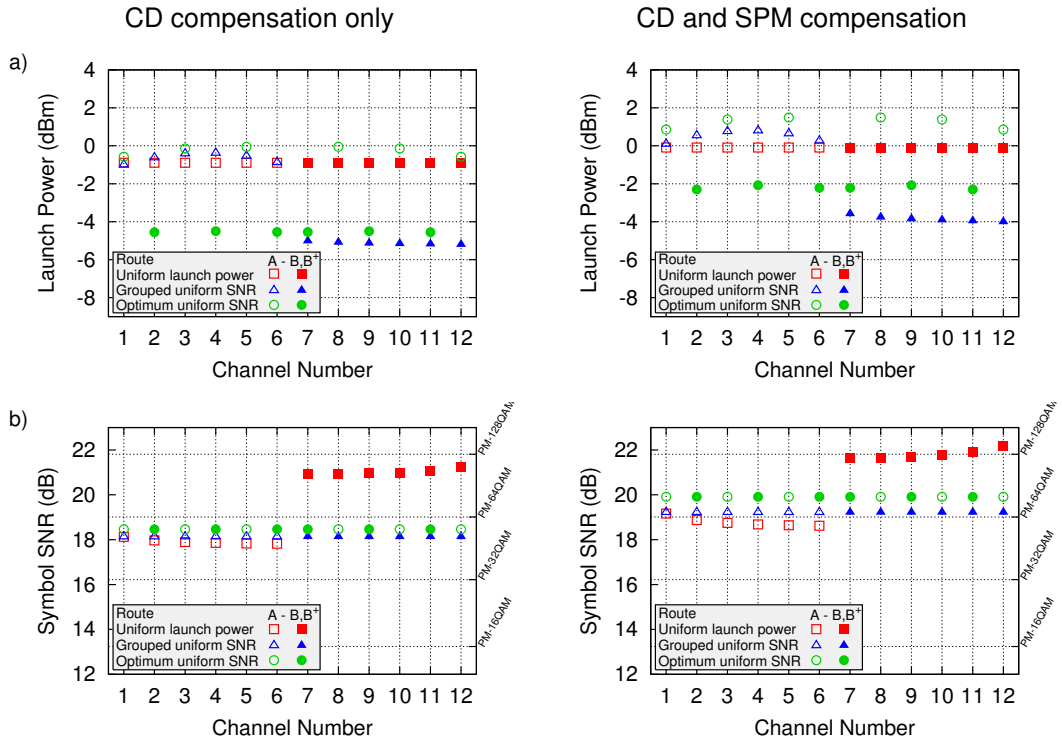

Figure 5.4: The launch power a) and symbol SNR b) for each channel under three SNR optimisation strategies. The results are shown for CD compensation only (left) and for CD and SPM compensation (right). The symbol SNR thresholds for 0.015 preFEC BER are also marked for various modulation formats.

Finally the routing, modulation format and launch powers were optimised to maximise the uniform throughput over connections "A", "B" and "B^+". That is to transport equal data between nodes 1 and 2, 1 and 3, and 2 and 3. An exhaustive search was carried out to search the routing and modulation format to maximise the SNR margin given the number of routes on each connection and the number transmitters utilising either a low or high modulation format. It has been shown that the optimum launch power and SNR is approximately uniform [75], see also the results of the Shannon capacity optimisation for a single link in section 5.1, so adjacent modulation formats are expected to give the optimum result. Thus given a throughput for the connections and the number of long and short routes to utilise the number of low and high format transceivers can be determined. Thence an exhaustive search of the channel allocations for each transceiver is carried out to maximise the SNR margin. The throughput for each connection was maximised while the SNR margin remained positive allowing error free transmission.

For CD only compensation it was found utilising 6 transceivers for each connection

the throughput was limited to 1.5 Tb.s^{-1} for each connection using PM-32QAM on all transceivers, it was not possible to find a channel and power allocation to give sufficient SNR for error free transmission if any transceivers for each connection was modulated using PM-64QAM. However if 7 transceivers were allocated to the long connection and 5 transceivers to each of the short connections "B" and "B^{+}" the maximum throughput for each connection was found to be 1.7 Tb·s^{-1}. The solution used 6 off PM-32QAM and 1 off PM-16QAM transceivers on the long route and 4 off PM-128QAM and 1 off PM-64QAM transceivers on the shorter route. This gives 7 channels operating near the optimal uniform power, 4 channels operating at a higher power and 1 at a lower power. Figure 5.5(left) shows the power and SNR for each channel showing the optimum routing occurs with high power channels at the band edges and well spaced to reduce nonlinear interference on these channels, note the equivalent solution reversing the channel numbers gave the same result.

For the CD and SPM compensation case it was found that utilising 6 transceivers for each connection, each utilising 5 off PM-64QAM and 1 off PM-128QAM gave the optimum error free uniform throughput of 1.85 Tb·s^{-1} for each connection. This solution uses 10 channels operating just below the optimal power and 2 higher power channels which are placed at the band edge to reduce the impact of nonlinear interference as shown in figure 5.5(right), note the equivalent solution reversing the channel numbers gave the same result.

The CD only compensation solution of figure 5.5(left) is counter intuitive to the results of figure 5.4 as the long routes have their launch power reduced while the shorter routes have their launch power increased. This occurs because the optimal solution utilises 5 channels over the short routes and 7 channels over the long route. To obtain equivalent throughput between the nodes the 5 channels must operate at significantly higher modulation order. Thus the result requires the SNR of the short route to be pushed above its flat launch power value while the SNR of the longer route can be significantly reduced. In the CD and SPM compensation solution of figure 5.5(right) the optimal solution has equal, 6, channels operating on all routes. Thus here the SNR are near their uniform optimum and the longer routes require higher launch power.

In this simple network where not all of the channels are transmitted across the same distance it is possible through correct channel and power allocation to improve the symbol

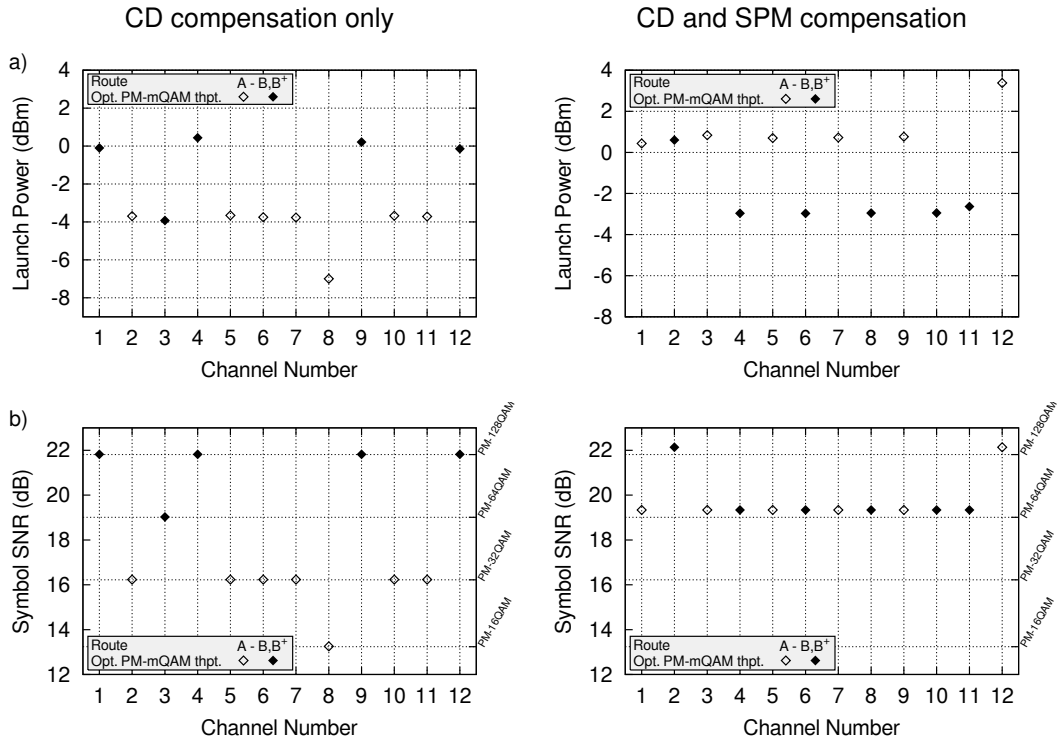

Figure 5.5: The launch power a) and symbol SNR b) for each channel under a PM-mQAM throughput optimisation strategy. The results are shown for CD compensation only (left) and for CD and SPM compensation (right). The symbol SNR thresholds for 0.015 preFEC BER are also marked for various modulation formats.

Table 5.2: Summary of four different optimization strategies for the simple 3 node network.

Optimisation Strategy	Metric	CD only	CD and SPM
Uniform power,	min SNR (dB)	17.8	18.6
grouped channels	Connection throughput (Tb.s^{-1})	1.50	1.55
Uniform SNR,	min SNR (dB)	18.1	19.2
grouped channels			
Uniform SNR,	min SNR (dB)	18.5	19.9
optimum channels			
PM-mQAM throughput	Connection throughput (Tb.s^{-1})	1.70	1.85
	with SNR margin (dB)	0.0	0.1

SNR of the worst channel by 0.7 dB and 1.3 dB respectively for CD only or for CD and SPM compensation. The redistribution of power was used to advantageously improve low SNR channels to allow a higher order modulation format to maximise the throughput of all the connections. For CD only compensation and equal launch power with grouped channels the throughput of each connection would be limited by the longer, low SNR routes to just 1.50 Tb·s^{-1}, since we require uniform throughput across all connections. This throughput can be increased to 1.70 Tb·s^{-1} by balancing the number of channels between long and short routes taking advantage of the naturally higher SNR on the shorter route and also by optimal channel and power allocation. For CD and SPM compensation the throughput of each connection is limited to 1.55 Tb·s^{-1} for uniform launch power and grouped channels but this can be increased to 1.85 Tb·s^{-1} by optimal channel and power allocation. Thus by optimising the modulation format, channel and power allocation the connection throughput of this simple network has been increased by 13 % and 19 % respectively for CD only and for CD and SPM compensation.

5.3 Comparison with Split Step Fourier Simulation

To confirm the validity of the quality of transmission model described in section 4 the interesting solution for the maximum PM-mQAM throughput in the 3 node network with CD only compensation was simulated using the split step fourier simulation [99] of the time domain signal.

The 17 signals, 7 for connection “A” and 5 for connection “B” and “B+”, were first separately generated in the time domain. Each signal comprised 64000 symbols created from $2m \times 64000$ random bits which were Gray mapped to the PM-mQAM symbols as required. The use of 64000 symbols ensures that for 32 GBaud the simulation time is also a multiple of 50 GHz. The simulation field of each signal was created by expanding the signal to 2 samples per symbol and filtering with an ideal rectangular Nyquist filter, a root raised cosine filter with roll off (1/32000). An ideal optical carrier was assumed with no phase, frequency offset or intensity noise.

The 12 signals for transmission through the first link were multiplexed together in the frequency domain. Each signal was ideally filtered to a 50 GHz channel width and the channels were stacked together in the required order and zero padded to give an overall

simulation bandwidth of 1280 GHz equivalent to 40 samples per symbol for the 32 GBaud signals.

The combined signal was transmitted through the first 6 spans. Each span was simulated using the split step Fourier solution to the Manakov equation [172] with fixed 10 m steps and followed by an ideal EDFA with gain to fully compensate the span loss and additive white Gaussian noise to simulate the ASE noise.

To simulate the second node the connection "B" signals were ideally demultiplexed in the frequency domain with ideal 50 GHz channel filters and dropped while the connection "B+" signals were ideally multiplexed to replace them. Transmission through the second link for the new combined signal was simulated as for the first. At the end node 3 the remaining 12 signals were ideally demultiplexed in the frequency domain using an ideal 50 GHz channel filter.

The 17 transmitted signals were expanded back to 2 samples per symbol by zero padding in the frequency domain before applying a matching filter and chromatic dispersion compensating filter. The compensated signal was equalised with a single tap Wiener-Hopf filter [173] to compensate for the average nonlinear phase rotation and to rescale the signal. The Wiener-Hopf filter tap was calculated by least squares minimisation of the error between the equalised symbols and the transmitted symbols. The filter is effectively trained by the whole data set. The signal quality was determined by calculating the SNR from the error vector magnitude, EVM [174]. The BER was calculated through a hard detection of the symbols and de-mapping to recover the data bits.

The overall simulation was repeated 16 times to improve the reliability of the SNR and BER estimates.

In figure 5.6 the simulated signal SNR are overlaid on the result of figure 5.5(b)(left). The split step Fourier simulation shows good agreement with the results calculated based on the GN model. The signal BER range from 1.18 % to 1.44 %, that is less than the FEC threshold of 1.5 % allowing error free performance on all signals. The SNR margin was found to be between 0.07 and 0.16 dB for the signals of connection "A" and between 0.15 and 0.45 dB for the signals of connection "B" and "B+". These margins are larger than those predicted by the GN model as the GN model over estimates the nonlinear interference for the early spans in the transmission. The signals on the shorter "B" and "B+" connections have a higher margin over the signals on the full length connection

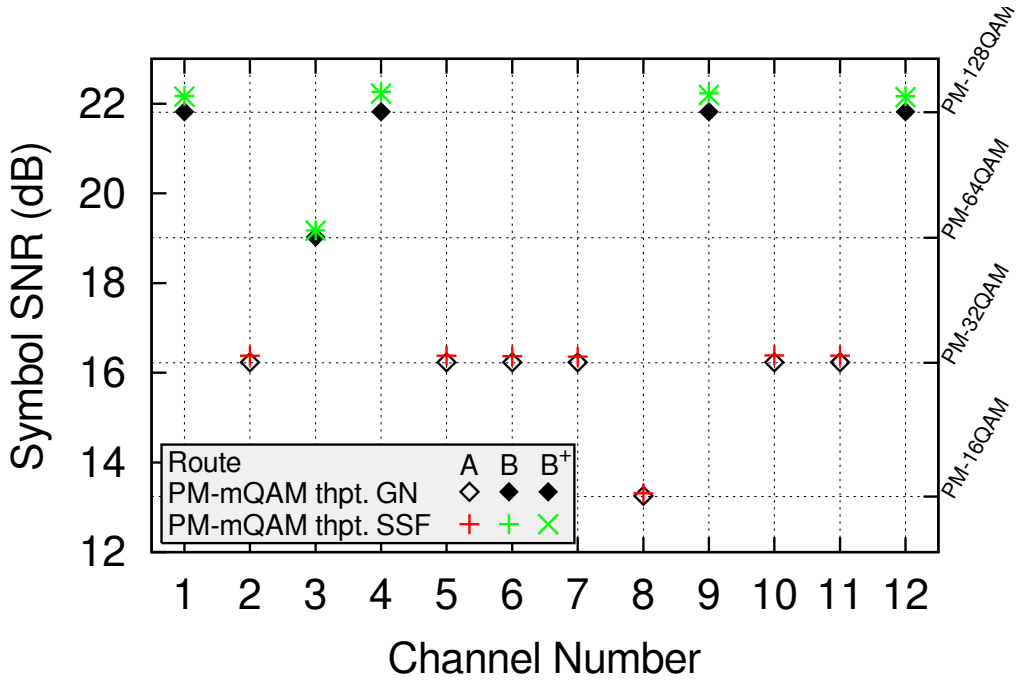

Figure 5.6: Comparison of the GN three node network solution described in figure 5.5 for CD compensation only with the split step Fourier simulated results

"A" as a result of their shorter transmission length. Also the signals on the connection "B" have slightly higher SNR than the equivalent signals on connection "B+" since the interfering signals from connection "A" have undergone more dispersion becoming more "Gaussian" before interfering. These differences are consistent with the assumptions and errors of the GN model and confirm that the GN model is robust and slightly under predicts performance.

5.4 Conclusions for Simple Networks

While the results and optimisations presented are specific to the link and networks shown they begin to shed some light on possible heuristic rules that lead to an optimised network.

- The Shannon capacity is optimised for a nearly flat, within ≈1 dB, launch power. This suggests that network capacity would be optimised with an approximately flat launch power. This is consistent with Serena et al. [75] who suggest a flat launch power will minimise the nonlinear interference.

- This launch power is approximately given by the optimized flat launch power obtained from equation (5.3). This is consistent with the local optimum global

optimum concept [77] where in a network of similar fibre with loss less nodes the local power optimum in each link leads to the global optimum across the whole network.

- When using transmitters utilising the PM-mQAM formats there is a large jump in required SNR between formats and this often results in a lower modulation format being used with potential excessive SNR margins. In this situation it is advantageous to minimise the launch power, while maintaining the require symbol SNR, as this reduces interference on neighbouring channels and may enable a neighbouring channel to increase its modulation format.

- Where transmitters are utilising different launch powers high power channels should not be spectrally grouped together but should be spaced with lower power channels to reduce the nonlinear interference on the high power channels.

- Where there is sufficient bandwidth, utilising multiple channels with lower order modulation and thus lower power will reduce the overall nonlinear interference within the network. For example in the case of the 3 node network above with CD only compensation it is possible to transmit 1.5 Tb·s^{-1} using 6 off PM-32QAM on all connections or by using 6 off PM-32QAM on the longer connection and 5 off PM-64QAM on the shorter connections, saving 1 transmitter. The former gives an optimum SNR margin of 2.2 dB while the latter only 1.9 dB, thus utilising spare bandwidth can improve the SNR margin.

6

Offline Static Network Optimisation

THIS chapter describes the use of the nonlinear quality of transmission model and the transmitter launch power optimisations to maximise the data throughput of a mesh network. The primary aim is to maximise the network throughput by adaptation of the routing, modulation format, DWDM spectrum and transmitter launch power. Where multiple degenerate solutions exist the secondary aims are to minimise the number of transceivers and maximise the available SNR margin for robust transmission. These ideas were first shown at the Optical Network Design and Modeling conference in Stockholm 2014 [175] and published as an extended paper in 2015 [176].

6.1 Outline of Optimisation Process

Figure 6.1 shows a flow diagram that outlines the overall process to optimise the routing and transceiver parameters to maximise the network throughput. The full joint optimisation of the network to maximise the throughput is a complex and nonlinear optimisation. Thus we divide the problem to make it tractable using the heuristics developed in chapter 5.

It has been shown in chapter 5 that the Shannon capacity is maximised for near equal launch powers. The network will also be heavily loaded to achieve the maximum throughput. Thus a worst case SNR based on fully loaded links can be used to initially estimate the highest order modulation format that can be utilised on each route. A pre-solve stage calculates the k-shortest routes between each node pair, the worst case SNR of each route and selects suitable modulation formats as described in section 6.2.

Linear programming techniques can be used to optimally solve the assignment of routes and DWDM channels within the network. Section 6.3 describes a relaxed mixed integer linear program, MILP, that is used to find an upper bound of the network throughput without invoking the wavelength continuity constraint. Section 6.4 details a mixed binary linear program, MBLP, that was used to allocate transmitters to routes and DWDM channels to maximise the network throughput within the constraint of the traffic profile and physical resources. Having found the maximum network throughput the MBLP is re-computed with the secondary objective to minimise the number of transmitters, minimise the likely nonlinear interference and group highly interfering DWDM channels. These processes are described in detail in section 6.4.

Given a network solution with transmitters allocated to routes and DWDM channels the next step is to optimise individual launch powers and assign spectrum to each DWDM channel. The highly interfering channels have been grouped, by the MBLP, as such, following the heuristic from the conclusion of chapter 5, the DWDM channels are not allocated sequential spectral slots but are dispersed to reduce the nonlinear interference. The process of assigning DWDM channels to physical spectrum and optimising individual launch powers is described in section 6.5. The aim of this process is to maximise the available SNR margin given a network solution developed in section 6.4.

If the process of spectral assignment and launch power optimisation reveals a large SNR margin the initial pre-solve stage is re-calculated on the temporary assumption that the modulation formats required SNR can be reduced, allowing higher order modulation, on some routes, than would initially have been allowed. The MBLP, launch power optimisation and spectral assignment are repeated to obtain new network solutions with potentially higher throughput but lower SNR margin. Provided the final SNR margin is greater than 0 dB the new network solution was deemed viable.

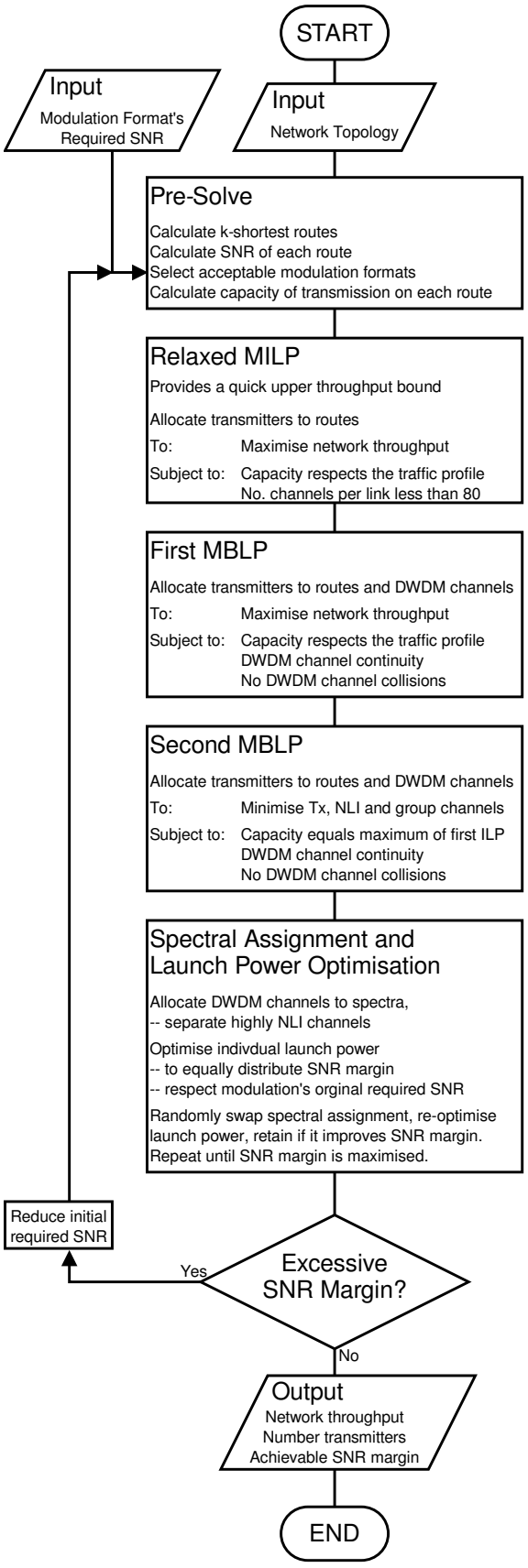

Figure 6.1: Flow diagram to illustrate the overall network optimisation process.

6.2 Pre-solve Stage

As a preliminary stage to solving the network optimisation problem, first the k-shortest routes [177], K=10, between each source-destination node pair were calculated and the worst case SNR, SNR_m, of each route was calculated from equation (6.1).

In order to remove the launch power consideration from the worst case SNR calculation the launch power was set to a constant and equal optimised power and similar to the LOGON [77] strategy all the DWDM channels were considered fully occupied with the optimum constant launch power. This assumption removes the exact routing and DWDM channel allocation from the worst case SNR estimation, decoupling the choice of modulation format from the routing and channel allocation. The symbol SNR of all the channels over a route was taken as the minimum SNR, SNR_m, on the worst case, central, channel such that

$$SNR_m = \frac{p_0}{N_s n_{ASE} + N_s X_{xpm} p_0^3 + N_s^{1+\varepsilon} X_{spm} p_0^3} \tag{6.1}$$

where p_0 is the equal launch power of all the channels, N_s is the number of fibre spans the signal traverses, n_{ASE} is the ASE noise accumulated in a single fibre span, $X_{xpm} = \max_j \sum_{i \neq j} X_{i,j}$, is the maximum nonlinear cross interference efficiency for a fully loaded single span and $X_{spm} = X_{0,0}$ is the nonlinear interference efficiency for SPM added if this has not been compensated, again for a single span. The launch power, p_0, is optimised to maximise the network throughput. In the case that SPM is ideally compensated the optimum launch power is independent of the route length since both noise terms depend linearly on the number of spans and the optimum launch power can be calculated using equation (5.3). For the case where only CD is compensated and SPM is included through the X_{spm} term in equation (6.1) the optimum launch power was found by solving the relaxed routing problem of section 6.3 with different launch powers and selecting the launch power that achieved the greatest throughput.

Given the worst case SNR of each route, the modulation formats where the route SNR exceeds the modulation formats required SNR were chosen for each route from those listed in Table 4.2 and the capacity of each route with each modulation format was calculated.

6.3 A Wavelength Continuity Relaxed Upper Bound

The routing and DWDM channel assignment problem can be considerably reduced by removing the wavelength continuity constraint, effectively assuming that ideal wavelength conversion is possible at every node. This relaxed problem requires the allocation of transceivers to routes from the previously calculated k-shortest routes to provide each node pair with the required capacity while ensuring that the bandwidth usage on any link does not exceed the fibre system bandwidth. There are two popular linear program formulations for solving routing and spectral assignment problems, those based on flow and those based on routes [178, 179]. Since here the channel capacity is route dependent the problem is formulated as a route based mixed integer linear problem, MILP. It should be noted that in this work the traffic matrix is symmetric, $T_{s,d} = T_{d,s}$, and the network is symmetric with fibre pairs, so as is customary the problem is reduced by solving for $d > s$ only.

In order to describe the MILP the following notation was used

Constants:

- N: number of nodes,
- L: number of links,
- K: number of shortest routes,
- W: number of DWDM channels,

Parameters:

- s,d: the source and destination nodes $\in \{1,2,\ldots,N\}$,
- l: a link $\in \{1,2,\ldots,L\}$,
- k: a shortest route $\in \{1,2,\ldots,K\}$,
- w: a DWDM channel $\in \{1,2,\ldots,W\}$,
- $T_{s,d}$: the normalized traffic demand between source, s, and destination ,d,
- $r_{s,d,k}$: the k^{th} shortest route between source, s, and destination ,d,
- $\delta^{L}_{s,d,k,l}$: is set to 1 if route $r_{s,d,k}$ traverses link l, 0 otherwise,

- $C_{s,d,k}$: the capacity of transmission of a single channel over the route $r_{s,d,k}$,

Variables:

- c: the total throughput of the network, a multiplying factor to the normalised traffic matrix **T** to define the actual traffic demand,
- $F_{s,d,k}$: is the number of active transceivers using route $r_{s,d,k}$,

The aim is to optimise c as a continuous variable and $F_{s,d,k}$ as integer variables, to maximise c such that

$$c_{max} = \max_{c,F_{s,d,k}} c \tag{6.2}$$

subject to the total capacity between all source, s, and destination, d, nodes exceeding the demand

$$\sum_{k} F_{s,d,k} C_{s,d,k} - cT_{s,d} >= 0 \qquad \forall \quad s,d > s. \tag{6.3}$$

and the number of signals in any link, l, does not exceed the system bandwidth of W channels,

$$\sum_{k} \sum_{s} \sum_{d>s} F_{s,d,k} \delta^{L}_{s,d,k,l} <= W \qquad \forall \quad l. \tag{6.4}$$

This problem has $1 + K \times N \times (N-1)/2$ variables, equal to 911 for $K = 10$ and $N = 14$, and $L + N \times (N-1)/2$ constraints, equal to 112 for $L = 21$ and $N = 14$. The MILP optimisation was solved using IBM CPLEX® and for the relaxed problem described here the computation took typically a few minutes on a dual quad core computer with 16 threads running at 2.3 GHz.

This relaxed optimisation was used to find the maximum network throughput for the three realistic networks topologies, described in section 3.8, as a function of the transmitter launch power. The optimum launch power that maximised the network throughput was used in subsequent wavelength continuity constrained optimisations. Figure 6.2 shows the relative network throughput found by solving the relaxed MILP optimisation as a function of transmitter launch power, also shown is the relative number of transceivers used to distinguish between equal throughput results. In the case of CD and SPM compensation the optimum launch power was equal to that calculated from equation (5.3) as the nonlinear interference and ASE noise scale linearly with the number of spans. For CD only compensation the optimum launch power was -1.5 dBm for the NSF and DTAG/T-systems network topologies while for CD and SPM compensation the optimum launch power was

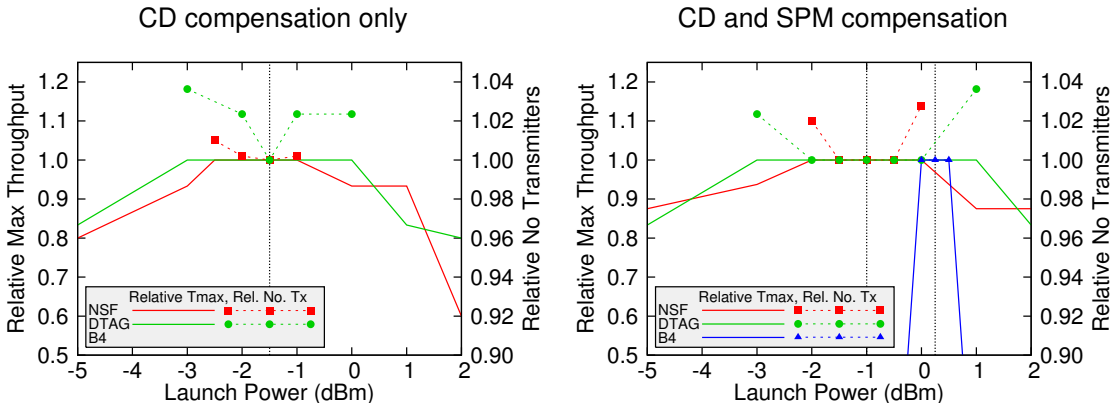

Figure 6.2: The relative maximum network throughput and relative number of transceivers utilised as a function of the launch power for the three network topologies considered. The results are shown for CD compensation only (left) and for CD and SPM compensation (right).

found to be -1.0 dBm for the NSF and DTAG/T-systems topologies. For the Google B4 topology the furthest separated nodes can only be connected error free with PM-BPSK modulation when SPM is compensated and for a wider grid spacing of 100 GHz. Under these conditions the optimum launch power was 0.25 dBm.

Given the optimum launch power the maximum network throughput for the three realistic network topologies described in section 3.8 was found as a function of the number of shortest paths, K. Figure 6.3 shows the relative network throughput found by solving the relaxed MILP optimisation as a function of the number of shortest paths, also shown is the relative number of transceivers used to distinguish between equal throughput. It can be seen that provided $K \geq 3$ the maximum network throughput is obtained for all the networks while for $K \geq 8$ the maximum network throughput utilising the minimum number of transceivers is obtained for all networks. Thus in this work $K = 10$ is used and assumed to be suitable for all the networks in section 3.8 when the wavelength continuity constraint is also applied.

6.4 Routing, Modulation and Channel Assignment

Next, the allocation of DWDM channels to routes was optimised as a mixed binary linear program, MBLP, in order to maximise the traffic throughput. This allows inclusion of the wavelength continuity constraint.

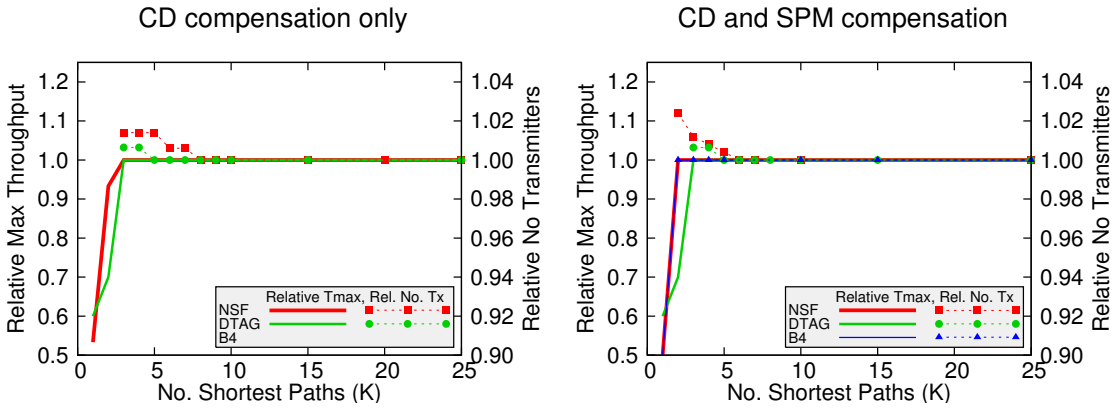

Figure 6.3: The relative maximum network throughput and relative number of transceivers utilised as a function of the number of k-shortest paths considered for the three network topologies considered. The results are shown for CD compensation only (left) and for CD and SPM compensation (right).

In order to describe the MBLP problem the following notation was used

Constants:

- N: number of nodes,
- L: number of links,
- K: number of shortest routes,
- W: number of DWDM channels,
- M: number of modulation formats available over a given route $r_{s,d,k}$,

Parameters:

- s,d: the source and destination nodes $\in \{1,2,\ldots,N\}$,
- l: a link $\in \{1,2,\ldots,L\}$,
- k: a shortest route $\in \{1,2,\ldots,K\}$,
- w: a DWDM channel $\in \{1,2,\ldots,W\}$,
- m: a modulation format $\in \{1,2,\ldots,M\}$,
- $T_{s,d}$: the normalized traffic demand between source, s, and destination ,d,

- $r_{s,d,k}$: the k^{th} shortest route between source, s, and destination ,d,
- $\delta^{L}_{s,d,k,l}$: is set to 1 if route $r_{s,d,k}$ traverses link l, 0 otherwise,
- $SNR^{M}_{s,d,k}$: the worst case symbol SNR for transmission over route $r_{s,d,k}$,
- $C_{s,d,k,m}$: the capacity of transmission on a single channel over the route $r_{s,d,k}$ with modulation format, m,
- $SNR^{R}_{s,d,k,m}$: the required symbol SNR for error free transmission over route $r_{s,d,k}$ with modulation format, m.

Variables:

- c: the total throughput of the network, a multiplying factor to the normalized traffic matrix $\mathbf{T}$ to define the actual traffic demand,
- $\delta^{F}_{s,d,k,m,w}$: is 1 if there is an active transceiver over route $r_{s,d,k}$ using modulation format, m, and DWDM channel w, 0 otherwise.

The aim is to optimise c as a continuous variable and $\delta^{F}_{s,d,k,m,w}$ as binary variables, so that

$$c_{max} = \max_{c,\delta^{F}_{s,d,k,m,w}} c \tag{6.5}$$

subject to the total capacity between all source, s, and destination, d, nodes exceeding the demand

$$\sum_{w}\sum_{m}\sum_{k} \delta^{F}_{s,d,k,m,w} C_{s,d,k,m} - cT_{s,d} >= 0 \qquad \forall \quad s,d > s \tag{6.6}$$

and the number of signals occupying DWDM channel, w, in any link, l, does not exceed 1,

$$\sum_{m}\sum_{k}\sum_{s}\sum_{d>s} \delta^{F}_{s,d,k,m,w}\delta^{L}_{s,d,k,l} <= 1 \qquad \forall \quad l,w. \tag{6.7}$$

The MBLP optimisation was solved using IBM CPLEX® and for the results presented in this paper the computation took typically a few hours on a dual quad core computer with 16 threads running at 2.3 GHz. The optimisation is assisted using prior knowledge of the maximum network throughput obtained from the solution of the relaxed problem.

Given that the maximum network throughput c_{max} has been calculated the MBLP was re-calculated with the secondary objective to group highly interfering channels, for later

separation, while minimising the total number of transmitters and the overall nonlinear interference. Optimise $\delta^F_{s,d,k,m,w}$ as binary variables to

$$\min_{\delta^F_{s,d,k,m,w}} \sum_w \sum_m \sum_k \sum_s \sum_{d>s} \delta^F_{s,d,k,m,w} \left[1000 + \frac{Z_{s,d,k}}{10000} \left(\frac{SNR^R_{s,d,k,m}}{SNR^M_{s,d,k}} \right)^2 \left(\frac{w}{10} + 100 \right) \right] \tag{6.8}$$

subject to the constraints of equations (6.6) and (6.7) where c has been replaced by c_{max}. The large constant in the objective function ensures that the minimum number of transmitters are used. The term $\frac{SNR^R_{s,d,k,m}}{SNR^M_{s,d,k}}$ is the ratio of the modulation formats' required SNR to the basic SNR of the route used in the routing stage, the worst case where all channels are occupied. This ratio is related to the expected transmitter power thus the square multiplied by the route length $Z_{s,d,k}$ denotes the channels likelihood to cause nonlinear interference. By dividing $Z_{s,d,k}$ by 10000 a constant of the order of the maximum of $Z_{s,d,k}$ the weight term $\frac{Z_{s,d,k}}{10000} \left(\frac{SNR^R_{s,d,k,m}}{SNR^M_{s,d,k}} \right)^2$ is of order 1. By weighting the objective function with the channel number, more highly interfering signals will be placed in the lowest available channel number, thus grouping them together. The constant added to the channel weight ensures that nonlinear interference is always more weighted than channel number. The objective function weight increases by order 1000 for additional transmitters, order < 100 for nonlinear interference and order < 10 for higher channel numbers. So this objective function tries to, in order of priority, minimise the number of transmitters, then minimise the nonlinear interference and finally group highly interfering signals. There is still some considerable scope to improve this objective function to more closely achieve these stated aims.

6.5 Launch Power and Spectral Assignment

The symbol SNR of individual channels can be estimated as described in section 4.8. Given that the i^{th} transmitter-receiver pair requires a symbol SNR, SNR^R_i, with an overall margin SNR_{margin} then the launch powers, $\mathbf{p}$ should be minimised to achieve a symbol SNR of $SNR_{margin}\mathbf{SNR}^R$.

The launch powers were iteratively optimised to achieve the required SNR and were initialised based on ASE noise alone using

$$p_i = SNR_{margin}\, SNR^R_i\, n_{ASE,i}. \tag{6.9}$$

For a given network state with launch powers, $\mathbf{p}$ the SNR of the i^{th} signal is given by,

$$SNR_i = \frac{p_i}{n_{ASE,i} + p_i \sum_j \left(X_{i,j}\, p_j^2 \right)} \tag{6.10}$$

where $X_{i,j}$ is an accumulated nonlinear interference as calculated by equation (4.44). The variation of the SNR with launch power around the current network state, $\frac{\mathrm{d}\mathbf{SNR}}{\mathrm{d}\mathbf{p}}$ is given by

$$\frac{\mathrm{d}SNR_i}{\mathrm{d}p_j} = SNR_i^2 \left[\frac{n_{ASE,i=j}}{p_i^2} - 2X_{i,j}\, p_j \right] \tag{6.11}$$

where $n_{ASE,i=j} = n_{ASE,i}$ for $i = j$, zero otherwise. The iteration update is given by

$$\Delta\mathbf{p} = \left(SNR_{margin}\mathbf{SNR}^R - \mathbf{SNR} \right) \left(\frac{\mathrm{d}\mathbf{SNR}}{\mathrm{d}\mathbf{p}} \right)^{-1}. \tag{6.12}$$

In order to improve the speed of convergence and dampen oscillations in the computation the iteration update was restricted at each step by multiplying by $\mu < 1$ where

$$\mu = \begin{cases} \min_i \left(\frac{0.1}{\Delta P_i} \right) & \text{for} \quad \min_i \left(\frac{0.1}{\Delta P_i} \right) < 1 \\ 1 & \text{otherwise} \end{cases} \tag{6.13}$$

the launch powers, $\mathbf{p}$ were then updated as

$$\mathbf{p} := \mathbf{p} + \mu\Delta\mathbf{p} \tag{6.14}$$

the iteration proceeds through equations (6.10) to (6.14) until the launch powers, $\mathbf{p}$, converge. The algorithm was found typically to converge within 20 iterations for ≈ 600 transmitters provided the required SNR with margin can be achieved. It was also found to be prudent to check that $\frac{\mathrm{d}SNR_i}{\mathrm{d}p_i} \geq 0$ as it is possible to achieve a symbol SNR by using too high a launch power, if the condition was false then the i^{th} launch power was reduced to achieve the same SNR on the i^{th} signal, while the other signals will have a slightly increased SNR, before continuing the launch power iteration.

The aim of the launch power optimisation was to maximise the SNR margin equally across all the signals, giving similar error rate performance across the signals. The SNR margin was increased incrementally and at each step the launch power optimised as described. The maximum achievable SNR margin was taken as the largest SNR margin for which a solution to the power optimisation converged and was possible.

The DWDM channels as obtained from the routing modulation and channel assignment MBLP, were then assigned to DWDM spectra. The separation of higher power signals

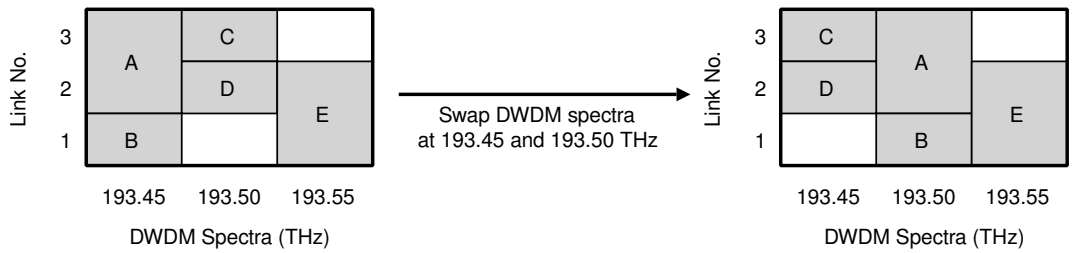

Figure 6.4: Illustration of DWDM spectrum swapping process. A-E refer to transmitted signals, grey block are occupied link-spectral slots. After swapping the spectral continuity and collision free constraints are maintained.

has been shown in section 5.2, and in [34], to give improved overall SNR performance. The assignment was initial done manually to separate the lower channel numbers by assigning them well separated spectra. Since we are considering a fixed grid, each DWDM channel from the solution of section 6.4, is self-contained, there is no spectral contiguity constraint. This allows all of the transmitters operating in a given DWDM channel to be moved to another spectra assignment without disturbing the spectral continuity or collision constraints. Thus we can swap the spectral assignment of one DWDM channel with that of another DWDM channel and this possibility was used to improve the DWDM channel spectral assignment. The process is illustrated in figure 6.4 for a simple network with three links and three DWDM channels. Thus the initial manual assignment was improved by swapping random pairs of DWDM channels and calculating the achievable SNR margin by following the iterative launch power optimisation described above. The new DWDM spectra assignment was then retained if this improved the achievable SNR margin or returned to the original spectral positions if it did not. Random pairs were swapped until no further improvement in achievable margin could be made.

For the NSF network utilising a fixed PM-QPSK modulation format with CD and SPM compensation the MBLP solution gave a worst case SNR margin of 2.8 dB under the equal launch power fully loaded links assumption used in section 6.4, keeping the grouped channel allocation and optimising the launch power gave an achievable SNR margin of 3.8 dB. Figure 6.5 (left) shows the total launch power, summed over all transmitters, in each DWDM channel after the individual launch powers have been optimised as described above but retaining the grouped channel assignments. Following spectral assignment the achievable SNR margin was increased to 4.5 dB and figure 6.5 (right) shows the total launch power, summed over all transmitters, in each DWDM channel, clearly showing that

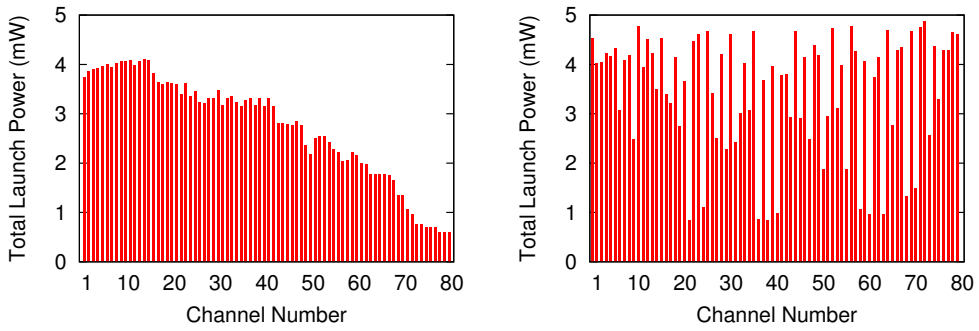

Figure 6.5: Total launch power across all transmitters in each DWDM channel for the NSF network for the fixed PM-QPSK modulation solution with CD and SPM compensation. Initial grouped DWDM channel assignments, giving 3.8 dB SNR margin (left) and Optimal DWDM channel assignments, giving 4.5 dB SNR margin (right).

high power channels have been spectrally separated.

6.6 Example Network Optimisations

For each of the three example networks shown in section 3.8, five network solutions were calculated each for CD only compensation and CD and SPM compensation at the receiver. The solutions differ in the following ways;

1) A baseline optimisation for a go anywhere fixed modulation format, with fixed launch power and worst case SNR assuming full channel occupancy in all links,

2) A go anywhere fixed modulation format as 1) but where the launch power and DWDM channel assignment have been optimised,

3) An adapted modulation format based on a worst case SNR for fixed launch power and assuming full channel occupancy in all links but where the launch power and DWDM channel assignment where subsequently optimised,

4) An adapted modulation format based on improved SNR expectation where the launch power and DWDM channel assignment have been optimised,

5) As 4) but removing the requirement to minimise the number of transmitters.

Beginning with the country scaled DTAG/T-Systems core network of figure 3.3, under the assumption of equal launch power and fully loaded links the SNR of the longest shortest-path route allows PM-32QAM modulation. Thus PM-32QAM is the baseline go anywhere case for this network as it is suitable for transmission between all node pairs. By optimising the routing and channel allocation using the MBLP described in section 6.4 while maintaining the fixed PM-32QAM modulation format a network throughput of 273.0 Tb·s^{-1} was achieved using 1092 transmitters and with a worst case SNR margin of 0.7 dB and 1.1 dB for the CD only and CD and SPM compensation cases respectively. Taking this fixed PM-32QAM routing solution and optimising the launch power and spectral allocation, as described in section 6.5, a SNR margin of 1.7 dB and 2.6 dB was possible, for the CD only and CD and SPM compensation cases respectively.

It is then the aim to utilise this margin to increase the network throughput. First the modulation format was adapted to the route by allowing the MBLP of section 6.4 the choice of all modulation formats on each route that have a required SNR less than the route worst case SNR calculated based on equal launch powers and fully loaded links. The adaptation of the modulation format allowed the number of transmitters to be reduced to 936 while maintaining the network throughput at 273.0 Tb·s^{-1}. To further access this margin the modulation formats required SNR were temporarily reduced during the initial routing, modulation and channel assignment. This allowed the network to increase its throughput slightly to 318.5 Tb·s^{-1} for the CD and SPM compensation case. Finally by removing the requirement to minimise the number of transmitters an increase in network throughput to 282.1 Tb·s^{-1} for the CD only compensated case was possible. Thus using more transmitters operating at with a lower order modulation allows a small improvement in SNR margin and or in the case of CD only compensation a small increase in throughput.

Thus by optimising the routing, modulation, launch power and spectral assignment the throughput has been increased by 3 % and 16 %, for the DTAG/T-Systems core network, over the baseline traditional go anywhere case for CD only and CD and SPM compensation respectively. These results are summarised in table 6.1.

Next consider the larger continental scale NSF network of figure 3.4, under the assumption of equal launch power and fully loaded links the SNR of the longest shortest-path route allows PM-QPSK modulation. Thus PM-QPSK is the baseline go anywhere format for this network as it is suitable for transmission between all node pairs. By

Table 6.1: Summary of results for the DTAG/T-Systems core network.

Optimisation	CD only compensation			CD and SPM compensation		
	Network Throughput ($Tb{\cdot}s^{-1}$)	Number of Transmitters	SNR Margin (dB)	Network Throughput ($Tb{\cdot}s^{-1}$)	Number of Transmitters	SNR Margin (dB)
1) Fixed PM-32QAM (MILP on worst SNR) Equal power Fully loaded links	273.0	1092	0.7	273.0	1092	1.1
2) Fixed PM-32QAM (MILP on worst SNR) Optimised power and channel assignment	273.0	1092	1.7	273.0	1092	2.6
3) Adapted PM-mQAM (MILP on worst SNR) Optimised power and channel assignment	273.0	936	0.8	273.0	936	1.6
4) Adapted PM-mQAM (MILP optimistic SNR) Optimised power and channel assignment	273.0	936	0.8	318.5	1018	0.3
5) Adapted PM-mQAM (MILP optimistic SNR and unlimited Tx) Optimised power and channel assignment	282.1	1650	0.2	318.5	1708	0.5

optimising the routing and channel allocation using the ILP described in section 6.4 while maintaining the fixed PM-QPSK modulation format a network throughput of 109.2 $Tb{\cdot}s^{-1}$ was achieved utilising 1092 transmitters and with a worst case SNR margin of 2.1 dB and 2.8 dB for the CD only and CD and SPM compensation cases respectively. Taking this fixed PM-QPSK routing solution and optimising the launch power and spectral allocation, as described in section 6.5, a SNR margin of 3.1 dB and 4.5 dB was possible for the CD only and CD and SPM compensation cases respectively.

Allowing the MILP of section 6.4 the choice of all modulation formats on each route that have a required SNR less than the worst case route SNR calculated based on equal launch powers and fully loaded links increased the network throughput to 136.5 $Tb{\cdot}s^{-1}$ and 145.6 $Tb{\cdot}s^{-1}$ using 1004 transmitters for the CD only and CD and SPM compensation cases respectively. Following optimisation of the launch power and spectral allocation a SNR

Table 6.2: Summary of results for the NSF network.

Optimisation	CD only compensation			CD and SPM compensation		
	Network Throughput ($Tb{\cdot}s^{-1}$)	Number of Transmitters	SNR Margin (dB)	Network Throughput ($Tb{\cdot}s^{-1}$)	Number of Transmitters	SNR Margin (dB)
1) Fixed PM-QPSK (MILP on worst SNR) Equal power Fully loaded links	109.2	1092	2.1	109.2	1092	2.8
2) Fixed PM-QPSK (MILP on worst SNR) Optimised power and channel assignment	109.2	1092	3.1	109.2	1092	4.5
3) Adapted PM-mQAM (MILP on worst SNR) Optimised power and channel assignment	136.5	1004	1.2	145.6	1004	2.0
4) Adapted PM-mQAM (MILP optimistic SNR) Optimised power and channel assignment	145.6	1036	0.7	182.0	1034	0.2
5) Adapted PM-mQAM (MILP optimistic SNR and unlimited Tx) Optimised power and channel assignment	154.7	1400	0.1	182.0	1484	0.5

margin of 1.2 dB and 2.0 dB was achieved. Temporarily reducing the modulation formats required SNR during the initial routing, modulation and channel assignment allowed a network throughput of 145.6 $Tb{\cdot}s^{-1}$ and 182.0 $Tb{\cdot}s^{-1}$ utilising 1036 and 1034 transmitters and following launch power and spectral allocation achieved a SNR margin of 0.7 dB and 0.2 dB. Finally by removing the requirement to minimise the number of transmitters allowed a network throughput of 154.7 $Tb{\cdot}s^{-1}$ and 182.0 $Tb{\cdot}s^{-1}$ utilising 1400 and 1484 transmitters and following launch power and spectral allocation achieved a SNR margin of 0.1 dB and 0.5 dB.

Thus by optimising the routing, modulation, launch power and spectral assignment the throughput has been increased by 41 % and 66 %, for the NSF network, over the baseline traditional go anywhere case for CD only and CD and SPM compensation respectively. These results are summarized in table 6.2.

Finally considering the much longer, inter-continental scale Google B4 network of figure 3.5 under the assumption of equal launch power and fully loaded links it is not possible to transmit the lowest order modulation format, PM-BPSK across the longest shortest-path route. In order to achieve a SNR suitable for PM-BPSK on the longest shortest-path route under the assumption of equal launch power and fully loaded links it was necessary to increase the channel spacing to 100 GHz and reduce the number of channels to 40. It was also necessary to use CD and SPM compensation at the receiver. By optimising the routing and channel allocation a baseline network throughput of 13.2 Tb·s^{-1} was achieved using 264 transmitters with a worst case SNR margin of 0.1 dB. Taking this fixed PM-BPSK routing solution and optimising the launch power and spectral assignment a SNR margin of 2.0 dB was possible.

To improve the network throughput the modulation format was adapted to the route by allowing the MBLP of section 6.4 the choice of all modulation formats on each route that have a required SNR less than the route worst case SNR calculated based on equal launch powers and fully loaded links. This allowed a network throughput of 26.4 Tb·s^{-1} utilising 304 transmitters and following launch power and spectral assignment optimisation a margin just above 0.2 dB was achieved. No further improvement in network throughput or SNR margin could be achieved by either reducing the initial SNR requirement or removing the requirement to minimise the number of tranmsitters.

Thus by optimising the routing, modulation, spectral assignment and launch power the throughput has been increased by 100 %, for the Google B4 network, over the baseline traditional route independent case. These results are summarised in table 6.3.

Figure 6.6 summarises the network throughput for each of the three test topologies for the baseline and optimised cases. It has been shown that for each of these three network topologies, with quite different diameters, the optimisation of the launch power and channel spectra assignment leads to an increase in the SNR margin of about 1 dB and 1.7 dB for the CD only and CD and SPM compensation cases respectively, for the fixed go anywhere baseline modulation format. This margin can be traded to increase the average modulation format order by approximately 1 b·s^{-1}·Hz^{-1}·pol^{-1} for each 3 dB of SNR margin, increasing the network throughput. For the smallest diameter DTAG/T-Systems National core network where the fixed modulation format is PM-32QAM, 5 b·s^{-1}·Hz^{-1}·pol^{-1}, the 1.7 dB and 2.6 dB SNR margins should allow an increase of 10 %

Table 6.3: Summary of results for the Google B4 network.

Optimisation	CD only compensation			CD and SPM compensation		
	Network Throughput ($Tb{\cdot}s^{-1}$)	Number of Transmitters	SNR Margin (dB)	Network Throughput ($Tb{\cdot}s^{-1}$)	Number of Transmitters	SNR Margin (dB)
1) Fixed PM-BPSK (MILP on worst SNR) Equal power Fully loaded links				13.2	264	0.1
2) Fixed PM-BPSK (MILP on worst SNR) Optimised power and channel assignment				13.2	264	2.0
3) Adapted PM-mQAM (MILP on worst SNR) Optimised power and channel assignment				26.4	304	0.2
4) Adapted PM-mQAM (MILP optimistic SNR) Optimised power and channel assignment				26.4	304	0.2
5) Adapted PM-mQAM (MILP optimistic SNR and unlimited Tx) Optimised power and channel assignment				26.4	420	0.2

and 17 % in network throughput for the CD only and CD and SPM compensation cases respectively. For the NSF network where the fixed modulation format is PM-QPSK, 2 $b{\cdot}s^{-1}{\cdot}Hz^{-1}{\cdot}pol^{-1}$, the 3.1 dB and 4.5 dB SNR margin should allow an increase of 50 % and 75 % in network throughput for the CD only and CD and SPM compensation cases respectively. Finally for the Google B4 network where the fixed modulation format is PM-BPSK, 1 $b{\cdot}s^{-1}{\cdot}Hz^{-1}{\cdot}pol^{-1}$, the 2.0 dB SNR margin should allow a 66 % improvement in network throughput. These expected improvements in network throughput are in general observed in the final optimised solutions. Thus it is seen the improvement in network throughput as a result of modulation format, spectrum and launch power assignment improves for longer networks as they start from a lower spectral efficiency such that adaptation can give a fractionally larger improvement.

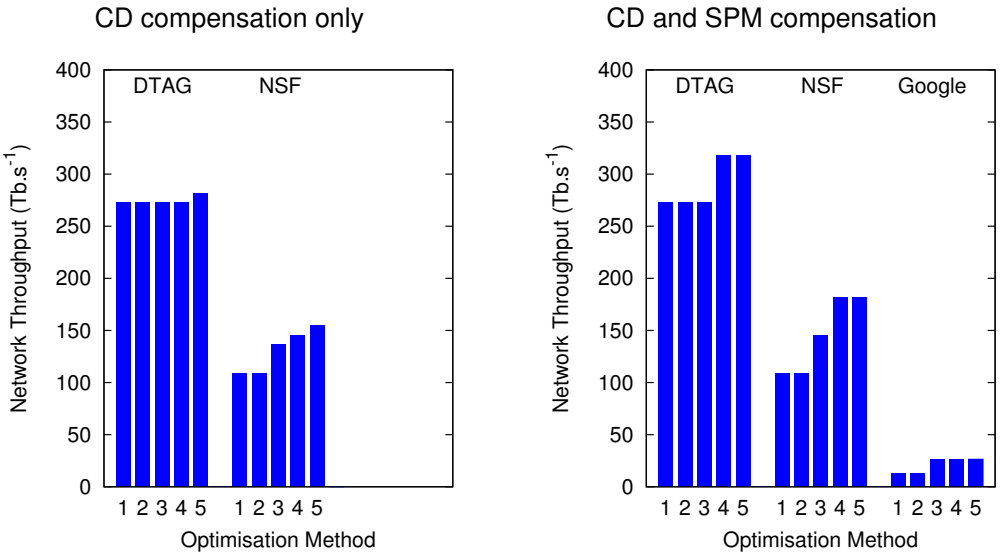

Figure 6.6: Total network throughput for the three test topologies for five different routing, wavelength and launch power assignment strategies, as described in section 6.6.

6.7 Adapting the FEC Overhead

In the previous sections, routing, modulation format, spectrum and launch power assignment was carried out to maximise the network throughput for a given traffic profile. Remaining with the fixed grid, fixed symbol rate paradigm there is still the option to adapt the FEC OH. That is, it is possible to use a higher FEC OH with stronger error correction to allow transmission with poor SNR at the expense of a reduced data throughput. The ideas of this section were presented at OFC 2015 [180].

In a network the different routes inevitably lead to signals with different SNR and the optimal use or control of this SNR is critical to better utilise the network resources. In the previous sections the network resources were more fully utilised by adapting the launch power, effectively adapting the signal SNR to that required by the modulation format. Adaptive FEC OH allows the adaptation of the required SNR to the SNR of the signal. However adapting the FEC OH leads to non-standard data rates which may cause complications with the client network interfaces. In this section the performance of square mQAM modulation formats with 100 Gb·s^{-1} client data rate granularity and adapting the routing, modulation format, spectrum and launch power assignment was compared with using a fixed launch power and adapting the routing, modulation format, spectrum and

FEC OH assignment with a 10 Gb·s^{-1} client data granularity.

Consider HD-FEC where the receiver output is an uncorrected binary sequence and this is subsequently independently corrected to give the client data. For an ideal binary symetric channel with a pre-FEC BER, P_b, the maximum hard decision code rate, R_c, that results in error free transmission is given by [87]

$$R_c = 1 + P_b \log_2(P_b) + (1 - P_b) \log_2(1 - P_b) \tag{6.15}$$

such that for PM-QPSK modulation at 32 GBaud the maximum error free information rate is $32 \times 4 \times R_c$ Gb·s^{-1}. Allowing a further 5 % overhead for the OTU framing leads to a maximum client data rate $\frac{1}{1.05} 32 \times 4 \times R_c$ Gb·s^{-1} for PM-QPSK modulation.

To solve the network optimisation problem it is necessary to find the required SNR for each client data rate considered, that is, for a given data rate choose the modulation format and FEC OH to minimise the required SNR for error free transmission. The client data rates will be in multiples of 10 GbE with 5 % framing OH, a data rate granularity of 10.5 Gb·s^{-1}. So for each modulation format the required code rate can be calculated thence from equation (6.15) the required pre-FEC BER, P_b can be found and finally the required SNR to achieve this pre-FEC BER can be calculated given the modulation format chosen. The required SNR for client data rates of 10 and 100 Gb·s^{-1} granularity transported using PM-QPSK, PM-16QAM, PM-64QAM and PM-256QAM are shown in table 6.4 and illustrated in figure 6.7. Note that the required SNR is slightly lower than in table 4.2 since here ideal HD-FEC is considered while previously a realised HD-FEC was considered. While these ideal HD-FEC codes may not exist realised soft decision FEC can achieve similar performance.

The use of variable FEC OH increases the possible network optimisation possibilities and complexity. The work presented at OFC [180] considered two network optimisation strategies to utilise the available network resources. The use of multiples of a fixed 100 GbE client rate and adapting the SNR through power adaptation to meet the required SNR for the modulation format following the network optimisation process of sections 6.2 to 6.5. Alternatively the use of a multiple of a 10 GbE client rate with adapted FEC OH utilising the full list of formats and coding rates taken from table 6.4 and the network optimisation process of sections 6.2 to 6.4.

Table 6.5 and 6.6 shows the throughput results for the 14-node 21-link NSF network topology and the 14-node 23-link DTAG/T-Systems national core network topology. Also

Table 6.4: Modulation formats, data rates and required symbol SNRs for the 32 GBaud variable code rate signals used.

Modulation Format	Code Rate	Information ($Gb{\cdot}s^{-1}$)	Client Data ($Gb{\cdot}s^{-1}$)	Required SNR (dB)
PM-QPSK	0.41	52.5	50	0.6
PM-QPSK	0.49	63.0	60	1.7
PM-QPSK	0.57	73.5	70	2.7
PM-QPSK	0.66	84.0	80	3.6
PM-QPSK	0.74	94.5	90	4.6
PM-QPSK	0.82	105.0	100	5.7
PM-16QAM	0.45	115.5	110	6.7
PM-16QAM	0.49	126.0	120	7.3
PM-16QAM	0.53	136.5	130	8.0
PM-16QAM	0.57	147.0	140	8.6
PM-16QAM	0.62	157.5	150	9.1
PM-16QAM	0.66	168.0	160	9.7
PM-16QAM	0.70	178.5	170	10.3
PM-16QAM	0.74	189.0	180	10.9
PM-16QAM	0.78	199.5	190	11.5
PM-16QAM	0.82	210.0	200	12.1
PM-16QAM	0.86	220.5	210	12.8
PM-16QAM	0.90	231.0	220	13.5
PM-16QAM	0.94	241.5	230	14.5
PM-64QAM	0.66	252.0	240	15.0
PM-64QAM	0.68	262.5	250	15.5
PM-64QAM	0.71	273.0	260	15.9
PM-64QAM	0.74	283.5	270	16.4
PM-64QAM	0.77	294.0	280	16.8
PM-64QAM	0.79	304.5	290	17.3
PM-64QAM	0.82	315.0	300	17.7
PM-64QAM	0.85	325.5	310	18.2
PM-64QAM	0.88	336.0	320	18.8
PM-64QAM	0.90	346.5	330	19.3
PM-64QAM	0.93	357.0	340	20.0
PM-64QAM	0.96	367.5	350	20.9
PM-256QAM	0.74	378.0	360	21.7
PM-256QAM	0.76	388.5	370	22.1
PM-256QAM	0.78	399.0	380	22.4
PM-256QAM	0.80	409.5	390	22.8
PM-256QAM	0.82	420.0	400	23.2
PM-256QAM	0.84	430.5	410	23.6
PM-256QAM	0.86	441.0	420	24.1
PM-256QAM	0.88	451.5	430	24.5
PM-256QAM	0.90	462.0	440	25.0
PM-256QAM	0.92	472.5	450	25.5

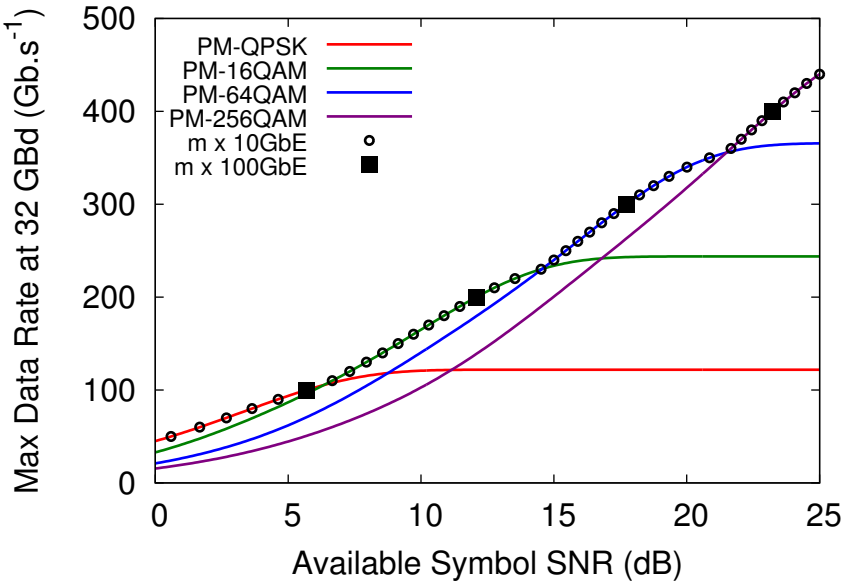

Figure 6.7: Graph of client data rate versus symbol SNR for various code rate and modulation formats.

Table 6.5: Network throughput solutions for NSF network topology with variable rate ideal HD FEC

	Network throughput ($Tb{\cdot}s^{-1}$) and Achievable SNR margin (dB)	
	CD only compensation	CD and SPM compensation
Fixed 100 GbE 22% FEC OH	109.2 (4.2)	109.2 (5.9)
Adapted m×100 GbE 22% FEC OH Adapted launch power	145.6 (1.2)	200.2 (0.2)
Adapted Modulation Variable FEC OH m×10 GbE steps	191.1 (0.8)	203.8 (0.9)

Table 6.6: Network throughput solutions for DTAG/T-Systems network topology with variable rate ideal HD FEC

	Network throughput ($Tb{\cdot}s^{-1}$) and Achievable SNR margin (dB)	
	CD only compensation	CD and SPM compensation
Fixed 200 GbE 22% FEC OH	218.4 (5.4)	218.4 (6.9)
Adapted m×100 GbE 22% FEC OH Adapted launch power	316.7 (0.6)	325.8 (1.5)
Adapted Modulation Variable FEC OH m×10 GbE steps	327.6 (0.9)	327.6 (0.9)

shown is the achievable SNR margin with launch power optimisation in each case, this serves to highlight the finer differences between CD only compensation and full CD and SPM compensation. The largest network throughput was achieved using the finer granularity m×10 GbE transmission rates with SPM compensation for the NSF network and using launch power adaptation for the DTAG network giving an overall increase in network throughput of 87 % and 50 % from the baseline for the two networks considered. Where SPM is compensated, launch power adaptation can allow m×100 GbE fixed clients to give a comparable network throughput to that using variable client rates in both networks. When using adapted modulation with adapted FEC OH the effect of compensating SPM increases the network throughput by just 7 % and 3 % for the two networks.

These results suggest that there is a choice of approaches that both give broadly similar gains in network throughput. Use a m×100 GbE client rate with launch power adaptation a more complex routing and spectral assignment to minimise nonlinear interference and perhaps SPM compensation or use a m×10 GbE variable client rate with a more complex FEC algorithm. The choice between these solutions will depend on the clients preference for a fixed 100 GbE data rate versus a variable client data rate weighted against the complexity of implementing more complex routing and spectral assignment, SPM compensation and adapted FEC.

7

Online Sequentially Loaded Networks

THE following work on sequentially loaded optical networks was undertaken in collaboration with BT at Adastral Park. The overall aim of the work was to better include the physical effects of nonlinearity in network simulations. BT provided a network simulation tool written in C# which included their 20+2 node UK core topology. Two pieces of work have resulted from this collaboration, an investigation of the network blocking load as a function of launch power [162] and an investigation of the use of lower bit rate lanes to avoid stranded capacity[1]. Throughout this chapter the launch power is set to be uniform across all channels. The novelty of the work is to include nonlinear effects through the GN model into network simulations. There is considerable scope to extend this work for example, by adapting launch power and by considering dynamic networks where demands are removed as well as added.

[1] A journal paper describing this work is in preparation.

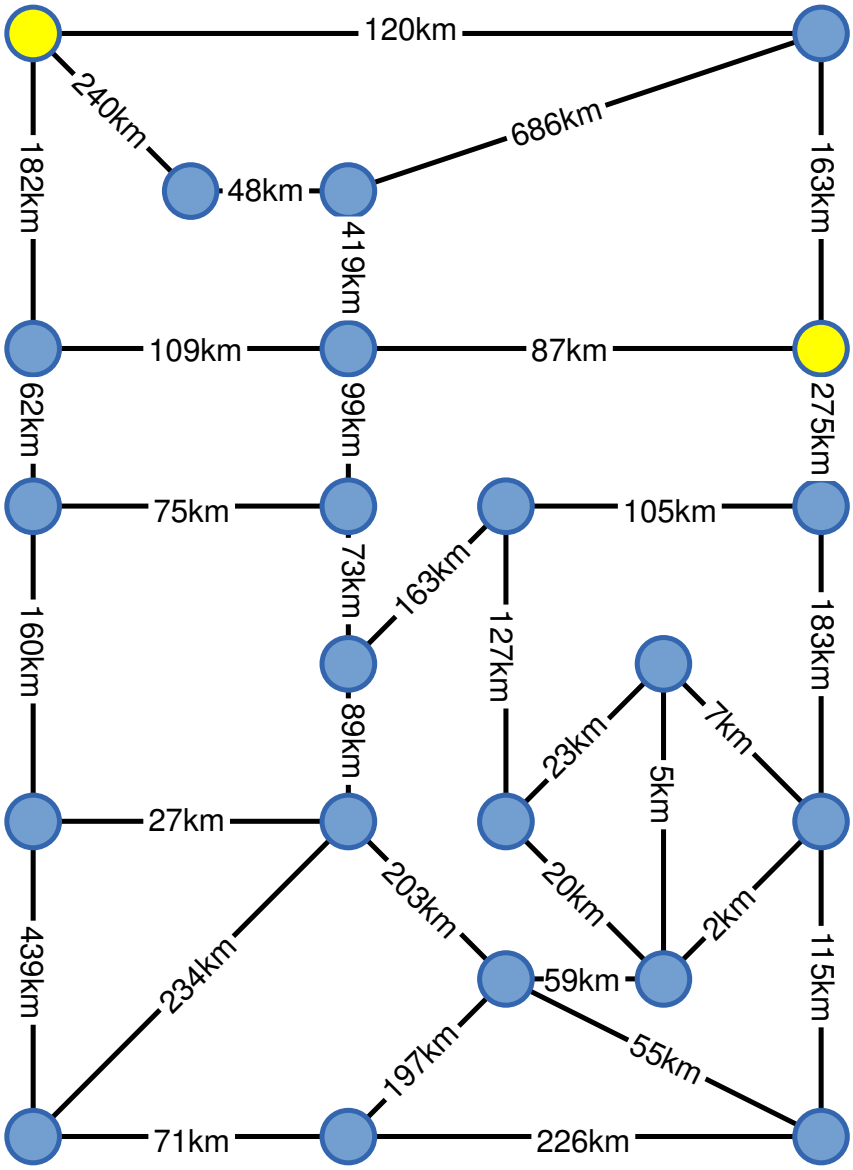

Figure 7.1: The BT 20+2 node UK core topology [29] showing link lengths in (km). The two yellow nodes do not supply or receiver traffic and are for routing purposes only.

7.1 BT Core Topology Parameters

This chapter utilises a different set of network parameters from the rest of this thesis to better reflect the network of BT, as such table 7.1 contains the fibre and system parameters used for the sequentially loaded network simulations. Figure 7.1 illustrates the BT 20+2 node UK core network topology and shows the link lengths used. The two yellow nodes do not supply or receive traffic and are included only for routing purposes.

One important difference in this network is the range of link lengths which can not

Table 7.1: Simulation parameters for the BT 20+2 node core network used throughout chapter 7.

Parameter	Symbol	Value	
Fibre Parameters			
Attenuation Coefficient		0.25	$dB \cdot km^{-1}$
	α	0.0576	km^{-1}
Chromatic Dispersion Coefficient		16.7	$ps \cdot nm^{-1} \cdot km^{-1}$
	β_2	-21.3	$ps^2 \cdot km^{-1}$
Nonlinear Coefficient	γ	1.3	$W^{-1} \cdot km^{-1}$
Amplifier Parameters			
Noise Figure	NF	4.5	dB
Max. Span Length		60	km

be satisfactorily rounded to a single realistic span length. Thus the network contains a large range of span lengths. To avoid repeated numerical integration of the GN model an approximation to describe the nonlinear interference with span length was required. As written in the GN model equation [41, (1)] it appears that the nonlinear interference scales with effective length squared L_{eff}^2 however it should be noted that $\rho(f_1, f_2, f)$ contains L_{eff}^{-2} effectively cancelling out this dependence and hence L_{eff} does not appear in equation (4.17).

From equation (4.22) and (4.23) it can be seen that when $4\pi^2\beta_2(f_1 - f)(f_2 - f)L_s$ is approximately 0, that is either $L = 0$, $(f_1 - f) = 0$ or $(f_2 - f) = 0$, i.e. for short spans or SPM interference then the cos term tends to 1 and the GN model scales as $(1 - e^{-\alpha L})^2$. When $L >> 0$ and $(f_1 - f) >> 0$ or $(f_2 - f) >> 0$, that is for reasonable spans and XPM interference then the GN model scales as $(1 - e^{-2\alpha L})$. This can be understood physically in that for SPM or short lengths where the dispersion is small the nonlinear interference scales coherently, with L_{eff}^2. For longer lengths and XPM the nonlinear interference scales incoherently due to the rapid walk off between the signals and increases linearly with the effective squared power length.

In the work of section 7.3, the nonlinear interference factor for a single span was calculated by numerical integration for a limited number of channel separations and span lengths and then estimated by interpolation to obtain the actual factor for a specific channel

separation and span length as required. The interpolation was carried out such that for $\Delta f = 0$, that is for SPM interference $X(0, L_s)$ is a one dimensional interpolation in the space $(1 - e^{-\alpha L_s})^2$ while for XPM interference $X(\Delta f, L_s)$ was a two dimensional interpolation in the space $\frac{1}{\Delta f}, (1 - e^{-2\alpha L_s})$. The numerical integration was carried out for channel spacings $\Delta f = 0, 75, 150, 225, 300, 375, 450, 600, 900, 1350, 1800, 2250, 4950$ and for span lengths $L = 2, 5, 7, 20, 40, 60$. The interpolation error was estimated by calculating the difference between the numerical integration and the interpolation midway between these points and was found to be less than 0.11 dB.

In the work of section 7.4 the equal launch power, fully loaded network paradigm was assumed and there is no need to calculate $X(\Delta f, L)$ but merely $X_m(L)$, the worst case nonlinearity factor as a function of span length. The worst case nonlinearity factor $X_m(L)$ was calculated by numerical integration of the GN model over the whole c-band for a limited number of span lengths. Considering the forms of the length dependence used above, it was found that $X_m(L)$ could be well approximated by

$$X_m(L) = X_m(\infty) \left[1 - \mathrm{e}^{-a_0 L}\right]^{a_1} \tag{7.1}$$

where for 100 channels spaced at 50 GHz operating at 32 Gbaud with Nyquist sinc pulses, $X_m(\infty) = 8.26 \times 10^{-4}$ mW^2·span^{-1} is the NLI for an infinite long span obtained by numerical integration of the GN model and a_0 and a_1 where found to be 0.0988 km^{-1} and 1.19 respectively by fitting the numerical data to minimise the sum of squares of the error between the analytic equation and the numerical results. The numerically integrated and analytical estimation of $X_m(L)$ are compared in figure 7.2 where the RMS difference was found to be 1.3×10^{-6} mW^{-2}·span^{-1}.

7.2 Simulation Methodology

The network simulation tool allows the simulation of a sequentially loaded BT 20+2 node UK core network. Uniformly chosen bi-directional traffic demands were sequentially applied to the network. The network simulation tool accept or blocks the demands following a routing procedure utilising the available network resources and a pool of transmitter profiles. The transmitter profiles contain the capacity and required signal SNR for transmission using a given symbol rate, modulation format and FEC overhead.

A number of demands much greater than the expected network capacity were

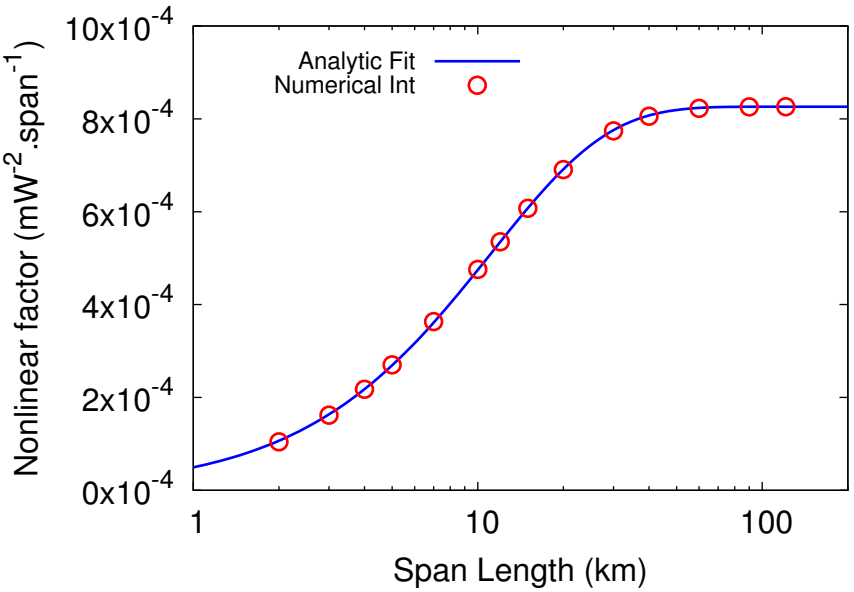

Figure 7.2: Graph of worst case nonlinear interference factor versus span length. Values for 100 channels on a 50 GHz grid operating at 32 Gbaud with Nyquist sinc pulses.

sequentially applied to the network and the network simulation tool records a running total of the number of demands accepted and blocked in the network. The simulation was repeated 10000 times to improve the statistics and the average number of accepted and blocked demands calculated as a function of the number of demands requested. The cumulative blocking probability after the i^{th} demand was calculated as, CBP_i,

$$\text{CBP}_i = \frac{\text{Block}_i}{i} \tag{7.2}$$

where Block_i is the mean accumulated blocking after the i^{th} demand. The probability that the next demand will be blocked, BP_i was calculated from the cumulative blocking probability as

$$\text{BP}_i = (i+1)\,\text{CBP}_{i+1} - i\,\text{CBP}_i \tag{7.3}$$

for a network accepted load after the i^{th} demand given by

$$\text{Load}_i = i\ (1-\text{CBP}_i)\,. \tag{7.4}$$

Table 7.2: Modulation formats, data rates and required symbol SNRs for the 56 GBaud signals used.

Modulation Format	Client Data ($Gb{\cdot}s^{-1}$)	Required SNR (dB)
PM-BPSK	100	5.5
PM-QPSK	200	8.5
PM-8QAM	300	12.5
PM-16QAM	400	15.1
PM-32QAM	500	18.1
PM-64QAM	600	21.1
PM-128QAM	700	23.9
PM-256QAM	800	26.8

7.3 Investigation of Optimal Launch Power

This work presented at OFC 2014 [162] showed an investigation to understand how the launch power affected the network load at 1% blocking probability and how best to include the nonlinear interference into the network model. The nonlinear interference was included based both on the actual network state and also as a worst case based on a channel in the centre of a fully loaded DWDM band where each channel is launched with equal power. For comparison an ASE noise only case was considered without nonlinear interference.

A fixed 75 GHz grid was used with 56 Gbaud signals utilising a root raised cosine shape with roll off 0.25. The transceivers were chosen from the pool shown in table 7.2 and have 100 $Gb{\cdot}s^{-1}$ client data granularity.

The demands were processed in the following way. If an active transceiver between the source and destination nodes has an SNR suitable for the next higher modulation format then the transceiver was uprated and the demand accept. In the absence of a suitable active transceiver the shortest route[2] (based on number of hops) between the source and destination was calculated and the available continuous spectrum checked. If spectrum was available then the first fit wavelength was assigned for a new transceiver. The SNR of the route was checked to ensure its suitability for PM-BPSK, the lowest order modulation format and the SNR of all the existing transceivers checked to ensure there was no detrimental effect on them. If all these conditions were satisfied the demand was accepted onto the new active transceiver if not the demand was deemed to have been

[2]In this first work with sequential networks only the shortest route between nodes was considered.

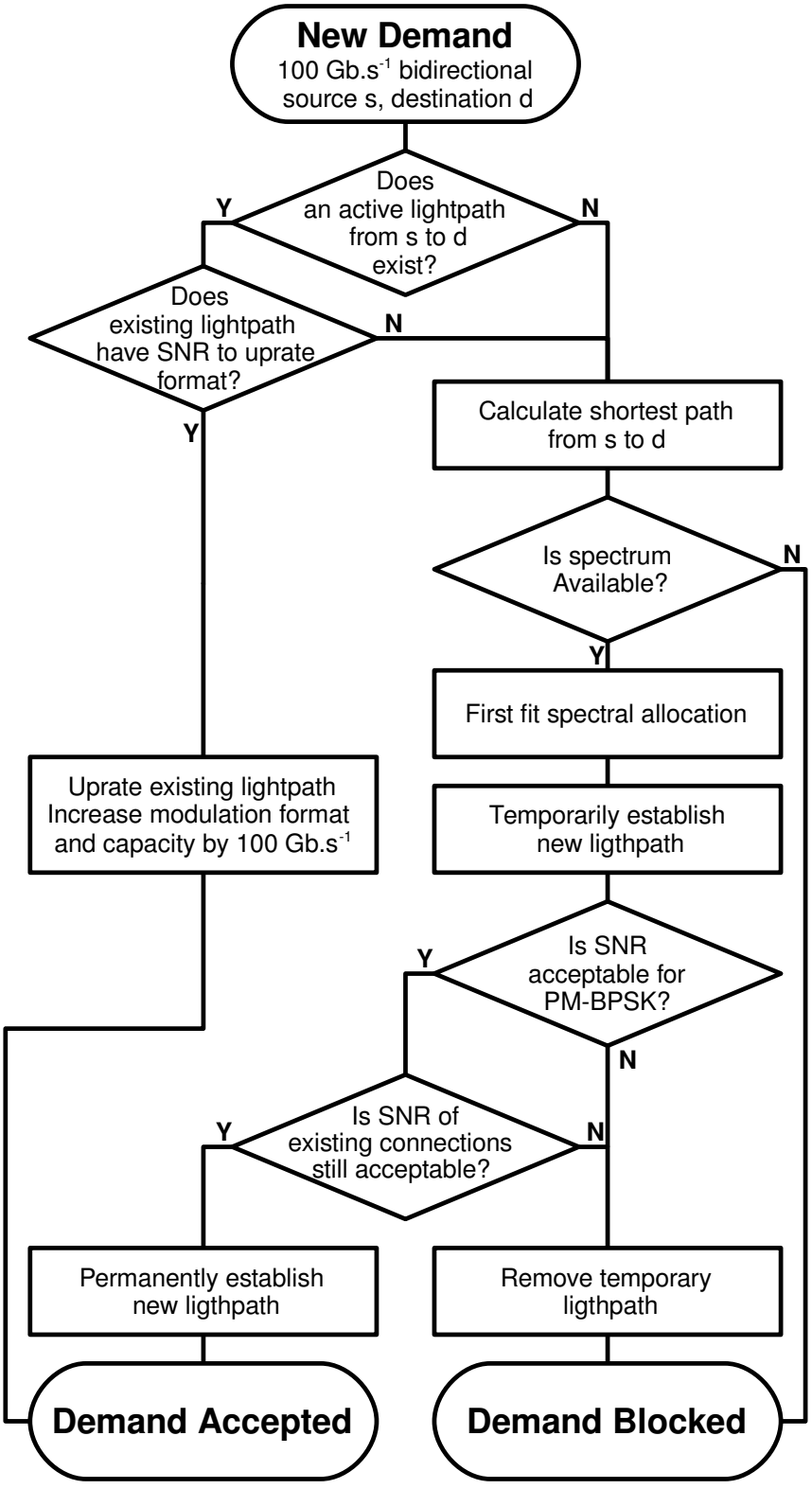

Figure 7.3: Flow chart of the routing and demand acceptance process.

blocked. The demand acceptance process is illustrated in the flow chart of figure 7.3.

3000 bidirectional demands were generated between uniformly random source and

destination pairs each with 100 Gb·s^{-1} capacity. These demands were applied to the network as described above and the cumulative blocking probability recorded. The blocking probability as a function of accepted load was calculated using equations (7.3) and (7.4). Finally the network load where the blocking probability was estimated to be 1 % was calculated by a quadratic fit of the blocking probability versus load over a blocking probability range of 0.3 % to 2 %. Figure 7.4 shows the 1 % blocking load of the BT 20+2 node UK core network as a function of the transmitter power for three nonlinear interference models.

- The linear case corresponds to the case where nonlinear interference has been neglected and X had been set to zero everywhere. In this case as the transmitter power is increased the highest order modulation and thus information capacity increases without bound.

- The greedy case corresponds to the case where each channel calculates its SNR based on the existing channel occupancy. We call this the greedy case since it does not take into account the future requirements of other channels. Future channel allocations will increase the nonlinear interference on existing channels leading to cross blocking.

- The egalitarian case corresponds to the limit where each channel calculates its symbol SNR assuming all the channels are fully loaded. In this case there is no problem of cross blocking of future channels as the SNR already accounts for the links being fully loaded.

Figure 7.4 shows that in the absence of nonlinear transmission the blocking load increases linearly with the logarithm of the transmitter launch power as expected from the Shannon information capacity equation. Including nonlinear interference through the GN model based on the actual network state, the greedy approach, leads to a significant decrease of the blocking load at moderate and higher launch powers. This greedy approach is so called since a channel that utilises all of the available SNR resource will cause blocking of future channels on the links it occupies since it is unable to tolerate any further nonlinear interference and future channels will be blocked during set up as a result of this cross channel blocking. In the egalitarian case all the channels assume that the network may become fully loaded and calculate SNR accordingly. Since the links are assumed to

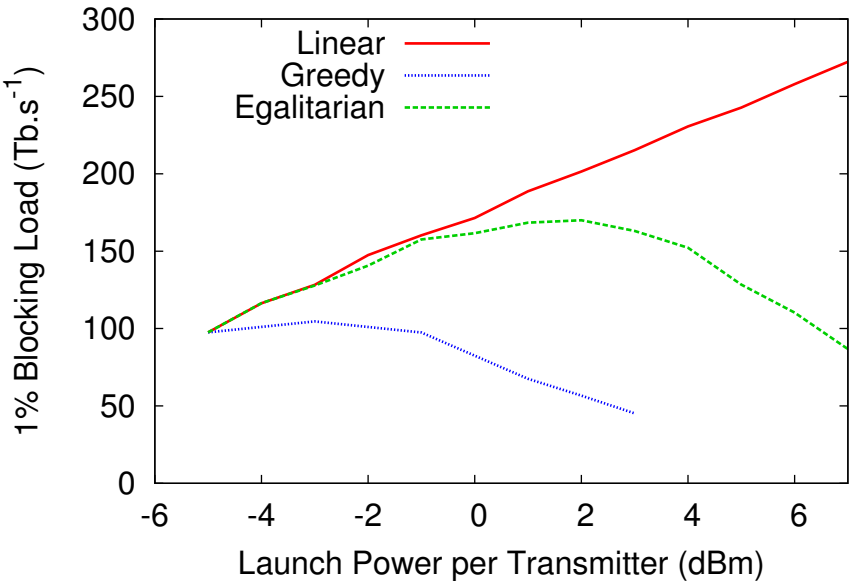

Figure 7.4: 1% blocking load as a function of launch power for the BT 20+2 node core network.

be fully loaded the addition of any future channels will not cause detrimental degradation to any of the existing channels. Thence the blocking load follows the linear performance at low launch powers while the blocking load is seen to decrease in the high launch power regime twice as fast as it increases, this was expected from the form of the SNR equation. Thus from an engineering tolerance perspective it is better to launch too little power than too much. The egalitarian approach gives both better performance, is easier to implement and more robust.

7.4 Investigation of the Utilisation of 25 GbE Lanes

In a wavelength routed optical network signals travel a variety of distances and routes and experience a variety of impairments leading to different signal SNRs. Thus the theoretical maximum error free spectral efficiency varies across the network. Contemporary networking has client side data rates that are fixed, for example following the Ethernet standard with 100 GbE client data rates such that transport networks are designed to transport multiples of 100 $\text{Gb}\cdot\text{s}^{-1}$ client data.

The variety of transmitted signal SNRs can be fully utilised with adaptive modulation and adaptive FEC OH [40, 88, 181] or alternatively the signal launch power can be adapted to effectively transfer SNR margin between channels to fit the required SNR of an adapted

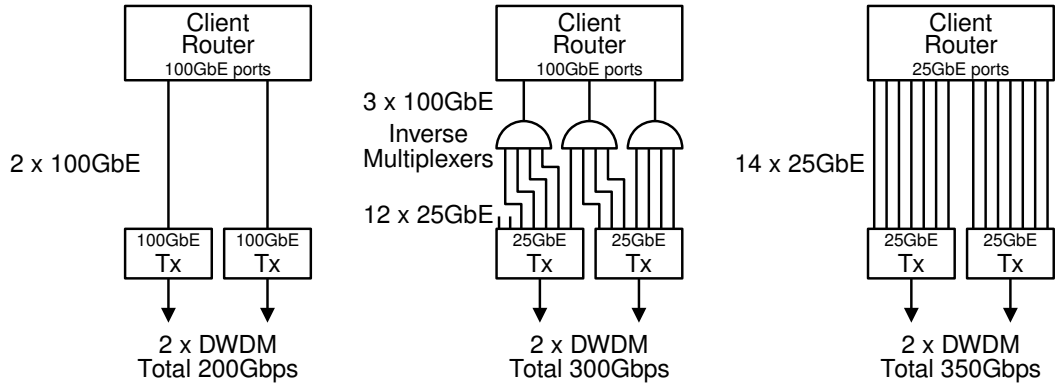

Figure 7.5: Illustration of the transceiver connection options considered.

modulation, fixed FEC overhead 100 GbE granularity [180]. The later requires more complex routing and wavelength assignment algorithms [175] and may not be suitable for sequential or dynamically loaded networks. The former leads to a variety of spectral efficiencies. Elastic bandwidth and flexible grids [62, 63] could be used to maintain a fixed client rate by adjusting the symbol rate for a given spectral efficiency but this again leads to more complex routing and wavelength assignment and the difficulties of spectral fragmentation with stranded bandwidth.

So consider the simpler paradigm of a fixed optical grid, fixed optimised launch power and use an adapted modulation and adaptive FEC OH leading to a variety of data rates. This simplifies the routing and wavelength assignment as each DWDM channel is now separately constrained and by considering a fully loaded network the nonlinear impairments can be estimated without requiring full knowledge of the network state [162]. Thus in general the optimal data rate will not align with the preferred 100 GbE client side rate leaving stranded capacity. As pointed out in [182], a flexible Ethernet is required to better match client and optical layers. The recent debates within IEEE 802.3 and the ethernet community suggest that 25 GbE is a data rate that can be transported over single electrical or OOK optical channels. So to more fully utilise the available data rates with adaptive modulation and adaptive FEC overhead, inverse multiplexing the fixed 100 GbE client rate onto four 25 GbE lanes and transmitting these on the available spare capacity of multiple transceivers as illustrated in figure 7.5 is considered. This is compared with traditional fixed 100 GbE and also using fixed 25 GbE demands.

For a given symbol SNR the modulation format and FEC coding are chosen to maximise

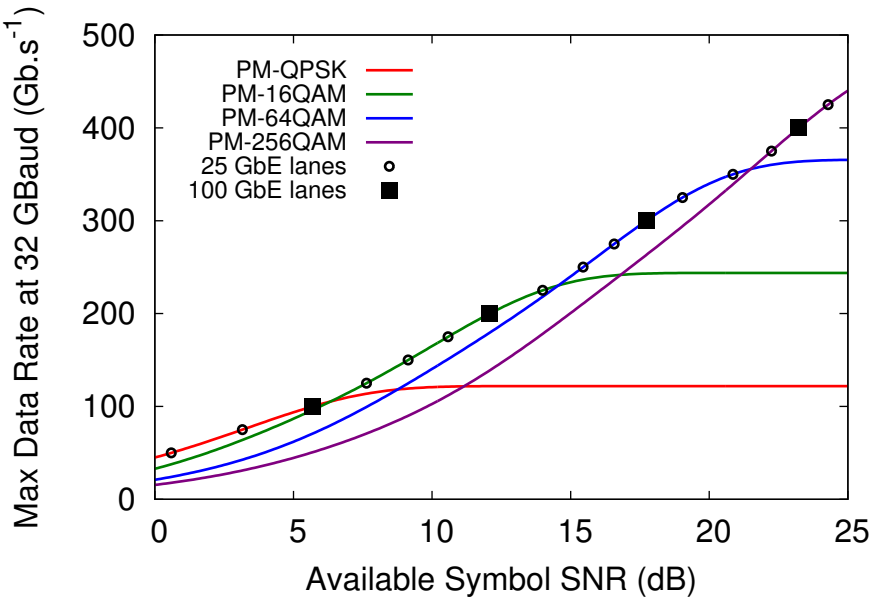

Figure 7.6: Graph of client data rate versus symbol SNR for various code rate and modulation formats.

the data throughput. Consider an ideal hard decision binary symetric channel using HD FEC, where for a pre-FEC BER, P_b, the maximum code rate, R_c, that results in error free transmission is given by [87]

$$R_c = 1 + P_b \log_2[P_b] + (1 - P_b)\log_2[1 - P_b]. \tag{7.5}$$

Thus for PM-QPSK modulation at 32 GBaud the maximum error free information rate is $32 \times 4 \times R_c$ Gb·s^{-1}. It is usual to including a 5% overhead for the OTU framing leading to a maximum client data rate $\frac{1}{1.05} 32 \times 4 \times R_c$ Gb·s^{-1} for the PM-QPSK modulation.

The reverse of this is solved, that is for a given data rate the modulation format and FEC overhead is chosen to minimise the required SNR for error free transmission. The data rates are chosen to be in multiples of 25 GbE with 5 % framing OH, giving a data rate granularity of 26.25 Gb·s^{-1}. So for each modulation format the required code rate can be calculated thence from equation (7.5) the required pre-FEC BER, P_b can be found and finally the required SNR to achieve this pre-FEC BER can be calculated given the modulation format. The required SNR for client data rates on 100 and 25 Gb·s^{-1} lanes transported using PM-QPSK, PM-16QAM, PM-64QAM and PM-256QAM are shown in table 7.3 and illustrated in figure 7.6.

In this section 32 Gbaud signals using Nyquist sinc pulses are considered with each fibre able to support 100 channels on a 50 GHz grid. Table 7.3 shows the available transceiver

Table 7.3: Modulation formats, data rates and required symbol SNRs for the 32 GBaud signals used.

Modulation Format	Code Rate	Information ($Gb{\cdot}s^{-1}$)	Client Data ($Gb{\cdot}s^{-1}$)	Required SNR (dB)
PM-QPSK	0.41	53	50	0.6
PM-QPSK	0.62	79	75	3.2
PM-QPSK	0.82	105	100	5.7
PM-16QAM	0.49	131	125	7.6
PM-16QAM	0.62	158	150	9.1
PM-16QAM	0.72	184	175	10.6
PM-16QAM	0.82	210	200	12.1
PM-16QAM	0.92	236	225	14.1
PM-64QAN	0.68	263	250	15.5
PM-64QAM	0.75	289	275	16.6
PM-64QAM	0.82	315	300	17.7
PM-64QAM	0.89	341	325	19.1
PM-64QAM	0.96	368	350	20.9
PM-256QAM	0.77	394	375	22.2
PM-256QAM	0.82	420	400	23.2
PM-256QAM	0.87	447	425	24.3
PM-256QAM	0.92	473	450	25.5

profiles used. For the fixed FEC OH only those transceiver profiles with a code rate of 0.82 were used.

To demonstrate the gains by fully utilising the available SNR, sequential loading of the BT 20+2 node UK core network was considered. Uniformly random demands were sequentially added to the network in the following way. If a transceiver with sufficient spare capacity was available between the source and destination nodes then the demand was accepted in full by that transceiver. If a transceiver was available between the source and destination nodes with insufficient spare capacity to fully accept the demand and a new transceiver can be set up following the same path the demand was accepted across the two transceivers. Otherwise a new transceiver was routed using the congestion aware shortest path (number of hops) based on [87] and if DWDM spectrum was available the first fit wavelength chosen to activate the transceiver. The SNR of the available route was calculated and the highest capacity signal format chosen from Table 7.3 where the SNR exceeds the required SNR for error free transmission. The demand was accepted onto the new transceiver. If all these options fail then the demand was deemed to have been blocked.

The process of routing and accepting a demand is illustrated in the flow chart of figure 7.7.

Either 2000, 100 Gb·s^{-1} or 8000, 25 Gb·s^{-1} bi-directional demands were requested in each simulation run with the simulation being repeated 10000 times to improve the statistics. The blocking probability was calculated as described in section 7.2 and the network load that gives a 0.1 %, 1 % and 10 % blocking probability were calculated by interpolation from a quadratic fit to the blocking probability versus load in the log domain over a blocking probability range of 0.05 % to 0.2 %, 0.5 % to 2 % and 6 % to 15 % respectively.

The simulation was carried out for four different sets of transceiver and demand profiles:

- for a fixed 200 Gb·s^{-1} PM-16QAM modulation format accepting upto 2 off 100 GbE demands,
- for an adapted PM-mQAM modulation format with fixed FEC overhead giving 100 Gb·s^{-1} client data granularity and accepting multiple 100 GbE demands in full,
- for an adapted PM-mQAM modulation format with adapted FEC overhead giving 25 Gb·s^{-1} client data granularity with the 100 GbE demands inverse multiplexed across four 25 GbE lanes and accepted across single or multiple transceivers
- and for an adapted format PM-mQAM with adapted FEC overhead giving 25 Gb·s^{-1} client data granularity with the multiple 25 GbE demands accepted in full.

Figure 7.8 shows the blocking probability versus accepted load for the different transceiver configurations described above. The network load at 0.1 %, 1 % and 10 % blocking probabilities are shown in table 7.4 and increase from 213 to 273 Tb·s^{-1} for 1 % blocking in going from fixed PM-16QAM modulation with fixed FEC OH and 100 GbE demands to adapted PM-mQAM modulation with adapted FEC OH and 25 GbE demands. For transceivers with 100 GbE client data granularity it is expected that on average 50 Gb·s^{-1} per transceiver of client data capacity will be stranded by incomplete utilisation of the available SNR, given that approximate 1000 transceivers are active then 50 Tb·s^{-1} of client data capacity is unused. This stranded capacity will fall to 50 Gb·s^{-1} per node pair when the demands are inverse multiplexed onto 25 GbE lanes, a total of 19 Tb·s^{-1} and fall further to 12.5 Gb·s^{-1} per transceiver when 25GbE client demands are used a total of just 12.5 Tb·s^{-1}. This view is consistent with the results shown in figure 7.8

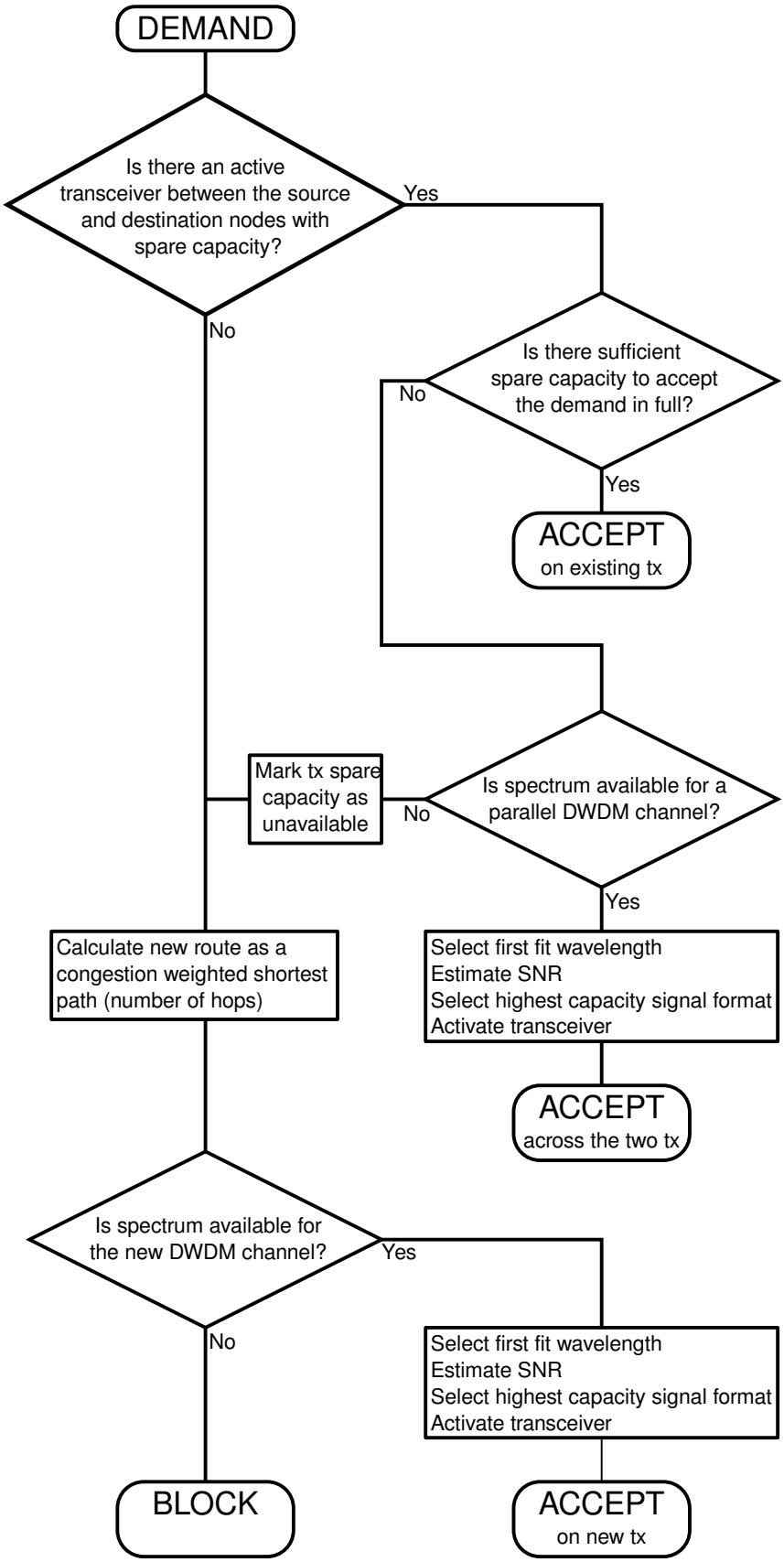

Figure 7.7: The flow process of routing and accepting sequential demands.

Table 7.4: Network load for a number of blocking probabilities and the number of active transceivers at a network load of 200 Tb·s^{-1} for the four transceiver configurations considered.

Transceiver Configuration	Network Load (Tb·s^{-1}) for blocking probability			No. Tx at load 200 Tb·s^{-1}
	0.1%	1%	10%	
Fixed PM-16QAM, fixed FEC Coding, 100 GbE demands.	206	213	223	1095
Adaptive PM-mQAM, fixed FEC coding, 100 GbE demands.	225	232	243	913
Adaptive PM-mQAM, adaptive FEC coding, 100 GbE demand.	251	265	281	854
Adaptive PM-mQAM, adaptive FEC coding, 25 GbE demands.	267	273	290	861

and suggests that moving to 100 GbE demands split across four 25 GbE lanes gives the lions share of capacity improvement.

Figure 7.9 shows the evolution of the number of active transceivers in the network as the network load is increased for the four different transceiver configurations. The points at which 0.1 %, 1 % and 10 % blocking probabilities occur are marked by triangle, circle and square symbols respectively. It can be seen that by using adaptive modulation and adaptive FEC OH fewer transceivers are required at the higher network loads. It also shows that at higher loads 100 GbE demands split across four 25 GbE lanes utilises approximately the same number of transceivers as using 25 GbE demands directly but suffers slightly earlier blocking. At low network loads the use of 25 GbE demands shows significantly more transceivers are required for a given network load this is because the smaller demands lead to a more rapid increase in the number of different source destination connections, but this low load regime is not an area of interest for future optical networking.

By comparing the number of transceivers used at the higher network load of 200 Tb·s^{-1}

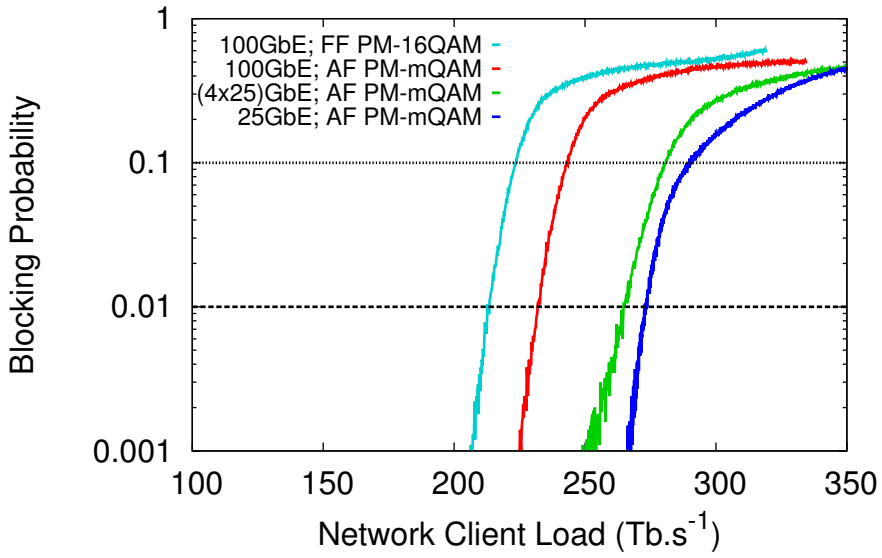

Figure 7.8: Blocking probability versus network load for the BT 20+2 node UK core network. For the four transceiver configurations considered, FF = fixed FEC-OH, AF = adaptive FEC-OH.

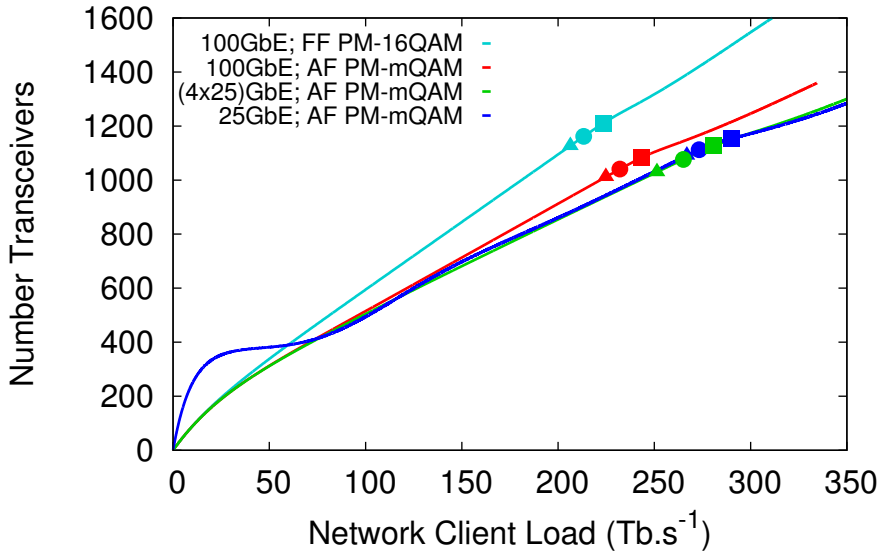

Figure 7.9: Number of active transceivers versus network load for the BT 20+2 node UK core network. For the four transceiver configurations considered, FF = fixed FEC-OH, AF = adaptive FEC-OH. The triangle, circle and square symbols correspond to blocking probabilities of 0.1, 1 and 10 % respectively.

it is possible to estimate the break even economic price for the different transceiver technologies. The final column of table 7.4 shows the average number of transceivers used to accept the load of 200 $\mathrm{Tb{\cdot}s^{-1}}$ under the four different transceiver configurations considered. For the technology to be economically acceptable then the price of an adaptive format transceiver needs to be less than 20 % more than a fixed PM-16QAM transceiver and the price of including adaptive FEC should not increase the transceiver price by more than a further 6 % of a fixed FEC overhead adaptive modulation transceiver.

8

Summary and Further Work

THE work of this thesis has looked at the area of "Coherent Optical Fibre Networking in the Nonlinear Regime" and consider the optimisation of overall network goals by adjusting the transceiver operating parameters and optical signal routing through the network.

8.1 Summary of This Work

This work began by reviewing the optical transmission impairments and developed a simple model for the estimation of the quality of transmission for a polarisation multiplexed coherent signal transmitted through an optical fibre in the weakly nonlinear regime. The model is heavily based on the recently published Gaussian noise model of nonlinear interference and is adapted to estimate the quality of transmission of individual light paths given the set of transmitter launch powers. The model was initially used to show how adaptation of the launch power can optimise the quality of transmission in a point-to-point link and a simple three node network [34]. It was shown how launch power optimisation

can balance the quality of transmission across channels improving the worst performing channel at the expense of a degradation to the better channels. The optimum theoretical Shannon capacity was achieved with a near flat launch power but with slightly greater launch power at the band edge where the noise is lower.

This work was extended to include the nonlinear impairment model in the routing and wavelength assignment to maximise the traffic throughput of a wavelength routed optical mesh network. The nonlinear impairment model was used to estimate the worst case quality of transmission of light paths through the network based on fully occupied links with equal launch power. This quality of transmission was used to allocate modulation formats and capacities to these light paths. The traffic throughput was maximised using an integer linear program formulation to assign transmitters to routes and wavelengths [45, 183]. Throughput gains of between 0 and 100 % over a baseline go anywhere modulation format were found. The wide variation in throughput gains depends on the network dimensions with large diameter networks showing greater gains. The throughput gains also depend on the exact transmission quality of the longest, shortest route in the baseline case since if this is just sufficient for a given modulation format then the improvements due to adaptation will be small, where as if the transmission quality of the longest, shortest route is not quite sufficient then a lower modulation format is used that can be upgraded with a small improvement in signal quality.

This initial inclusion of nonlinear impairments was based on the worst case, central channel for equal transmitter launch power and fully loaded links. Given the routing and wavelength assignment solution the individual launch powers were optimised to evenly distribute the SNR margin across all the active transceivers. This showed that the quality of transmission can be improved from the worst case by adapting the individual transmitter launch powers and this increase in quality of transmission was used to improve the traffic throughput [175, 176]. The adaptation of the individual launch power and wavelength assignment gave an improvement in SNR of 1 dB for the transceivers with CD only compensation and an improvement of between 1.5 and 1.9 dB when CD and SPM compensation was applied. The greater improvement in SNR when SPM is compensated was found for longer networks. The overall throughput gains were found to be between 3 and 42 % for CD only compensation and between 17 and 100% for CD and SPM compensation.

Adapting the modulation format to the quality of transmission is quite a coarse optimisation since there are a limited number of suitable modulation formats. Better optimisation of the signal to the quality of transmission can be achieved by adapting the FEC OH to provide the maximum error free data transmission rate. The throughput optimisation of a mesh network was compared for fixed launch power with adapted modulation format and FEC OH and optimised launch power with adapted modulation format alone in [180]. The two approaches gave similar throughput gains but in the case of optimised FEC OH the launch power is constant and there are fewer constraints to consider in the wavelength assignment while adapting the launch power required SPM compensation to obtain the best results.

Current operational networks tend to be sequential loaded, that is they are not fully loaded on day one and future demands are added. When the network cannot accept some fraction of the requests a new network is installed. In collaboration with BT the blocking load, the load at which an unacceptable number of demands was blocked, as a function of the launch power was investigated. It was shown that an Egalitarian approach where the worst case nonlinear noise for fully loaded links was assumed equally for all channels gave the best blocking load [162]. Where the nonlinear noise was estimated from the actual network state then some routes greedily assumed high SNR which led to blocking of future signals within the network. The granularity of using 100 GbE signals leads to some considerable stranded capacity and one final piece of work demonstrates that utilising finer granularity 25 GbE signals can increase the blocking load by avoiding this stranded capacity.

8.2 Further Work

Within the specific area of work of this thesis there are a number of improvements and ideas to be followed.

The nonlinear impairments based on the GN model should be extended to allow for Nyquist spaced channels, flexible symbol rate channels and to consider the effect of different modulation formats through the EGN model. A possible avenue to extend the current matrix based nonlinear impairments to allow for close packed channels was described in chapter 4 to allow for the noise spectrum being broader than the signal

spectrum and interference noise leaking into neighbouring signals. The work of Poggiolini et al [35] and Johannisson et al [36] have closed form expressions suitable for flexible symbol rate signals and flexible well spaced channels, the accuracy of the approximations in these closed form expressions could be improved. The GN model assumption of Gaussian signal statistics leads to an over estimation of the nonlinear interference, this can be removed by using the EGN model [168, 169]. In order to fully evaluate the nonlinear interference in a mesh network context using the EGN model, knowledge of the modulation format, pre-dispersion and distance of co-propagation of any interfering signals is required. Even in fixed grid systems with well spaced channels this will lead to a large increase in the number of possible interference types such that a simple lookup table of numerically integrated interference factors may prove difficult. Thus good accuracy closed form expressions for the EGN nonlinear interference parameters are required extending and improving the accuracy of those already provide [184].

In the case where nonlinear compensation is applied, using for example using full field DBP, the quality of such compensation needs to be estimated. In particular the effect of stochastic properties and processes in the transmission link, for example PMD and ASE noise, need to be more fully investigated. Also if nonlinear effects are mitigated the overall quality of transmission will be improved by increasing the launch power and this may introduce higher order perturbations into the nonlinear propagation. Such higher order perturbations are not included in the GN model so new models or extensions may be required.

The quality of transmission model should be extended for the impairments caused by filtering and isolation in ROADMs due to the wavelength selective switches (WSS) and also for the non-ideal properties of the EDFAs. The isolation and filtering effects in ROADMs have been shown to be a significant source of impairment [126, 127]. Also the effect of PDL within ROADM and EDFA should be considered as this also alters the SNR between the two polarisation multiplexed signals. Models exist for the non-ideal properties of EDFA, the gain tilt, noise flatness and spectral hole burning but these models are based on population dynamics and provide a significant burden to the overall impairment calculation. A simplified but accurate amplifier model with a complexity reduction similar to utilising the GN model over the split step Fourier simulation for transmission is required.

From a network optimisation point of view it would be better to jointly optimise all of

the transmitter parameters rather than the multiple stage iterative process used in chapter 6. Yan et al. at Chalmers University [46, 185] have looked at using nonlinear programs to solve this problem for very simple links but it remains an open question if this can be extend to a mesh networks with solvable complexity.

The work undertaken in chapter 6 suggests that the optimisation and adaptation of modulation format, routing, wavelength, coding and launch power leads to increases in the maximum network throughput between 42 % and 100 % with the larger gains for smaller diameter networks. These results on real mesh network topologies could be better underpinned by carry out an estimation of the throughput gains on regular networks with different diameters and different degrees of connectivity. Also the effect of variations in the traffic matrix need to be understood.

While Korotky et al [92] estimates the theoretical gains from network adaptation and optimisation the approach assumes a small perturbation on a existing network routing solution. It would be interesting to understand the gains in network throughput by considering a theoretical uniform network of nodes and links. A linear network and a planar network where the traffic demand is equal between all linear or areal elements and the total signal is limited in bandwidth or bandwidth per unit cross length for the linear or planar network. Then from a flow based restriction it would be possible to calculate the change in flow if the transmission format is adapted from a fixed rate based on the longest shortest path to a rate based on the actual shortest path.

Considering the broader directions the real benefit of this work is to inform the management of the network resources on the relative benefits of different optimisation strategies and allow inform decisions based on the complexity of those optimisations as to how best to organise the use of resources. Software defined networking has gained a lot of momentum in the last few years as a better way to control the network from the higher layers [186]. SDN decouples the management of the network from the data flows allowing cheap white box routers to be used and controlled from a logically centralised management controller. This work will help to decide how the centralised controller should be informed of the physical layer transmission impairments so that decisions on routing can be more properly made.

The centralised control of network resources allows a consistent view of the network state and allows the network to be divided and sold on as separate services. The infrastructure as

a service paradigm requires that a network can be sliced into multiple virtual networks and sold to multiple tenants and that there is no detrimental interaction between the slices that may affect the quality of service to any one tenant due to the traffic of another [187]. In this respect the knowledge of physical layer impairments is required to inform the construction and operation of the multiple virtual networks.

The whole area of network virtualisation requires the abstraction of the various optical components. Such abstractions must capture in a simple but sufficiently accurate way the properties of these components such that the performance and quality of the end to end transmission over a light path can be calculated. For established light paths the actual measured performance should be feedback allowing the network controller to learn and enhance its understanding of the component properties within the network. Performance monitoring is well established but in multi-tenanted networks some form of policing and identification of rogue or damaging signals will be required by the central controller. This would also allow tenants to lodge complaints if they can identify the source of aggressive signals. Accurate abstractions of the physical optical layer will also allow the network management functions to be virtualised. This network function virtualisation, NFV [188] allows, for example routing, load balancing and impairment awareness, to be carried out in remote data centres using commodity computing.

The work of this thesis will help to inform the process to design systems and methods that ensure reliable operation of multiple virtual networks through simple, accurate abstractions of the optical physical layer.

Bibliography

[1] A. SALEH & J. M. SIMMONS, "Architectural principles of optical regional and metropolitan access networks," *Journal of Lightwave Technology*, **Vol. 17**, **No. 12**, 1999, pp. 2431–2448. [doi: 10.1109/50.809662]

[2] J. BALIGA, R. W. A. AYRE, K. HINTON, & R. S. TUCKER, "Green Cloud Computing: Balancing Energy in Processing, Storage, and Transport," *Proceedings of the IEEE*, **Vol. 99**, **No. 1**, Jan. 2011, pp. 149–167. [doi: 10.1109/JPROC.2010.2060451]

[3] A. SALEH & J. M. SIMMONS, "All-Optical Networking— Evolution, Benefits, Challenges, and Future Vision," *Proceedings of the IEEE*, **Vol. 100**, **No. 5**, May 2012, pp. 1105–1117. [doi: 10.1109/JPROC.2011.2182589]

[4] M. W. CHBAT & H.-J. SCHMIDTKE, "Falling Boundaries from Metro to ULH Optical Transport Equipment," in *Optical Fiber Communication Conference*, Anaheim, CA. (USA), Mar. 2007, paper NTuA3. [doi: 10.1109/OFC.2007.4348516]

[5] "Minnesota Internet Traffic Studies (MINTS)," University of Minnesota, Aug. 2009. [Available: http://www.dtc.umn.edu/mints/home.php]

[6] "Cisco Visual Networking Index: Forecast and Methodology, 2014-2019," Cisco, May 2015. [Available: http://www.cisco.com/c/en/us/solutions/collateral/service-provider/ip-ngn-ip-next-generation-network/white_paper_c11-481360.pdf]

[7] S. K. KOROTKY, "Traffic Trends: Drivers and Measures of Cost-Effective and Energy-Efficient Technologies and Architectures for Backbone Optical Networks,"

in *Optical Fiber Communication Conference*, Los Angeles, CA. (USA), Mar. 2012, paper OM2G.1. [doi: 10.1364/OFC.2012.OM2G.1]

[8] "Fixed (wired)-broadband subscriptions," ITU, Jan. 2014. [Available: http://www.itu.int/en/ITU-D/Statistics/Documents/statistics/2014/Fixed_broadband_2000-2013.xls]

[9] "Telecomunications market data tables, Q3 2014," Ofcom, Nov. 2014. [Available: http://stakeholders.ofcom.org.uk/binaries/research/cmr/telecoms/Q3-2014.pdf]

[10] "UK fixed-line broadband performance, November 2014 - The performance of fixed-line broadband provided to UK residential consumers," Ofcom, Nov. 2014. [Available: http://stakeholders.ofcom.org.uk/binaries/research/broadband-research/november2014/Fixed_bb_speeds_November_2014.pdf]

[11] "Monthly Performance Pack," BBC iPlayer, May 2015. [Available: http://downloads.bbc.co.uk/mediacentre/iplayer/iplayer-performance-may2015.pdf]

[12] H. KOGELNIK, "High-capacity optical communications: personal recollections," *IEEE Journal of Selected Topics in Quantum Electronics*, **Vol. 6**, **No. 6**, Nov. 2000, pp. 1279–1286. [doi: 10.1109/2944.902179]

[13] R. W. TKACH, "Scaling optical communications for the next decade and beyond," *Bell Labs Technical Journal*, **Vol. 14**, **No. 4**, Feb. 2010, pp. 3–9. [doi: 10.1002/bltj.20400]

[14] R.-J. ESSIAMBRE & R. W. TKACH, "Capacity Trends and Limits of Optical Communication Networks," *Proceedings of the IEEE*, **Vol. 100**, **No. 5**, May 2012, pp. 1035–1055. [doi: 10.1109/JPROC.2012.2182970]

[15] R. MEARS, L. REEKIE, I. JAUNCEY, & D. PAYNE, "Low-noise erbium-doped fibre amplifier operating at 1.54μm," *Electronics Letters*, **Vol. 23**, **No. 19**, 1987, p. 1026. [doi: 10.1049/el:19870719]

[16] F. DERR, "Coherent optical QPSK intradyne system: concept and digital receiver realization," *Journal of Lightwave Technology*, **Vol. 10**, **No. 9**, Sep. 1992, pp. 1290–1296. [doi: 10.1109/50.156881]

[17] P. J. WINZER, "High-Spectral-Efficiency Optical Modulation Formats," *Journal of Lightwave Technology*, **Vol. 30**, **No. 24**, Dec. 2012, pp. 3824–3835. [doi: 10.1109/JLT.2012.2212180]

[18] S. BEPPU, K. KASAI, M. YOSHIDA, & M. NAKAZAWA, "2048 QAM (66 Gbit/s) single-carrier coherent optical transmission over 150 km with a potential SE of 153 bit/s/Hz," *Optics Express*, **Vol. 23**, **No. 4**, Feb. 2015, pp. 4960–4969. [doi: 10.1364/OE.23.004960]

[19] A. SANO, T. KOBAYASHI, S. YAMANAKA, A. MATSUURA, H. KAWAKAMI, Y. MIYAMOTO, K. ISHIHARA, & H. MASUDA, "102.3-Tb/s (224 x 548-Gb/s) C- and Extended L-band All-Raman Transmission over 240 km Using PDM-64QAM Single Carrier FDM with Digital Pilot Tone," in *Optical Fiber Communication Conference*, Los Angeles, CA. (USA), 2012, paper PDP5C.3. [doi: 10.1364/OFC.2012.PDP5C.3]

[20] J.-X. CAI, H. G. BATSHON, M. MAZURCZYK, H. ZHANG, Y. SUN, O. V. SINKIN, D. FOURSA, & A. N. PILIPETSKII, "64QAM Based Coded Modulation Transmission over Transoceanic Distance with $>$ 60 Tb/s Capacity," in *Optical Fiber Communication Conference*, Los Angeles, CA. (USA), 2015, paper Th5C.8. [doi: 10.1364/OFC.2015.Th5C.8]

[21] F. FORGHIERI, R. W. TKACH, A. CHRAPLYVY, & D. MARCUSE, "Reduction of four-wave mixing crosstalk in WDM systems using unequally spaced channels," *IEEE Photonics Technology Letters*, **Vol. 6**, **No. 6**, Jun. 1994, pp. 754–756. [doi: 10.1109/68.300184]

[22] E. IP & J. M. KAHN, "Compensation of Dispersion and Nonlinear Impairments Using Digital Backpropagation," *Journal of Lightwave Technology*, **Vol. 26**, **No. 20**, Oct. 2008, pp. 3416–3425. [doi: 10.1109/JLT.2008.927791]

[23] G. LIGA, T. XU, A. ALVARADO, R. I. KILLEY, & P. BAYVEL, "On the performance of multichannel digital backpropagation in high-capacity long-haul optical transmission," *Optics Express*, **Vol. 22**, **No. 24**, Nov. 2014, pp. 30 053–30 062. [doi: 10.1364/OE.22.030053]

[24] J. SAKAGUCHI, W. KLAUS, J. M. DELGADO MENDINUETA, B. J. PUTTNAM, R. S. LUIS, Y. AWAJI, N. WADA, T. HAYASHI, T. NAKANISHI, T. WATANABE, Y. KOKUBUN, T. TAKAHATA, & T. KOBAYASHI, "Realizing a 36-core, 3-mode Fiber with 108 Spatial Channels," in *Optical Fiber Communication Conference*, Los Angeles, CA. (USA), 2015, paper Th5C.2. [doi: 10.1364/OFC.2015.Th5C.2]

[25] N. K. FONTAINE, R. RYF, H. CHEN, A. V. BENITEZ, B. GUAN, R. SCOTT, B. ERCAN, S. J. B. YOO, L. E. GRÜNER-NIELSEN, Y. SUN, R. LINGLE, E. ANTONIO-LOPEZ, & R. AMEZCUA-CORREA, "30×30 MIMO Transmission over 15 Spatial Modes," in *Optical Fiber Communication Conference*, Los Angeles, CA. (USA), 2015, paper Th5C.1. [doi: 10.1364/OFC.2015.Th5C.1]

[26] S. GRINGERI, B. BASCH, V. SHUKLA, R. EGOROV, & T. J. XIA, "Flexible architectures for optical transport nodes and networks," *IEEE Communications Magazine*, **Vol. 48**, **No. 7**, Jul. 2010, pp. 40–50. [doi: 10.1109/MCOM.2010.5496877]

[27] ITU-T, *Spectral grids for WDM applications: DWDM frequency grid*, ITU-T Std. ITU-T G.694.1, 2012. [Available: http://www.itu.int]

[28] I. TOMKOS, S. AZODOLMOLKY, J. SOLE-PARETA, D. CAREGLIO, & E. PALKOPOULOU, "A Tutorial on the Flexible Optical Networking Paradigm: State of the Art, Trends, and Research Challenges," *Proceedings of the IEEE*, **Vol. 102**, **No. 9**, Sep. 2014, pp. 1317–1337. [doi: 10.1109/JPROC.2014.2324652]

[29] P. WRIGHT, A. LORD, & S. NICHOLAS, "Comparison of Optical Spectrum Utilization Between Flexgrid and Fixed Grid on a Real Network Topology," in *Optical Fiber Communication Conference*, Los Angeles, CA. (USA), 2012, paper OTh3B.5. [doi: 10.1364/OFC.2012.OTh3B.5]

[30] M. JINNO, B. KOZICKI, H. TAKARA, A. WATANABE, Y. SONE, T. TANAKA, & A. HIRANO, "Distance-adaptive spectrum resource allocation in spectrum-sliced elastic optical path network," *IEEE Communications Magazine*, **Vol. 48**, **No. 8**, Aug. 2010, pp. 138–145. [doi: 10.1109/MCOM.2010.5534599]

[31] A. NAG, M. TORNATORE, & B. MUKHERJEE, "Optical Network Design With Mixed Line Rates and Multiple Modulation Formats," *Journal of Lightwave Technology*, **Vol. 28**, **No. 4**, Feb. 2010, pp. 466–475. [doi: 10.1109/JLT.2009.2034396]

[32] C. SARADHI & S. SUBRAMANIAM, "Physical layer impairment aware routing (PLIAR) in WDM optical networks: issues and challenges," *IEEE Communications Surveys & Tutorials*, **Vol. 11**, **No. 4**, 2009, pp. 109–130. [doi: 10.1109/SURV.2009.090407]

[33] A. G. RAHBAR, "Review of Dynamic Impairment-Aware Routing and Wavelength Assignment Techniques in All-Optical Wavelength-Routed Networks," *IEEE Communications Surveys & Tutorials*, **Vol. 14**, **No. 4**, Jan. 2012, pp. 1065–1089. [doi: 10.1109/SURV.2011.101911.00023]

[34] D. J. IVES & S. J. SAVORY, "Transmitter Optimized Optical Networks," in *National Fiber Optic Engineers Conference*, Anaheim, CA. (USA), 2013, paper JW2A.64. [doi: 10.1364/NFOEC.2013.JW2A.64]

[35] P. POGGIOLINI, G. BOSCO, A. CARENA, V. CURRI, Y. JIANG, & F. FORGHIERI, "The GN-Model of Fiber Non-Linear Propagation and its Applications," *Journal of Lightwave Technology*, **Vol. 32**, **No. 4**, Feb. 2014, pp. 694–721. [doi: 10.1109/JLT.2013.2295208]

[36] P. JOHANNISSON & E. AGRELL, "Modeling of Nonlinear Signal Distortion in Fiber-Optic Networks," *Journal of Lightwave Technology*, **Vol. 32**, **No. 23**, Dec. 2014, pp. 3942–3950. [doi: 10.1109/JLT.2014.2361357]

[37] R. M. SCHMOGROW, D. HILLERKUSS, M. DRESCHMANN, M. HUEBNER, M. WINTER, J. MEYER, B. NEBENDAHL, C. KOOS, J. BECKER, W. FREUDE, & J. LEUTHOLD, "Real-Time Software-Defined Multiformat Transmitter Generating 64QAM at 28 GBd," *IEEE Photonics Technology Letters*, **Vol. 22**, **No. 21**, Nov. 2010, pp. 1601–1603. [doi: 10.1109/LPT.2010.2073698]

[38] H. Y. CHOI, T. TSURITANI, & I. MORITA, "BER-adaptive flexible-format transmitter for elastic optical networks," *Optics Express*, **Vol. 20**, **No. 17**, Aug. 2012, pp. 18 652–18 658. [doi: 10.1364/OE.20.018652]

[39] K. ROBERTS & C. LAPERLE, "Flexible Transceivers," in *European Conference on Optical Communications*, Amsterdam (NL), 2012, paper We.3.A.3. [doi: 10.1364/ECEOC.2012.We.3.A.3]

[40] D. A. A. MELLO, A. N. BARRETO, T. C. DE LIMA, T. F. PORTELA, L. BEYGI, & J. M. KAHN, "Optical Networking With Variable-Code-Rate Transceivers," *Journal of Lightwave Technology*, **Vol. 32**, **No. 2**, Jan. 2014, pp. 257–266. [doi: 10.1109/JLT.2013.2292298]

[41] P. POGGIOLINI, "The GN Model of Non-Linear Propagation in Uncompensated Coherent Optical Systems," *Journal of Lightwave Technology*, **Vol. 30**, **No. 24**, Dec. 2012, pp. 3857–3879. [doi: 10.1109/JLT.2012.2217729]

[42] R. PASTORELLI, G. BOSCO, S. PICIACCIA, & F. FORGHIERI, "Network Planning Strategies for Next-Generation Flexible Optical Networks [Invited]," *Journal of Optical Communications and Networking*, **Vol. 7**, **No. 3**, Feb. 2015, p. A511. [doi: 10.1364/JOCN.7.00A511]

[43] H. CUKURTEPE, M. TORNATORE, A. YAYIMLI, & B. MUKHERJEE, "Dynamic traffic provisioning in Mixed-Line-Rate networks with launch power determination," in *International Conference on Transparent Optical Networks*, Cartagena (ES), Jun. 2013, paper We.D4.6. [doi: 10.1109/ICTON.2013.6603015]

[44] B. BIRAND, H. WANG, K. BERGMAN, D. KILPER, T. NANDAGOPAL, & G. ZUSSMAN, "Real-Time Power Control for Dynamic Optical NetworksAlgorithms and Experimentation," *IEEE Journal on Selected Areas in Communications*, **Vol. 32**, **No. 8**, Aug. 2014, pp. 1615–1628. [doi: 10.1109/JSAC.2014.2335371]

[45] D. J. IVES, P. BAYVEL, & S. J. SAVORY, "Adapting Transmitter Power and Modulation Format to Improve Optical Network Performance Utilizing the Gaussian Noise Model of Nonlinear Impairments," *Journal of Lightwave Technology*, **Vol. 32**, **No. 21**, Nov. 2014, pp. 3485–3494. [doi: 10.1109/JLT.2014.2346582]

[46] L. YAN, E. AGRELL, & H. WYMEERSCH, "Resource Allocation in Nonlinear Flexible-Grid Fiber-Optic Networks," in *Optical Fiber Communication Conference*, Los Angeles, CA. (USA), 2015, paper Tu2I.5. [doi: 10.1364/OFC.2015.Tu2I.5]

[47] S. AZODOLMOLKY, M. KLINKOWSKI, E. MARIN, D. CAREGLIO, J. S. PARETA, & I. TOMKOS, "A survey on physical layer impairments aware routing and wavelength assignment algorithms in optical networks," *Computer Networks*, **Vol. 53**, **No. 7**, May 2009, pp. 926–944. [doi: 10.1016/j.comnet.2008.11.014]

[48] A. NAG & M. TORNATORE, "Transparent optical network design with mixed line rates," in *International Symposium on Advanced Networks and Telecommunication Systems*, Mumbai (IN), Dec. 2008, pp. 1–3. [doi: 10.1109/ANTS.2008.4937771]

[49] A. NAG & M. TORNATORE, "Optical network design with mixed line rates," *Optical Switching and Networking*, **Vol. 6**, **No. 4**, Dec. 2009, pp. 227–234. [doi: 10.1016/j.osn.2009.08.010]

[50] A. NAG, M. TORNATORE, & B. MUKHERJEE, "Power Management in Mixed Line Rate Optical Networks," in *Photonics in Switching*, Monterey, CA. (USA), 2010, paper PTuB4. [doi: 10.1364/PS.2010.PTuB4]

[51] P. CHOWDHURY, M. TORNATORE, A. NAG, E. IP, T. WANG, & B. MUKHERJEE, "On the Design of Energy-Efficient Mixed-Line-Rate (MLR) Optical Networks," *Journal of Lightwave Technology*, **Vol. 30**, **No. 1**, Jan. 2012, pp. 130–139. [doi: 10.1109/JLT.2011.2177441]

[52] A. NAG, T. WANG, & B. MUKHERJEE, "Robust Design of Spectrum-Efficient Green Optical Backbone Networks," *Journal of Lightwave Technology*, **Vol. 31**, **No. 7**, Apr. 2013, pp. 1138–1144. [doi: 10.1109/JLT.2013.2245301]

[53] M. BATAYNEH, D. A. SCHUPKE, M. HOFFMANN, A. KIRSTAEDTER, & B. MUKHERJEE, "Optical Network Design for a Multiline-Rate Carrier-Grade Ethernet Under Transmission-Range Constraints," *Journal of Lightwave Technology*, **Vol. 26**, **No. 1**, 2008, pp. 121–130. [doi: 10.1109/JLT.2007.913027]

[54] M. BATAYNEH, D. A. SCHUPKE, M. HOFFMANN, A. KIRSTAEDTER, & B. MUKHERJEE, "On Routing and Transmission-Range Determination of Multi-Bit-Rate Signals Over Mixed-Line-Rate WDM Optical Networks for Carrier Ethernet," *IEEE/ACM Transactions on Networking*, **Vol. 19**, **No. 5**, Oct. 2011, pp. 1304–1316. [doi: 10.1109/TNET.2011.2107748]

[55] R. APARICIO-PARDO, P. PAVON-MARINO, & S. ZSIGMOND, "Mixed line rate virtual topology design considering nonlinear interferences between amplitude and phase modulated channels," *Photonic Network Communications*, **Vol. 22**, **No. 3**, Jul. 2011, pp. 230–239. [doi: 10.1007/s11107-011-0322-2]

[56] K. CHRISTODOULOPOULOS, K. MANOUSAKIS, & E. A. VARVARIGOS, "Reach Adapting Algorithms for Mixed Line Rate WDM Transport Networks," *Journal of Lightwave Technology*, **Vol. 29**, **No. 21**, Nov. 2011, pp. 3350–3363. [doi: 10.1109/JLT.2011.2167596]

[57] K. CHRISTODOULOPOULOS, "Adapting the transmission reach in mixed line rates WDM transport networks," in *Optical Network Design and Modeling*, Bologna (IT), Feb. 2011, pp. 1–6.

[58] N. SAMBO, M. SECONDINI, F. CUGINI, G. BOTTARI, P. IOVANNA, F. CAVALIERE, & P. CASTOLDI, "Modeling and Distributed Provisioning in 10\40\100\-Gb/s Multirate Wavelength Switched Optical Networks," *Journal of Lightwave Technology*, **Vol. 29**, **No. 9**, May 2011, pp. 1248–1257. [doi: 10.1109/JLT.2011.2122245]

[59] H. CUKURTEPE, M. TORNATORE, A. YAYIMLI, & B. MUKHERJEE, "Impairment-aware lightpath provisioning in mixed line rate networks," in *IEEE International Conference on Advanced Networks and Telecommunciations Systems (ANTS)*, Dec. 2012, pp. 18–23. [doi: 10.1109/ANTS.2012.6524221]

[60] S. CHANDRASEKHAR & X. LIU, "Mixed 10/40/100-Gb/s transmission through bandwidth-managed ROADMs," in *Joint Conference of the Opto-Electronics and Communications Conference and the Australian Conference on Optical Fibre Technology*, Sydney (AU), Jul. 2008, pp. WeQ–1. [doi: 10.1109/OECCA-COFT.2008.4610626]

[61] M. JINNO, H. TAKARA, B. KOZICKI, Y. TSUKISHIMA, T. YOSHIMATSU, T. KOBAYASHI, Y. MIYAMOTO, K. YONENAGA, A. TAKADA, O. ISHIDA, & S. MATSUOKA, "Demonstration of Novel Spectrum-Efficient Elastic Optical Path Network with Per-Channel Variable Capacity of 40 Gb / s to Over 400 Gb / s," in *European Conference on Optical Communications*, Brussels (BE), Sep. 2008, paper Th.3.F.6. [doi: 10.1109/ECOC.2008.4729581]

[62] M. JINNO, H. TAKARA, B. KOZICKI, Y. TSUKISHIMA, Y. SONE, & S. MATSUOKA, "Spectrum-efficient and scalable elastic optical path network:

architecture, benefits, and enabling technologies," *IEEE Communications Magazine*, **Vol. 47**, **No. 11**, Nov. 2009, pp. 66–73. [doi: 10.1109/MCOM.2009.5307468]

[63] O. GERSTEL, M. JINNO, A. LORD, & S. J. B. YOO, "Elastic optical networking: a new dawn for the optical layer?" *IEEE Communications Magazine*, **Vol. 50**, **No. 2**, Feb. 2012, pp. s12–s20. [doi: 10.1109/MCOM.2012.6146481]

[64] B. KOZICKI, H. TAKARA, Y. SONE, A. WATANABE, & M. JINNO, "Distance-Adaptive Spectrum Allocation in Elastic Optical Path Network (SLICE) with Bit per Symbol Adjustment," in *Optical Fiber Communication Conference*, San Diego, CA. (USA), 2010, paper OMU3. [doi: 10.1364/OFC.2010.OMU3]

[65] T. TAKAGI, H. HASEGAWA, K.-I. SATO, T. TANAKA, B. KOZICKI, Y. SONE, & M. JINNO, "Algorithms for maximizing spectrum efficiency in elastic optical path networks that adopt distance adaptive modulation," in *European Conference on Optical Communication*, Torino (IT), Sep. 2010, pp. 1–3. [doi: 10.1109/ECOC.2010.5621146]

[66] T. TAKAGI, H. HASEGAWA, K.-I. SATO, Y. SONE, B. KOZICKI, A. HIRANO, & M. JINNO, "Dynamic Routing and Frequency Slot Assignment for Elastic Optical Path Networks that Adopt Distance Adaptive Modulation," in *Optical Fiber Communication Conference*, Washington, D.C., 2011, paper OTuI.7. [doi: 10.1364/OFC.2011.OTuI7]

[67] B. KOZICKI, H. TAKARA, T. TANAKA, Y. SONE, A. HIRANO, K. YONENAGA, & M. JINNO, "Distance-Adaptive Path Allocation in Elastic Optical Path Networks," *IEICE Transactions on Communications*, **Vol. E94-B**, **No. 7**, 2011, pp. 1823–1830. [doi: 10.1587/transcom.E94.B.1823]

[68] L. ZHANG, W. LU, X. ZHOU, & Z. ZHU, "Dynamic RMSA in spectrum-sliced elastic optical networks for high-throughput service provisioning," in *International Conference on Computing, Networking and Communications*, Jan. 2013, pp. 380–384. [doi: 10.1109/ICCNC.2013.6504113]

[69] K. CHRISTODOULOPOULOS, P. KOKKINOS, K. MANOUSAKIS, & E. A. VARVARIGOS, "Impairment Aware RWA in Optical Networks: Over-provisioning

or Cross Optimization?" *Journal of Networks*, **Vol. 5**, **No. 11**, Nov. 2010, pp. 1271–1278. [doi: 10.4304/jnw.5.11.1271-1278]

[70] K. CHRISTODOULOPOULOS, I. TOMKOS, & E. A. VARVARIGOS, "Elastic Bandwidth Allocation in Flexible OFDM-Based Optical Networks," *Journal of Lightwave Technology*, **Vol. 29**, **No. 9**, May 2011, pp. 1354–1366. [doi: 10.1109/JLT.2011.2125777]

[71] F. FORGHIERI, R. W. TKACH, & A. CHRAPLYVY, "WDM systems with unequally spaced channels," *Journal of Lightwave Technology*, **Vol. 13**, **No. 5**, May 1995, pp. 889–897. [doi: 10.1109/50.387806]

[72] V. THING, P. SHUM, & M. RAO, "Bandwidth-Efficient WDM Channel Allocation for Four-Wave Mixing-Effect Minimization," *IEEE Transactions on Communications*, **Vol. 52**, **No. 12**, Dec. 2004, pp. 2184–2189. [doi: 10.1109/TCOMM.2004.838684]

[73] A. ADHYA & D. DATTA, "Design methodology for WDM backbone networks using FWM-aware heuristic algorithm," *Optical Switching and Networking*, **Vol. 6**, **No. 1**, Jan. 2009, pp. 10–19. [doi: 10.1016/j.osn.2008.05.006]

[74] A. ADHYA & D. DATTA, "Lightpath Topology Design for Wavelength-Routed Optical Networks in the Presence of Four-Wave Mixing," *Journal of Optical Communications and Networking*, **Vol. 4**, **No. 4**, Apr. 2012, pp. 314–325. [doi: 10.1364/JOCN.4.000314]

[75] P. SERENA & A. BONONI, "An Alternative Approach to the Gaussian Noise Model and its System Implications," *Journal of Lightwave Technology*, **Vol. 31**, **No. 22**, Nov. 2013, pp. 3489–3499. [doi: 10.1109/JLT.2013.2284499]

[76] E. PALKOPOULOU, G. BOSCO, A. CARENA, D. KLONIDIS, P. POGGIOLINI, & I. TOMKOS, "Nyquist-WDM-Based Flexible Optical Networks: Exploring Physical Layer Design Parameters," *Journal of Lightwave Technology*, **Vol. 31**, **No. 14**, Jul. 2013, pp. 2332–2339. [doi: 10.1109/JLT.2013.2265324]

[77] P. POGGIOLINI, G. BOSCO, A. CARENA, R. CIGLIUTTI, V. CURRI, F. FORGHIERI, R. PASTORELLI, & S. PICIACCIA, "The LOGON Strategy for Low-

Complexity Control Plane Implementation in New-Generation Flexible Networks," in *Optical Fiber Communication Conference*, Anaheim, CA. (USA), 2013, paper OW1H.3. [doi: 10.1364/OFC.2013.OW1H.3]

[78] R. PASTORELLI, G. BOSCO, A. NESPOLA, S. PICIACCIA, & F. FORGHIERI, "Network Planning Strategies for Next-Generation Flexible Optical Networks," in *Optical Fiber Communication Conference*, San Francisco, CA. (USA), 2014, paper M2B.1. [doi: 10.1364/OFC.2014.M2B.1]

[79] R. PASTORELLI, "Network Optimization Strategies and Control Plane Impacts," in *Optical Fiber Communication Conference*, Los Angeles, CA. (USA), 2015, paper M2I.6. [doi: 10.1364/OFC.2015.M2I.6]

[80] H. BEYRANVAND & J. A. SALEHI, "A Quality-of-Transmission Aware Dynamic Routing and Spectrum Assignment Scheme for Future Elastic Optical Networks," *Journal of Lightwave Technology*, **Vol. 31**, **No. 18**, Sep. 2013, pp. 3043–3054. [doi: 10.1109/JLT.2013.2278572]

[81] B. BIRAND, H. WANG, K. BERGMAN, & G. ZUSSMAN, "Measurements-based Power Control - A Cross-layered Framework," in *National Fiber Optic Engineers Conference*, Anaheim, CA. (USA), 2013, paper JTh2A.66. [doi: 10.1364/NFOEC.2013.JTh2A.66]

[82] H. NAKASHIMA & Y. AKIYAMA, "Launch Power Optimization Co-operated with Digital Nonlinear Compensator for Elastic Optical Network," in *Opto Electronics and Communications Conference*, Shanghai (CN), Jul. 2015, paper JThB.105.

[83] Q. YANG, W. SHIEH, & Y. MA, "Bit and Power Loading for Coherent Optical OFDM," *IEEE Photonics Technology Letters*, **Vol. 20**, **No. 15**, Aug. 2008, pp. 1305–1307. [doi: 10.1109/LPT.2008.926879]

[84] H. CUKURTEPE, M. TORNATORE, A. YAYIMLI, & B. MUKHERJEE, "Provisioning of dynamic traffic in mixed-line-rate optical networks with launch power determination," *Photonic Network Communications*, **Vol. 27**, **No. 3**, Apr. 2014, pp. 154–166. [doi: 10.1007/s11107-014-0435-5]

[85] G. GAO, J. ZHANG, W. GU, Z. FENG, & Y. YE, "Dynamic power control for mixed line rate transparent wavelength switched optical networks," in *European Conference on Optical Communication*, Torino (IT), Sep. 2010, paper We.8.D.6. [doi: 10.1109/ECOC.2010.5621447]

[86] G. GAO, X. CHEN, & W. SHIEH, "Influence of PMD on fiber nonlinearity compensation using digital back propagation," *Optics Express*, **Vol. 20**, **No. 13**, Jun. 2012, pp. 14 406–14 418. [doi: 10.1364/OE.20.014406]

[87] S. J. SAVORY, "Congestion Aware Routing in Nonlinear Elastic Optical Networks," *IEEE Photonics Technology Letters*, **Vol. 26**, **No. 10**, May 2014, pp. 1057–1060. [doi: 10.1109/LPT.2014.2314438]

[88] M. ARABACI, I. B. DJORDJEVIC, L. XU, & T. WANG, "Nonbinary LDPC-Coded Modulation for Rate-Adaptive Optical Fiber Communication Without Bandwidth Expansion," *IEEE Photonics Technology Letters*, **Vol. 24**, **No. 16**, Aug. 2012, pp. 1402–1404. [doi: 10.1109/LPT.2012.2204973]

[89] H. D. THANH, M. MORVAN, P. GRAVEY, F. CUGINI, & I. CERUTTI, "On the spectrum-efficiency of transparent optical transport network design with variable-rate forward error correction codes," in *International Conference on Advanced Communication Technology*, Pyeongchang (KR), Feb. 2014, pp. 1173–1177. [doi: 10.1109/ICACT.2014.6779143]

[90] Y. LI, H. DAI, G. SHEN, & S. K. BOSE, "Adaptive FEC-based lightpath routing and wavelength assignment in WDM optical networks," *Optical Switching and Networking*, **Vol. 14**, Aug. 2014, pp. 241–249. [doi: 10.1016/j.osn.2014.05.021]

[91] A. ALVARADO, D. J. IVES, S. J. SAVORY, & P. BAYVEL, "On Optimal Modulation and FEC Overhead for Future Optical Networks," in *Optical Fiber Communication Conference*, Los Angeles, CA. (USA), 2015, paper Th3E.1. [doi: 10.1364/OFC.2015.Th3E.1]

[92] S. K. KOROTKY, R.-J. ESSIAMBRE, & R. W. TKACH, "Expectations of optical network traffic gain afforded by bit rate adaptive transmission," *Bell Labs Technical Journal*, **Vol. 14**, **No. 4**, Feb. 2010, pp. 285–295. [doi: 10.1002/bltj.20416]

[93] S. MAKOVEJS, C. BEHRENS, R.-P. BRAUN, S. TEN, C. TOWERY, I. ROUDAS, K. KORESHKOV, T. NATH, & A. GLADISCH, "Impact of Adaptive-Rate Transponders and Fiber Attributes on the Achievable Capacity," *Journal of Optical Communications and Networking*, **Vol. 7**, **No. 3**, Feb. 2015, p. 172. [doi: 10.1364/JOCN.7.000172]

[94] D. B. PAYNE & J. STERN, "Transparent single-mode fiber optical networks," *Journal of Lightwave Technology*, **Vol. 4**, **No. 7**, 1986, pp. 864–869. [doi: 10.1109/JLT.1986.1074812]

[95] G. HILL, "A wavelength routing approach to optical communications networks," in *IEEE INFOCOM '88,Seventh Annual Joint Conference of the IEEE Computer and Communcations Societies. Networks: Evolution or Revolution?*, New Orleans, LA (USA), 1988, pp. 354–362. [doi: 10.1109/INFCOM.1988.12937]

[96] S. BARONI & P. BAYVEL, "Wavelength Requirements in Arbitrarily Connected Wavelength-Routed Optical Networks," *Journal of Lightwave Technology*, **Vol. 15**, **No. 2**, Feb. 1997, pp. 242–251. [doi: 10.1109/50.554330]

[97] J. BERTHOLD, A. SALEH, L. BLAIR, & J. M. SIMMONS, "Optical Networking: Past, Present, and Future," *Journal of Lightwave Technology*, **Vol. 26**, **No. 9**, May 2008, pp. 1104–1118. [doi: 10.1109/JLT.2008.923609]

[98] W. J. DUFFIN, *Electricity and Magnetism*. McGraw-Hill Book Company (UK) Ltd, 1980.

[99] G. P. AGRAWAL, *Nonlinear Fiber Optics*, 3rd ed., P. L. KELLY, I. P. KAMINOW, & G. P. AGRAWAL, Eds. Harcourt Place, 32 Jamestown Road, London NW1 7BY, UK: Academic Press, 2001.

[100] T. KATO, Y. SUETSUGU, & M. NISHIMURA, "Estimation of nonlinear refractive index in various silica-based glasses for optical fibers," *Optics Letters*, **Vol. 20**, **No. 22**, Nov. 1995, p. 2279. [doi: 10.1364/OL.20.002279]

[101] G. P. AGRAWAL, *Fiber-Optic Communication Systems*, 4th ed., K. CHANG, Ed. Hoboken, New Jersey, USA.: John Wiley & Sons, 2010.

[102] M. G. TAYLOR, "Coherent Detection Method Using DSP for Demodulation of Signal and Subsequent Equalization of Propagation Impairments," *IEEE Photonics Technology Letters*, **Vol. 16**, **No. 2**, Feb. 2004, pp. 674–676. [doi: 10.1109/LPT.2003.823106]

[103] S. J. SAVORY, "Digital Coherent Optical Receivers: Algorithms and Subsystems," *IEEE Journal of Quantum Electronics*, **Vol. 16**, **No. 5**, Sep. 2010, pp. 1164–1179. [doi: 10.1109/JSTQE.2010.2044751]

[104] R. MAHER, T. XU, L. GALDINO, M. SATO, A. ALVARADO, K. SHI, S. J. SAVORY, B. C. THOMSEN, R. I. KILLEY, & P. BAYVEL, "Spectrally Shaped DP-16QAM Super-Channel Transmission with Multi-Channel Digital Back-Propagation," *Scientific Reports*, **Vol. 5**, **No. 8214**, Feb. 2015, pp. 1–8. [doi: 10.1038/srep08214]

[105] A. MOREA, N. BROGARD, F. LEPLINGARD, J.-C. ANTONA, T. ZAMI, B. LAVIGNE, & D. BAYART, "QoT function and Aˆ* routing: an optimized combination for connection search in translucent networks," *Journal of Optical Networking*, **Vol. 7**, **No. 1**, 2008, p. 42. [doi: 10.1364/JON.7.000042]

[106] S. ZSIGMOND, "Routing in Optical Networks based on Physical Effects," PhD, Budapest University of Technology and Economics, 2010.

[107] T. CHIANG, N. KAGI, M. MARHIC, & L. KAZOVSKY, "Cross-phase modulation in fiber links with multiple optical amplifiers and dispersion compensators," *Journal of Lightwave Technology*, **Vol. 14**, **No. 3**, Mar. 1996, pp. 249–260. [doi: 10.1109/50.485582]

[108] A. CARTAXO, "Cross-phase modulation in intensity modulation-direct detection WDM systems with multiple optical amplifiers and dispersion compensators," *Journal of Lightave Technology*, **Vol. 17**, **No. 2**, Feb. 1999, pp. 178–190. [doi: 10.1109/50.744218]

[109] H. J. THIELE, R. I. KILLEY, & P. BAYVEL, "Investigation of Cross-Phase Modulation-Induced Transmission Penalties Using the Pump-Probe Technique," *Optical Fiber Technology*, **Vol. 8**, **No. 1**, Jan. 2002, pp. 71–81. [doi: 10.1006/ofte.2002.0363]

[110] S. PACHNICKE, J. REICHERT, S. SPALTER, & E. VOGES, "Fast analytical assessment of the signal quality in transparent optical networks," *Journal of Lightwave Technology*, **Vol. 24**, **No. 2**, Feb. 2006, pp. 815–824. [doi: 10.1109/JLT.2005.862472]

[111] W. LIN, T. HAHN, R. S. WOLFF, & B. MUMEY, "A distributed impairment aware QoS framework for all-optical networks," *Optical Switching and Networking*, **Vol. 8**, **No. 1**, Jan. 2011, pp. 56–67. [doi: 10.1016/j.osn.2010.05.003]

[112] C. CANTRELL, "Transparent optical metropolitan-area networks," in *Annual Meeting of the IEEE Lasers and Electro-Optics Society*, 2003, pp. 608–609. [doi: 10.1109/LEOS.2003.1252947]

[113] B. LAVIGNE, F. LEPLINGARD, L. LORCY, E. BALMEFREZOL, J.-C. ANTONA, T. ZAMI, & D. BAYART, "Method for the Determination of a Quality-of-Transmission Estimator along the Lihtpaths of Partially Transparent Networks," in *European Conference on Optical Communication*, Berlin (DE), Sep. 2007, paper 08.5.2.

[114] F. CUGINI, N. SAMBO, N. ANDRIOLLI, A. GIORGETTI, L. VALCARENGHI, P. CASTOLDI, E. LE ROUZIC, & J. POIRRIER, "Enhancing GMPLS Signaling Protocol for Encompassing Quality of Transmission (QoT) in All-Optical Networks," *Journal of Lightwave Technology*, **Vol. 26**, **No. 19**, Oct. 2008, pp. 3318–3328. [doi: 10.1109/JLT.2008.925674]

[115] B. RAMAMURTHY, D. DATTA, H. FENG, J. HERITAGE, & B. MUKHERJEE, "Impact of transmission impairments on the teletraffic performance of wavelength-routed optical networks," *Journal of Lightwave Technology*, **Vol. 17**, **No. 10**, Oct. 1999, pp. 1713–1723. [doi: 10.1109/50.793740]

[116] J. STRAND & A. CHIU, *Impairments and Other Constraints on Optical Layer Routing*, IETF Std. RFC4054, 2005. [Available: https://www.ietf.org]

[117] A. SPLETT, C. KURTSKE, & K. PETERMANN, "Ultimate transmission capacity of amplified optical fiber communication systems taking into account fiber nonlinearities," in *European Conference on Optical Communications*, Montreux (CH), 1993, paper MoC2.4.

[118] P. P. MITRA & J. B. STARK, "Nonlinear limits to the information capacity of optical fibre communications." *Nature*, **Vol. 411**, **No. 6841**, Jun. 2001, pp. 1027–30. [doi: 10.1038/35082518]

[119] J. TANG, "The channel capacity of a multispan DWDM system employing dispersive nonlinear optical fibers and an ideal coherent optical receiver," *Journal of Lightwave Technology*, **Vol. 20**, **No. 7**, Jul. 2002, pp. 1095–1101. [doi: 10.1109/JLT.2002.800344]

[120] H. LOUCHET, A. HODZIC, & K. PETERMANN, "Analytical model for the performance evaluation of DWDM transmission systems," *IEEE Photonics Technology Letters*, **Vol. 15**, **No. 9**, Sep. 2003, pp. 1219–1221. [doi: 10.1109/LPT.2003.816133]

[121] H. KOGELNIK & A. YARIV, "Considerations of noise and schemes for its reduction in laser amplifiers," *Proceedings of the IEEE*, **Vol. 52**, **No. 2**, 1964, pp. 165–172. [doi: 10.1109/PROC.1964.2805]

[122] E. DESURVIRE, D. BAYART, B. DESTHIEUX, & S. BIGO, *Erbium-Doped Fiber Amplifiers*. New York, USA: John Wilet and Sons Inc., 2002.

[123] A. YARIV, "Signal-to-noise considerations in fiber links with periodic or distributed optical amplification," *Optics Letters*, **Vol. 15**, **No. 19**, Oct. 1990, pp. 1064–1066. [doi: 10.1364/OL.15.001064]

[124] "A Performance Comparison of WSS Switch Engine Technologies," JDSU, May 2009. [Available: http://www.jdsu.com/ProductLiterature/wsscomp_wp_cms_ae.pdf]

[125] A. DEVARAJAN, K. SANDESHA, R. GOWRISHANKAR, B. S. KISHORE, G. PRASANNA, R. JOHNSON, & P. VORUGANTI, "Colorless, Directionless and Contentionless multi-degree ROADM architecture for mesh optical networks," in *International Conference on Communication Systems and Networks*, Bangalore (IN), Jan. 2010, pp. 1–10. [doi: 10.1109/COMSNETS.2010.5431987]

[126] M. M. FILER & S. TIBULEAC, "N-degree ROADM Architecture Comparison: Broadcast-and-Select versus Route-and-Select in 120 Gb/s DP-QPSK Transmission Systems," in *Optical Fiber Communication Conference*, San Francisco, CA. (USA), Mar. 2014, paper Th1I.2. [doi: 10.1364/OFC.2014.Th1I.2]

[127] F. HEISMANN, "System Requirements for WSS Filter Shape in Cascaded ROADM Networks," in *Optical Fiber Communication Conference*, San Diego, CA. (USA), Mar. 2010, paper OThR1. [doi: 10.1364/OFC.2010.OThR1]

[128] D. MONOYIOS & K. VLACHOS, "Multiobjective Genetic Algorithms for Solving the Impairment-Aware Routing and Wavelength Assignment Problem," *Journal of Optical Communications and Networking*, **Vol. 3**, **No. 1**, Dec. 2011, p. 40. [doi: 10.1364/JOCN.3.000040]

[129] R. RAMASWAMI & K. SIVARAJAN, "Design of logical topologies for wavelength-routed all-optical networks," in *Proceedings of INFOCOM'95*, Boston, MA (USA), Apr. 1995, paper 10c.4.1. [doi: 10.1109/INFCOM.1995.516012]

[130] S. JAIN, M. ZHU, J. ZOLLA, U. HÖLZLE, S. STUART, A. VAHDAT, A. KUMAR, S. MANDAL, J. ONG, L. POUTIEVSKI, A. SINGH, S. VENKATA, J. WANDERER, & J. ZHOU, "B4: Experience with a Globally-Deployed Software Defined WAN," in *Special Interest Group on Data Communication*, Hong Kong (CN), Aug. 2013, pp. 3–14. [doi: 10.1145/2486001.2486019]

[131] ETSI, *Network Aspects (NA); Availability performance of path elements of international digital paths*, ETSI Std. EN 300 416, Aug. 1998.

[132] J. P. SNYDER, "Map Projections - A Working Manual," U.S. Geological Survey Proffesional Paper 1395, Washington, D.C., 1987.

[133] R. W. SINNOT, "Virtues of the Haversine," *Sky and Telescope*, **Vol. 68**, **No. 2**, Aug. 1984, p. 159.

[134] M. SINCLAIR, "Improved model for European international telephony traffic," *Electronics Letters*, **Vol. 30**, **No. 18**, 1994, p. 1468. [doi: 10.1049/el:19941037]

[135] A. DWIVEDI & R. WAGNER, "Traffic model for USA long-distance optical network," in *Optical Fiber Communication Conference*, Baltimore, MA. (USA), Mar. 2000, paper TuK1.1. [doi: 10.1109/OFC.2000.868400]

[136] W.-K. WONG, "Comparing the fit of the gravity model for different cross-border flows," *Economics Letters*, **Vol. 99**, **No. 3**, Jun. 2008, pp. 474–477. [doi: 10.1016/j.econlet.2007.09.018]

[137] I. HEGGIE, "Are gravity and interactance models a valid technique for planning regional transport facilities?" *Operational Research Quarterly*, **Vol. 20**, **No. 1**, Mar. 1969, pp. 93–110.

[138] Y. ZHANG, M. ROUGHAN, C. LUND, & D. DONOHO, "An information-theoretic approach to traffic matrix estimation," in *Special Interest Group on Data Communication*, Karlsruhe (DE), Aug. 2003, pp. 301–312. [doi: 10.1145/863955.863990]

[139] S. K. KOROTKY & K. N. OIKONOMOU, "Scaling of the most likely traffic patterns of hose- and cost-constrained ring and mesh networks," *Journal of Optical Networking*, **Vol. 7**, **No. 6**, Jun. 2008, pp. 550–563. [doi: 10.1364/JON.7.000550]

[140] E. PALKOPOULOU, C. MERKLE, D. A. SCHUPKE, C. G. GRUBER, & A. KIRSTÄDTER, "Traffic models for future backbone networks - a service-oriented approach," *European Transactions on Telecommunications*, **Vol. 22**, **No. 4**, Jun. 2011, pp. 137–150. [doi: 10.1002/ett.1464]

[141] J. G. PROAKIS, *Digital Communications*, 4th ed. Singapore: McGraw-Hill, 2001.

[142] P. K. VITTHALADEVUNI, M.-S. ALOUINI, & J. KIEFFER, "Exact BER computation for cross QAM constellations," *IEEE Transactions on Wireless Communications*, **Vol. 4**, **No. 6**, Nov. 2005, pp. 3039–3050. [doi: 10.1109/TWC.2005.857997]

[143] J. SMITH, "Odd-Bit Quadrature Amplitude-Shift Keying," *IEEE Transactions on Communications*, **Vol. 23**, **No. 3**, Mar. 1975, pp. 385–389. [doi: 10.1109/TCOM.1975.1092806]

[144] K. CHO & D. YOON, "On the general BER expression of one- and two-dimensional amplitude modulations," *IEEE Transactions on Communications*, **Vol. 50**, **No. 7**, Jul. 2002, pp. 1074–1080. [doi: 10.1109/TCOMM.2002.800818]

[145] O. I. FORUM, "100G Forward Error Correction White Paper," Optical Internetworking Forum, 2010.

[146] M. SCHOLTEN, T. COE, & J. DILLARD, "Continuously-Interleaved BCH (CI-BCH) FEC delivers best in class NECG for 40G and 100G metro applications," in *National Fiber Optic Engineers Conference*, San Diego, CA. (USA), Mar. 2010, paper NTuB3.

[147] F. CHANG, K. ONOHARA, & T. MIZUOCHI, "Forward Error Correction for 100 G Transport Networks," *IEEE Communications Magazine*, **Vol. 3**, Mar. 2010, pp. S48–S55. [doi: 10.1109/MCOM.2010.5434378]

[148] G. TZIMPRAGOS, C. KACHRIS, I. DJORDJEVIC, M. CVIJETIC, D. SOUDRIS, & I. TOMKOS, "A Survey on FEC Codes for 100G and Beyond Optical Networks," *IEEE Communications Surveys & Tutorials*, 2014, pp. 1–1. [doi: 10.1109/COMST.2014.2361754]

[149] A. CARENA, G. BOSCO, V. CURRI, P. POGGIOLINI, M. T. TAIBA, & F. FORGHIERI, "Statistical characterization of PM-QPSK signals after propagation in uncompensated fiber links," in *European Conference on Optical Communication*, Torino (IT), Sep. 2010, paper P4.07. [doi: 10.1109/ECOC.2010.5621509]

[150] F. VACONDIO, C. SIMONNEAU, L. LORCY, J.-C. ANTONA, A. BONONI, & S. BIGO, "Experimental characterization of Gaussian-distributed nonlinear distortions," in *European Conference on Optical Communications*, Geneve (CH), Sep. 2011, paper We.7.B.1. [doi: 10.1364/ECOC.2011.We.7.B.1]

[151] F. VACONDIO, O. RIVAL, C. SIMONNEAU, E. GRELLIER, A. BONONI, L. LORCY, J.-C. ANTONA, & S. BIGO, "On nonlinear distortions of highly dispersive optical coherent systems," *Optics Express*, **Vol. 20**, **No. 2**, Jan. 2012, pp. 1022–1032. [doi: 10.1364/OE.20.001022]

[152] A. CARENA, V. CURRI, G. BOSCO, P. POGGIOLINI, & F. FORGHIERI, "Modeling of the Impact of Nonlinear Propagation Effects in Uncompensated Optical Coherent Transmission Links," *Journal of Lightwave Technology*, **Vol. 30**, **No. 10**, May 2012, pp. 1524–1539. [doi: 10.1109/JLT.2012.2189198]

[153] Z. WANG, Y. QIAO, Y. XU, & Y. JI, "Statistical characterization of the nonlinear noise in 28 Tbit/s PDM-16QAM CO-OFDM system," *Optics Express*, **Vol. 21**, **No. 15**, Jul. 2013, pp. 18 034–18 042. [doi: 10.1364/OE.21.018034]

[154] P. SERENA & A. BONONI, "On the accuracy of the Gaussian nonlinear model for dispersion-unmanaged coherent links," in *European Conference on Optical Communications*, London (UK), Sep. 2013, paper Th.1.D.3.

[155] X. CHEN & W. SHIEH, "Closed-form expressions for nonlinear transmission performance of densely spaced coherent optical OFDM systems." *Optics Express*, **Vol. 18**, **No. 18**, Aug. 2010, pp. 19 039–19 054. [doi: 10.1364/OE.18.019039]

[156] P. JOHANNISSON, "Analytical Modeling of Nonlinear Propagation in a Strongly Dispersive Optical Communication System," *arXiv*, **No. 1205.2193**, May 2012. [arXiv: 1205.2193]

[157] A. BONONI & P. SERENA, "An Alternative Derivation of Johannisson's Regular Perturbation Model," *arXiv*, **No. 1207.4729**, Jul. 2012. [arXiv: 1207.4729]

[158] P. POGGIOLINI, G. BOSCO, A. CARENA, V. CURRI, Y. JIANG, & F. FORGHIERI, "A Detailed Analytical Derivation of the GN Model of Non-Linear Interference in Coherent Optical Transmission Systems," *arXiv*, **No. 1209.0394**, Sep. 2012. [arXiv: 1209.0394]

[159] P. JOHANNISSON & M. KARLSSON, "Perturbation Analysis of Nonlinear Propagation in a Strongly Dispersive Optical Communication System," *Journal of Lightwave Technology*, **Vol. 31**, **No. 8**, Apr. 2013, pp. 1273–1282. [doi: 10.1109/JLT.2013.2246543]

[160] R. DAR, M. FEDER, A. MECOZZI, & M. SHTAIF, "Properties of nonlinear noise in long, dispersion-uncompensated fiber links," *Optics Express*, **Vol. 21**, **No. 22**, Nov. 2013, pp. 25 685–25 699. [doi: 10.1364/OE.21.025685]

[161] M. SECONDINI, E. FORESTIERI, & G. PRATI, "Achievable Information Rate in Nonlinear WDM Fiber-Optic Systems With Arbitrary Modulation Formats and Dispersion Maps," *Journal of Lightwave Technology*, **Vol. 31**, **No. 23**, Dec. 2013, pp. 3839–3852. [doi: 10.1109/JLT.2013.2288677]

[162] D. J. IVES, A. LORD, P. WRIGHT, & S. J. SAVORY, "Quantifying the Impact of Non-linear Impairments on Blocking Load in Elastic Optical Networks," in *Optical Fiber Communication Conference*, San Francisco, CA. (USA), Mar. 2014, paper W2A.55. [doi: 10.1364/OFC.2014.W2A.55]

[163] S. J. SAVORY, "Approximations for the Nonlinear Self-Channel Interference of Channels With Rectangular Spectra," *IEEE Photonics Technology Letters*, **Vol. 25**, **No. 10**, May 2013, pp. 961–964. [doi: 10.1109/LPT.2013.2255869]

[164] G. BOSCO, R. CIGLIUTTI, A. NESPOLA, A. CARENA, V. CURRI, F. FORGHIERI, Y. YAMAMOTO, T. SASAKI, Y. JIANG, & P. POGGIOLINI, "Experimental Investigation of Nonlinear Interference Accumulation in Uncompensated Links," *IEEE Photonics Technology Letters*, **Vol. 24**, **No. 14**, Jul. 2012, pp. 1230–1232. [doi: 10.1109/LPT.2012.2200672]

[165] G. TURIN, "An introduction to matched filters," *IEEE Transactions on Information Theory*, **Vol. 6**, **No. 3**, Jun. 1960, pp. 311–329. [doi: 10.1109/TIT.1960.1057571]

[166] R. DAR, M. FEDER, A. MECOZZI, & M. SHTAIF, "Properties of nonlinear noise in long, dispersion-uncompensated fiber links," *arXiv*, **No. 1307.7401**, Jul. 2013. [arXiv: 1307.7401]

[167] R. DAR, M. FEDER, A. MECOZZI, & M. SHTAIF, "Time varying ISI model for nonlinear interference noise," *arXiv*, **No. 1310.6132**, Oct. 2013. [arXiv: 1310.6132]

[168] R. DAR, M. FEDER, A. MECOZZI, & M. SHTAIF, "Accumulation of nonlinear interference noise in fiber-optic systems," *Optics Express*, **Vol. 22**, **No. 12**, Jun. 2014, pp. 14 199–14 211. [doi: 10.1364/OE.22.014199]

[169] A. CARENA, G. BOSCO, V. CURRI, Y. JIANG, P. POGGIOLINI, & F. FORGHIERI, "EGN model of non-linear fiber propagation," *Optics Express*, **Vol. 22**, **No. 13**, Jun. 2014, pp. 16 335–16 362. [doi: 10.1364/OE.22.016335]

[170] M. I. YOUSEFI, F. R. KSCHISCHANG, & G. KRAMER, "Kolmogorov-Zakharov Model for Optical Fiber Communication," *arXiv*, **Vol. 1411.6550**, Nov. 2014. [arXiv: 1411.6550]

[171] M. SECONDINI & E. FORESTIERI, "On XPM Mitigation in WDM Fiber-Optic Systems," *IEEE Photonics Technology Letters*, **Vol. 26**, **No. 22**, Nov. 2014, pp. 2252–2255. [doi: 10.1109/LPT.2014.2353217]

[172] C. R. MENYUK, "Application of multiple-length-scale methods to the study of optical fiber transmission," *Journal of Engineering Mathematics*, **Vol. 36**, **No. 1**, Aug. 1999, pp. 113–136. [doi: 10.1023/A:1017255407404]

[173] S. HAYKIN, *Adaptive filter theory*, 4th ed. Upper Saddle River, NJ, USA: Prentice Hall, 2001.

[174] IEC, *Fibre optic communication system design guides Part 10: Characterization of the quality of optical vector-modulated signals with the error vector magnitude*, IEC Std. PD IEC/TR 61 282-10:2013, 2013. [Available: http://www.iec.ch]

[175] D. J. IVES, P. BAYVEL, & S. J. SAVORY, "Physical Layer Transmitter and Routing Optimization to Maximize the Traffic Throughput of a Nonlinear Optical Mesh Network," in *Optical Network Design and Modeling*, Stockholm (SE), May 2014, pp. 168–173.

[176] D. J. IVES, P. BAYVEL, & S. J. SAVORY, "Routing, modulation, spectrum and launch power assignment to maximize the traffic throughput of a nonlinear optical mesh network," *Photonic Network Communications*, **Vol. 29**, **No. 3**, Mar. 2015, pp. 244–256. [doi: 10.1007/s11107-015-0488-0]

[177] J. Y. YEN, "Finding the K Shortest Loopless Paths in a Network," *Management Science*, **Vol. 17**, **No. 11**, 1971, pp. 712–716. [doi: 10.2307/2629312]

[178] D. BANERJEE & B. MUKHERJEE, "A practical approach for routing and wavelength assignment in large wavelength-routed optical networks," *IEEE Journal on Selected Areas in Communications*, **Vol. 14**, **No. 5**, Jun. 1996, pp. 903–908. [doi: 10.1109/49.510913]

[179] N. WAUTERS & P. DEMEESTER, "Design of the optical path layer in multiwavelength cross-connected networks," *IEEE Journal on Selected Areas in Communications*, **Vol. 14**, **No. 5**, Jun. 1996, pp. 881–892. [doi: 10.1109/49.510911]

[180] D. J. IVES, P. BAYVEL, & S. J. SAVORY, "Assessment of Options for Utilizing SNR Margin to Increase Network Data Throughput," in *Optical Fiber Communication Conference*, Los Angeles, CA. (USA), Mar. 2015, paper M2I.3. [doi: 10.1364/OFC.2015.M2I.3]

[181] G.-H. GHO & J. M. KAHN, "Rate-Adaptive Modulation and Coding for Optical Fiber Transmission Systems," *Journal of Lightwave Technology*, **Vol. 30**, **No. 12**, Jun. 2012, pp. 1818–1828. [doi: 10.1109/JLT.2012.2189435]

[182] X. ZHAO, V. VUSIRIKALA, B. KOLEY, V. KAMALOV, & T. HOFMEISTER, "The prospect of inter-data-center optical networks," *IEEE Communications Magazine*, **Vol. 51**, **No. 9**, Sep. 2013, pp. 32–38. [doi: 10.1109/MCOM.2013.6588647]

[183] D. J. IVES & S. J. SAVORY, "Fixed versus Flex Grid with Route Optimised Modulation Formats and Channel Rates of 400 Gbits and Above," in *European Conference on Optical Communications*, London (UK), Sep. 2013, paper P.5.11.

[184] P. POGGIOLINI, G. BOSCO, A. CARENA, V. CURRI, Y. JIANG, & F. FORGHIERI, "A Simple and Effective Closed-Form GN Model Correction Formula Accounting for Signal Non-Gaussian Distribution," *Journal of Lightwave Technology*, **Vol. 33**, **No. 2**, Jan. 2015, pp. 459–473. [doi: 10.1109/JLT.2014.2387891]

[185] L. YAN, E. AGRELL, H. WYMEERSCH, P. JOHANNISSON, R. TARANTO, & M. BRANDT-PEARCE, "Link-Level Resource Allocation for Flexible-Grid Nonlinear Fiber-Optic Communication Systems," *IEEE Photonics Technology Letters*, 2015. [doi: 10.1109/LPT.2015.2415586]

[186] D. KREUTZ, F. M. V. RAMOS, P. E. VERISSIMO, C. E. ROTHENBERG, S. AZODOLMOLKY, & S. UHLIG, "Software-Defined Networking: A Comprehensive Survey," *Proceedings of the IEEE*, **Vol. 103**, **No. 1**, Jan. 2015, pp. 14–76. [doi: 10.1109/JPROC.2014.2371999]

[187] S. PENG, R. NEJABATI, & D. SIMEONIDOU, "Impairment-Aware Optical Network Virtualization in Single-Line-Rate and Mixed-Line-Rate WDM Networks," *Journal of Optical Communications and Networking*, **Vol. 5**, **No. 4**, Mar. 2013, p. 283. [doi: 10.1364/JOCN.5.000283]

[188] J. MATIAS, J. GARAY, N. TOLEDO, J. UNZILLA, & E. JACOB, "Toward an SDN-enabled NFV architecture," *IEEE Communications Magazine*, **Vol. 53**, **No. 4**, Apr. 2015, pp. 187–193. [doi: 10.1109/MCOM.2015.7081093]